وزارة التعليم العالي والبحث العلمي

**Ministry of Higher Education and Scientific Research**

المدرسة الوطنية العليا لعلوم البحر وتهيئة الساحل

**National Higher School of Marine Sciences and Coastal Management**

**Final Year Thesis for the Degree of State Engineer in Marine Sciences**

**Option: Coastal Management and Protection**

**Topic:**

# Mapping the vulnerability of the Skikda coastline to the risks of erosion, coastal flooding, and inundation

Presented by:

HAMMA Wissal

BRANIA Aymen

Presented on 01/06/2025, in front of the jury composed of:

| | | |
|---|---|---|
| Mr. DAHMANI A. | Assistant Professor - ENSSMAL | President |
| Mr. MEZOUAR K. | Professor - ENSSMAL | Supervisor |
| Mr. GREBICI M. L | Engineer - ALDIPH | Co-Supervisor |
| Mrs. SALEM CHRIF Y. | Assistant Professor - ENSSMAL | Examiner |

**academic year: 2024/2025**

## Acknowledgements

We thank God, the Almighty, for granting us the strength, patience, and wisdom necessary to carry out this work. Without His blessing, none of this would have been possible.

We express our deepest gratitude to **Mr. Mezouar K.**, our supervisor, for his trust, valuable advice, and continuous support throughout this project. His expertise and rigor enabled us to move forward with clarity and motivation.

Our sincere thanks also go to **Mr. Grebici M.L.**, our co-supervisor, for his commitment, availability, and always insightful guidance. His support was a major asset at every stage of our work.

We warmly thank the members of the jury **Mr. DAHMANI A.** and **Mrs. SALEM CHRIF Y.** for agreeing to evaluate our thesis, and for their constructive and enriching remarks which will undoubtedly help improve the quality of our study.

We also thank **Mrs. Keraghel M.** and **Mr. Sallaye M.** for their technical support, attentive listening, and patience, which greatly facilitated our progress.

We take this opportunity to thank all the teaching staff of **ENSSMAL** for their instruction, guidance, and dedication throughout our training.

Finally, we extend a heartfelt thank you to everyone who, directly or indirectly, contributed to the success of this thesis. Their help, presence, and encouragement made all the difference.

# *Dedication*

*I would first like to thank God for granting me the strength and perseverance to complete this journey.*

*To my dear mother, GRAZZA Fadila, thank you for your endless love, your unwavering support, and for always believing in me, no matter the circumstances. Your presence in my life is my greatest blessing.*

*To my father, HAMMA Hafnaoui, I am deeply grateful for your guidance, your sacrifices, and for always pushing me to be the best version of myself. Your wisdom has shaped who I am today.*

*To my siblings, Thabet, Farah, and Youcef, thank you for being my constant source of joy and inspiration. Your encouragement and love mean the world to me.*

*To my friends, Nibras, Meriem, Yousra, Hayem, and Ikram, thank you for being by my side through the highs and lows, and for making this journey more enjoyable and memorable with your friendship and support.*

*To our GPL (Gestion et Protection du Littoral) program, it has been a privilege to share this experience with such a dedicated and passionate group. We've learned so much together.*

*I want also to express my appreciation to the company ALDIPH for its warm welcome and the resources made available to us during our internship. A big thank you to all the staff for their availability and valuable assistance during my time with them.*

*To our co-supervisor, thank you for your guidance and support throughout this project. Even though it was your first experience supervising, your commitment and dedication have been invaluable in helping us navigate this process.*

*And finally, to myself, for all the hard work, persistence, and resilience I've shown in completing this project. I truly believe I've earned this moment.*

*Wissal*

# *Dedication*

*I dedicate this work to my beloved parents. May God always protect them. Without their unconditional love and unwavering support, I could never have made it this far. I carry endless gratitude in my heart for everything they've done.*

*To the memory of my dear brother, Noureddine, who left this world far too soon. Your absence is deeply felt every day, but your love and your smile live on in me forever. May God have mercy on your soul and grant you peace in His vast paradise.*

*To my wonderful sisters, the true pillars of my life and the closest to my heart. Your love, strength, and kindness are with me in every step I take. Thank you for always being there.*

*To my project partner thank you for your support, your presence, and the shared moments that helped ease the challenges along the way.*

*And to my friends and colleagues Halim, Anis, Fadi, Chemsou, Saife Eddine, Oussama, Mourad, and Alla thank you for the laughs, the encouragement, and all the memories we've shared along the way.*

*Aymen*

# Table of Contents

## List of Figures

List of Appendices

## List of Tables

## List of Equations

## List of Abbreviations

**UNFCCC:** United Nations Framework Convention on Climate Change.

**OA:** Ocean Acidification.

**IPCC:** Intergovernmental Panel on Climate Change.

**NOAA:** National Oceanic and Atmospheric Administration.

**UNDP:** United Nations Development Program.

**KHK-HKH:** Horton index.

**POT:** Peaks Over Threshold.

**DHI:** Dansk Hydraulisk Institut.

**FM:** Flexible Mesh.

**ASCII:** American Standard Code for Information Interchange**.**

**GIS:** Geographic Information System.

**DSAS:** Digital Shoreline Analysis System.

**EPR:** End Point Rate.

**NSM:** Net Shoreline Movement.

**DEM:** Digital Elevation Model.

**SAETI:** Algerian Company for Infrastructure Studies.

# General Introduction

# General Introduction

Coastal areas are some of the most dynamic and vulnerable places on Earth. controlled by natural forces such as waves, storms, tides, and sea level rise, or human activity. The impacts of climate change are putting coastal zones at high risk of erosion, coastal flooding, and inundation.

In Algeria, these pressures are clearly visible along it's coastline. The country faces significant challenges protecting the zone and insuring development. Many regions are located in vulnerable areas, near oueds mouths or unstable cliffs, making them particularly exposed previously mentioned risks.

The Skikda coastline, in northeastern Algeria includes sensitive environments, such as wetlands and oueds mouths, that are highly exposed to both natural hazards and human impacts from industrial activity to harbor operations. Numerous studies have been carried out in bays such as Algiers Bay, Bou Ismaïl Bay, and Zemmouri Bay, providing valuable data on coastal dynamics and risks. However, there remains a clear lack of research focused on Skikda Bay, resulting in significant gaps in knowledge that impact effective coastal management and protection in this area.

The goal of this work is to better understand the risks facing the Skikda coastline and identify the regions most vulnerable. To do that so we organized this research into seven chapters:

- **Chapter I** In this chapter we defined the scientific concepts related to our study in a general way
- **Chapter II** We took a close look at the Skikda region, examining its geology, oueds, climate, and ocean conditions to understand how these factors influence the coast's behavior and vulnerability.
- **Chapter III** Focuses on Coastline Evaluation. We look at how the coastline has changed over time and predict how it might continue to evolve, identifying both the most stable and the most vulnerable areas.
- **Chapter IV** We used the Peaks Over Threshold (POT) method to estimate the risk and impact of major coastal flooding events.
- **Chapter V** Using the MIKE21 model we simulated how waves behave along the coast. These simulations helped us understand how different parts of the coastline respond to storm conditions and where flooding is most likely to occur.
- **Chapter VI** We used the results from the extreme events and hydrodynamic modeling to map the areas that are most vulnerable to flooding.
- **Chapter VII** We analyzed inundation caused by oued overflow, using the HEC-RAS model to simulate how water might spread from the Saf-Saf oued and the bridge that spans it.

Through these chapters, we hope to provide a comprehensive understanding of the challenges that the Skikda coastline faces now and in the future. By offering clear understanding to al the

risks, we hope to support better decision making for protecting the coastal environment and the communities that depend on it.

# Chapter I: Overview

# I.1 Introduction

Coastal regions are dynamic yet vulnerable environments, exposed to various natural hazards, including erosion, coastal flooding and inundation. Climate change and increasing urbanization exacerbate these phenomena, posing significant risks to people, infrastructure, and ecosystems. As these risks grow, it has become imperative to understand their causes and result to develop effective preventive and adaptive measures. This issue is particularly critical in a context where the resilience of coastal regions has emerged as a major challenge for the future.

# I.2 Coastal Environment and Landscapes

## I.2.1 Coasts

Coasts are complex areas, characterized by land–sea interaction **(AUGUSTINUS, 2003)**, as a result, it is home to three influences:

Continental factors: These refer to the geological structure of the area in question, which determines the type and resistance of rocks against erosion.

Marine factors: These encompass the effects of variations in mean sea level and processes driven by hydrodynamic forces such as waves, tides, and currents. The sea's influence extends beyond erosion, as it can also play a constructive role through sediment deposition and coastal progradation.

Atmospheric factors: These involve subaerial agents such as wind, temperature fluctuations, and water in its various forms. These elements contribute to rock weathering and influence the movement of sediments in both coastal and inland environments **(PASKOFF, 2010)**.

## I.2.2 Beaches

a beach is understood as a coastal landform primarily composed of unconsolidated sandy sediments, shaped by wave and current action, and including features such as berms that reflect depositional energy conditions **(PERERA et al., 2023)**.

It's a sloping coastal landform covered in loose sand, gravel, pebbles, or seashell fragments **(MARINE CONSERVATION SCIENCE, 2012)**.

## I.2.3 Cliff

It is a steep, vegetation-free slope with an inclination ranging from 15° to near-vertical, of highly variable height, located at the interface between land and sea, and shaped by marine processes or presence. **(PASKOFF, 2010)**.

There are two types of cliffs:

**Active cliffs**: characterized by a generally steep escarpment, constantly eroded by waves.

**Inactive cliffs**: which are no longer affected by marine processes.

### I.2.4 Dune

Is an accumulation of sand formed by the wind along shorelines, resulting from the transport and deposition of sediments carried by waves, marine currents, and cliff erosion. Its formation depends on the availability of sand, wind action, and specific conditions such as the moisture content of the grains and wind speed **(GOUGUET, 2018)**.

### I.2.5 Watershed

A watershed is defined as the area above a certain point which drains water through that particular point, i.e., outlet. In other words, it is an area of land which drains or sheds all of the incoming excess precipitation at the same place, toward the same body of water or the same low elevation area resulting from its topography. This means that a watershed's boundary is defined by its topographic high points. The precipitation that falls within the boundary of a watershed would flow as excess precipitation towards its outlet, i.e., point of lowest elevation. Depending on the location of the outlet, the watershed area would be different. A watershed is fairly simple to identify in hilly areas because its boundaries are well defined by ridges **(ABRAR et al., 2020).**

An ungauged watershed is one with inadequate records (in terms of both data quantity and quality) of hydrological observations to enable computation of hydrological variables of interest (both water quantity or quality) at the appropriate spatial and temporal scales, and to the accuracy acceptable for practical applications **(SIVAPALAN et al., 2003).**

A watershed having the measured hydrological parameters such as rainfall, runoff and others is called gauged watershed **(SURESH, 2020).**

## I.3 Coastal Space and System

### I.3.1 Coastal System

Coastal system includes both the physical coast and the dynamic processes that shape it (dynamic interfaces where land meets ocean and atmosphere). Through a multitude of physical processes, the three environments interact continuously along the shoreline. Interaction among these environments occurs at varying spatial and temporal scales, ranging from large-scale coastal dynamics down to the intricate relationships between water movement and sediment transport.

### I.3.2 Coastal space

Areas where various coastal activities are mapped and firmly anchored to specific locations, laying the basis for defining those spaces **(JOHNSEN et al., 2014)**. It is the human use and management of coastal regions.

### I.3.3 Coastal Domain

A broader spatial area influenced by coastal processes, including both land and sea and based on hydrodynamic processes the coastal domain is sectioned into 4 zones: Offshore zone, Surf zone, Shoaling zone, Swash zone.

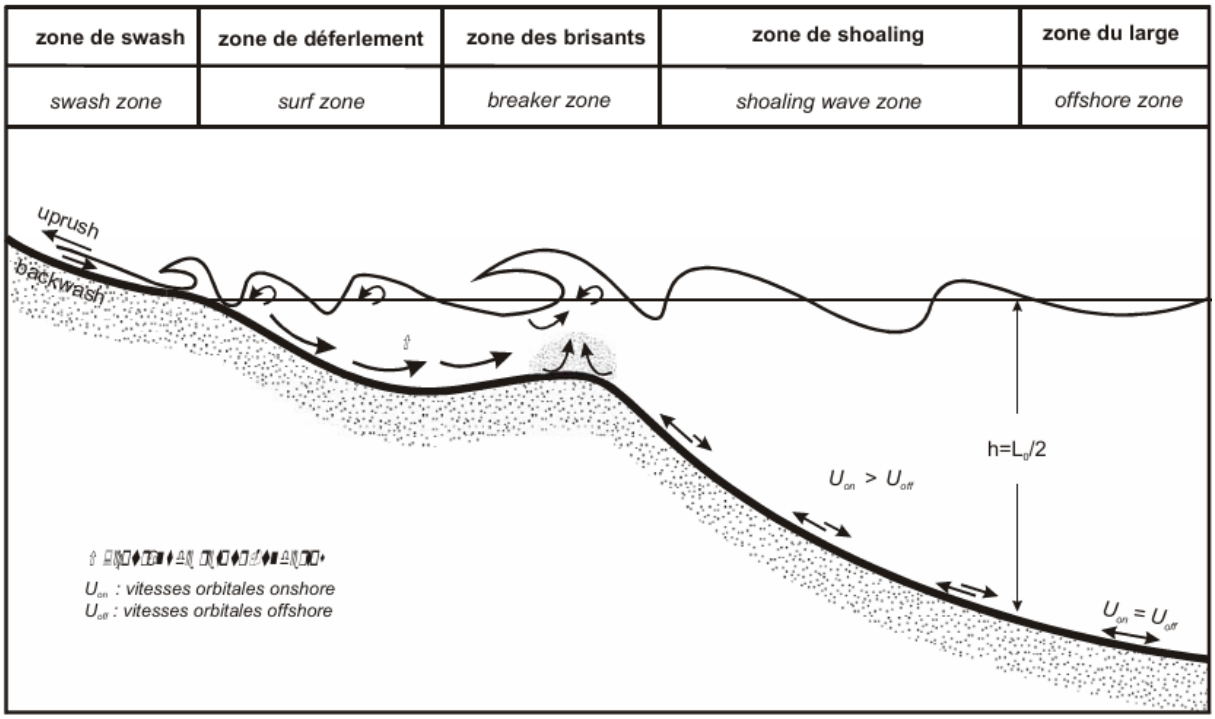


Figure 1: Diagram representing the zones of the coastal domain **(STEPANIAN, 2002)**.

## I.4 Climate and Climate Change

### I.4.1 Climate

Climate is the synthesis of the day-to-day weather conditions in a given area. The actual climate is characterized by long-term statistics (such as mean values, variances, probabilities of extreme values) of the state of the atmosphere in that area, or of the meteorological elements in that area. Synthesis implies much more than simple averaging. Various methods are used to represent climate; for example, average and extreme values, frequencies of values within stated ranges, and the frequencies of weather types with associated values of elements. The main climate elements are precipitation, temperature, humidity, sunshine and wind velocity, and phenomena such as fog, frost, thunder, and gales. Cloudiness, evaporation, grass minimum temperatures, and soil temperatures at various depths, and other items **(MAUNDER, 1992)**.

### I.4.2 Climate change

The Fifth Assessment Report published by the IPCC in 2013 reinforced the distinction between human-induced and natural climate change by stating with 95% certainty that human activities, particularly the burning of fossil fuels, deforestation, and industrial processes, have been the primary drivers of global warming since the mid-20th century. This has led to significant environmental transformations, including increasing global temperatures, rising sea levels, ocean acidification, and more extreme weather events. The IPCC also emphasized that the rate of climate change has accelerated in recent decades, with each of the last three decades being warmer than the previous one, surpassing any recorded temperature levels since 1850 **(IPCC, 2013).**

A change in the state of the climate that can be identified by changes in the mean and/or the variability of its properties and that persists for an extended period, typically decades or longer,

is defined as climate change in the IPCC 2021 report. Climate change may result from natural internal processes or external forces such as solar cycles, volcanic eruptions, or persistent human (anthropogenic) changes in the atmosphere or land use. The United Nations Framework Convention on Climate Change (UNFCCC), however, defines climate change more narrowly in its Article 1 as: "a change of climate which is attributed directly or indirectly to human activity that alters the composition of the global atmosphere and which is in addition to natural climate variability observed over comparable time periods". This definition by the UNFCCC makes a clear distinction between human-caused climate change and natural climate variability. **(IPCC, 2021).**

## I.5 Coastal Dynamic Agents

### I.5.1 Erosion

Erosion is a geomorphic process that detaches and removes material (soil, rock debris, and associated organic matter) from its primary location by some natural erosive agents or through human or animal activity **(ZORN et al., 2016)**.

### I.5.2 Sediment accumulation

The process by which sediment is deposited and stored in various coastal environments. This process is influenced by factors such as sediment supply, hydrodynamic conditions, and coastal topography.

### I.5.3 Sediment transport

Sediment transport has been defined as those processes by which sedimentary materials are removed from one location and transported to a downstream deposition site, from which a new cycle of sediment transport may start again **(BREBBIA et al., 1982)**.

### I.5.4 Storm

A storm refers to a disturbed or turbulent state in the natural environment, typically characterized by significant changes in atmospheric conditions such as wind, precipitation, pressure, and temperature. On Earth or other astronomical bodies, storms arise due to dynamic interactions within the atmosphere, leading to phenomena such as strong winds, thunderstorms, heavy rainfall, snow, or even dust storms. These events often result from atmospheric instabilities caused by thermal contrasts, moisture content, or planetary rotation **(LOBETO et al., 2024)**.

## I.6 Coastal Flooding and Inundation

### I.6.1 Coastal flooding

Coastal flooding refers to the temporary inundation of low-lying coastal areas due to the overflow of seawater onto normally dry land. It is primarily caused by storm surges, high tides, tsunamis, or rising sea levels associated with climate change. The severity of coastal flooding depends on factors such as storm intensity, coastal topography, and the presence of natural or man-made barriers **(IPCC, 2019)**.

### I.6.2 Inundation

Temporary, natural, or artificial submersion of a land area. This flooding generally affects land adjacent to a watercourse or a body of water with variable levels. It occurs when excess water cannot be drained through natural or artificial channels designed for this purpose.

Inundation of land areas along the coast, is caused by storms where water is driven onto land from an adjacent body of water **(NOAA, 2016)**.

### I.6.3 Sea Level

Sea level corresponds to the average height of the ocean, serving as a reference for studying maritime variations at different scales. It is calculated by considering the mean of high and low tides over a long period while excluding temporary effects caused by waves and storms. Generally, two types of measurements are distinguished: absolute sea level, which is determined relative to a geodetic reference, and relative sea level, which takes into account vertical land movements, such as subsidence or tectonic phenomena.

Beyond daily fluctuations, a gradual rise in global sea levels has been observed, mainly due to climate change. According to findings from the Intergovernmental Panel on Climate Change **(IPCC)** published in 2021, the global sea level rose by approximately 0.20m between 1901 and 2018, with an accelerating trend over recent decades. The rate of sea level rise increased from 1.3 mm/year between 1901 and 1971 to 3.7 mm/year between 2006 and 2018, indicating a significant acceleration of the phenomenon **(IPCC, 2021)**.

# Chapter II: Characterization of the Study Area

# II.1 Study Area

## II.1.1 Geographical Situation of the Study Area

The wilaya of Skikda, located in the northeastern coastal region of Algeria, covers an area of 4141 km². Its coastline covers over 250.19 km, 68% of which consists of rocky shores and steep cliffs, and features 34 beaches accessible to visitors.

It is bordered by:

- The Mediterranean Sea to the north
- Jijel Province to the west
- Mila Province to the southwest
- Constantine Province to the south
- Guelma Province to the southeast
- Annaba Province to the east

It is located between:

- Latitude: Between 36° 23' 40" and 37° 4' 40" North
- Longitude: Between 6° 13' 50" and 7° 24' 10" East

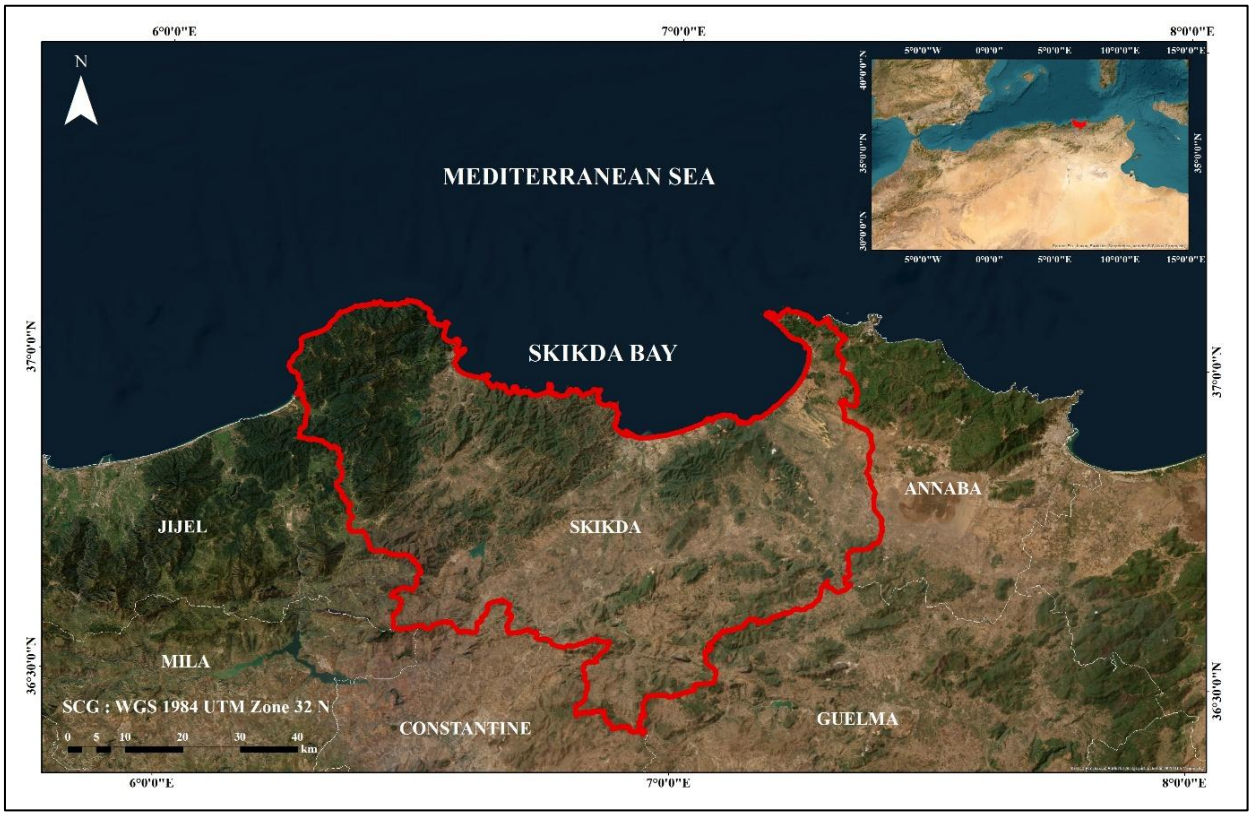


Figure 2: Map of the geographical location of the study area.

## II.1.2 Coastal Domain

The wilaya of Skikda comprises 38 communes, including 14 coastal ones, and had a total population of 1,018,000 in 2011, of which 418,682 lived in coastal areas **(MEGHZILI, 2015).**

Table 1: Coastal zone area per commune **(MEGHZILI, 2015).**

| Commune | Area of the commune (km²) | Coastal domain area (km²) | % Coastal domain area / Area of the commune | Coastline (km) | Population | Density (hab/km²) |
|---|---|---|---|---|---|---|
| **El Marsa** | 114,4 | 76,70 | 67,04 | 37,22 | 6 334 | 56 |
| **Ben Azzouz** | 213,7 | 56,95 | 87,38 | 7,26 | 30 809 | 144 |
| **Djendel 1 Saâdi Mohamed** | 213,7 | 56,95 | 26,65 | 5,15 | 9 143 | 43 |
| **Filfila** | 70,02 | 28,46 | 40,64 | 22,14 | 30 635 | 438 |
| **Skikda** | 56,38 | 40,06 | 71,05 | 28,69 | 172 860 | 3 066 |
| **Ain Zouit** | 113 | 23,32 | 20,63 | 35,03 | 2 086 | 19 |
| **Tamalous** | 177,4 | 4,867 | 2,74 | 7,66 | 54 158 | 305 |
| **Kerkera** | 85,93 | 115,48 | 18,01 | 23,99 | 24 714 | 287 |
| **Collo** | 24,41 | 16,87 | 69,11 | 25,52 | 37 300 | 1 528 |
| **Chéraïa** | 71,13 | 14,23 | 20,00 | 15,58 | 19 819 | 279 |
| **Kanoua** | 65,73 | 19,95 | 30,35 | 13,38 | 7 389 | 112 |
| **Ouled Attia** | 106,9 | 11,56 | 10,81 | 7,33 | 11 466 | 107 |
| **Kheng Mayoun** | 45,03 | 23,48 | 52,14 | 20,12 | 4 843 | 108 |
| **Oued Zhor** | 87,73 | 1,742 | 1,98 | 1,12 | 7 126 | 81 |
| **Total** | 1471,66 | 451,23 | 30,66 | 250,19 | 418 682 | 285 |

## II.2 Geological and Geomorphological Framework

Skikda's coastline is distinguished by its remarkable geomorphological diversity. Indeed, it is home not only to magnificent rocky shores, shaped by erosion, but also to vast stretches of fine sandy beaches that extend along the Mediterranean Sea, offering a striking contrast with the surrounding terrain. Moreover, an extensive dune field completes this landscape, playing an essential role in the natural protection of the coast and in maintaining the region's ecological balance

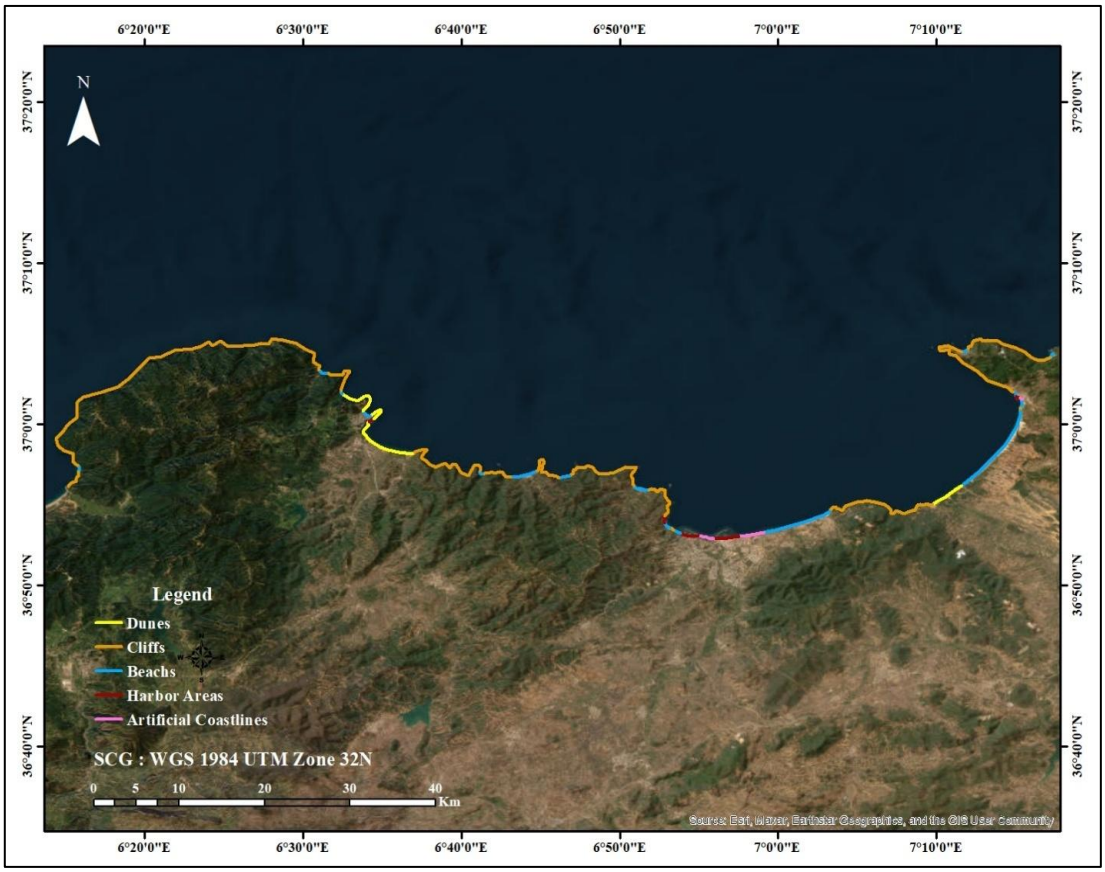


Figure 3: Coastal Typology of Skikda Bay.

### II.2.1 Dunes

#### Benazouz Dune Cordon

As part of the Guerbes-Sanhadja wetland complex, this dune cordon is important for biodiversity and ecosystem stability. A restoration project plans to stabilize 75 hectares of dunes in this area to prevent degradation and protect water resources. The vegetation includes species such as *Ammophila arenaria* and *Retama boveï*, which play a key role in dune fixation **(BOUHIDEL, 2022)**.

#### Guerbes-Sanhadja Dune System

Extending across the broader 42,100 hectares wetland complex, this dune system consists of various interconnected sand formations **(NATIONS UNIES, 2020)**. The dunes act as a natural barrier against coastal erosion, but they are increasingly threatened by agricultural expansion and human activities. Conservation efforts are underway to preserve their ecological functions **(UNDP, 2019).**

#### Filfila Dune Cordon

Located within the Guerbes-Sanhadja region, this dune system is particularly fragile. While specific data on its exact size is limited, it is known to be affected by overgrazing, sand

extraction, and trampling. Sustainable management strategies are needed to mitigate its degradation **(BOUHIDEL, 2022)**.

**Larbi Ben M'Hidi Dune System**

Spanning 206 hectares, this coastal area near Skikda features a succession of sandy beaches covering 45 hectares, backed by a vegetated dune cordon. However, urban development and tourism projects, which allocate 56 hectares for infrastructure, pose a growing threat to the dune ecosystem **(Algérie 360°, 2011).**

### II.2.2 Cliffs

10% of the Skikda coastline consists of rocky shores with limited recreational potential, while 58% comprises inaccessible cliffs **(MEGHZILI, 2015).**

The rocky cliffs dominate from Esrah Point to the Stora Cove site, with several rocky islets—including Sirigina, The Lion, the Macaque Islet, and the Monkeys Islet—located near the shoreline. The cliffs' topography is primarily composed of metamorphic rocks consisting of gneiss, schist, and bluish-gray mica schist **(GUEDDAH, 2003).**

The sheer cliffs of the Skikda coastline are subject to erosion caused by marine currents and chemical and biological phenomena linked to the aggressiveness of the waters, especially since the bay is known for frequent storms **(CEMALI et al., 2019).**

### II.2.2 Beaches

17% of the Skikda coastline consists of sandy beaches, distributed across a total of 65 sites.

Table 2: List of beaches in the wilaya of Skikda **(VITAMINEDZ, 2020).**

| No. | Beach Name | Daira/Commune | Observations |
|---|---|---|---|
| **1** | Lamguisba Cove | Kanoua | Small cove surrounded by cliffs |
| **2** | Marsa Zitoune Cove | Kheneg Mayoun | Bay nestled between two capes |
| **3** | Grande Plage | Ain Zouit | Wide stretch of fine sand |
| **4** | Aghalad or Khrayef Beach | Kheneg Mayoun | Rocky beach with coves |
| **5** | Ain Doula Beach | Collo | Wild beach bordered by forest |
| **6** | Ain Oum El Gssab Beach | Collo | Hard-to-reach,crystal-clear water |
| **7** | Awrar Beach | Kheneg Mayoun | Small isolated cove |
| **8** | Ayla Beach | Kheneg Mayoun | Golden sand beach |
| **9** | Belhadj Beach | Ain Zouit | Beach surrounded by cliffs |
| **10** | Ben Said Beach | Collo | Natural protected bay |
| **11** | Ben Zouit Beach | Kerkera | Fine sand, turquoise water |
| **12** | Bikini Beach | Skikda | Popular and touristy beach |
| **13** | Boumarouane Beach | El Marsa | Isolated, accessible by boat |
| **14** | Bouncheme Beach | Kanoua | Small bay between two rocks |
| **15** | Cap de Fer Beach | El Marsa | Rocky point with coves |

| | | | |
|---|---|---|---|
| **16** | Casino and Lido Beach | Skikda | Urban beach, close to hotels |
| **17** | Château Vert Beach | Skikda | Beach with a green cliff |
| **18** | Cheikh Rabah Beach | El Marsa | Hard-to-reach, beautiful cove |
| **19** | Collo Beach | Collo | Main beach of the town |
| **20** | Stora Beach | Skikda | Natural port, sandy beach |
| **21** | Platanes Beach | Filfila | Bordered by plane tree forests |
| **22** | Cap Bougaroun Beach | Kanoua | Deep waters, rich marine life |
| **23** | Eddamous or Damous Beach | Ouled Attia | Bay with panoramic view |
| **24** | El Marsa Beach | El Marsa | Natural port, coastal village |
| **25** | Guerbes or Guebez Beach | Skikda | Long wild beach |
| **26** | Hellala Beach | Kanoua | Small rocks and golden sand |
| **27** | Kef Fatma Beach | Benazouz | Crystal-clear waters, hard to access |
| **28** | Kssir El Baz Beach | Collo | Preserved natural environment |
| **29** | Bay of Young Girls Beach | Collo | Hidden small bay |
| **30** | La Carrière Beach | Skikda | Rocks and sea caves |
| **31** | La Jetée Beach (Horses' Beach) | Skikda | Stunning sea view |
| **32** | La Presqu'île Beach | Collo | Rocky peninsula |
| **33** | Labrarek Beach | Collo | Wild, little frequented |
| **34** | Laksar Beach | Kerkera | Fine sand and clear water |
| **35** | Larbi Ben M'hidi (Ex Jeanne d'Arc) Beach | Djendel | Large historic beach |
| **36** | Les Calatines Beach | Skikda | Rocky beach with coves |
| **37** | Marquette Beach | Skikda | Family-friendly beach |
| **38** | Marsa Zitoun or El Fnar Beach | Kheneg Mayoun | Clear waters, untouched nature |
| **39** | Military Beach | Skikda | Restricted access |
| **40** | Miramar Beach | Skikda | Close to hotel resorts |
| **41** | Mollo Beach | Skikda | Rocks and fine sand |
| **42** | Nor Beach | Skikda | Little frequented |
| **43** | Oued Bibi Beach | Ain Zouit | Bordered by a river |
| **44** | Oued El Gat Beach | Filfila | Preserved beach, rich marine life |
| **45** | Oued Lagsab Beach | Filfila | Natural beach |
| **46** | Oued Righa Beach | Filfila | Wide beach with dunes |
| **47** | Oued Saboun Beach | Filfila | Isolated and wild beach |
| **48** | Oued Tanji or Tangi or Tanger Beach | Ain Zouit | Picturesque beach |
| **49** | Oued Zhor Beach | Oued Zehour | Beach surrounded by mountains |
| **50** | Paradise Beach | Skikda | Idyllic location |
| **51** | Petit Port Beach | El Marsa | Small natural harbor |
| **52** | Ravin des Lions Beach | Skikda | Massive rock formations |
| **53** | Ravin des Singes Beach | Skikda | Cliff and wild cove |
| **54** | Rmila Beach | El Marsa | Fine sand, forest nearby |

| | | | |
|---|---|---|---|
| **55** | Kanoua Wild Beach | Kanoua | Little frequented, natural beauty |
| **56** | Sidi Abderahmane Beach | Kheneg Mayoun | Accessible by trail |
| **57** | Sidi Akacha Beach | El Marsa | Authentic beach |
| **58** | Taleza or Telza Beach | Collo | Protected bay |
| **59** | Tamanart Beach | Cheraia | Surrounded by lush vegetation |
| **60** | Zakkor or Zeghor Beach | Tamalous | Clear water and fine sand |
| **61** | Zmamria Beach | Kanoua | Wild and isolated |
| **62** | Cap de Fer East Flank Beaches | El Marsa | Stunning rocky landscape |
| **63** | Cap de Fer West Flank Beaches | El Marsa | Discreet cove |
| **64** | Beaches between El Marsa and Cap de Fer | El Marsa | Series of small coves |
| **65** | Wild Beaches | Skikda | Various unregulated beaches |

## II.3 Hydrographic Framework

### II.3.1 The Wadis

The hydrographic basin of the Gulf of Skikda is drained by several major wadis:

**Oued El Kebir**

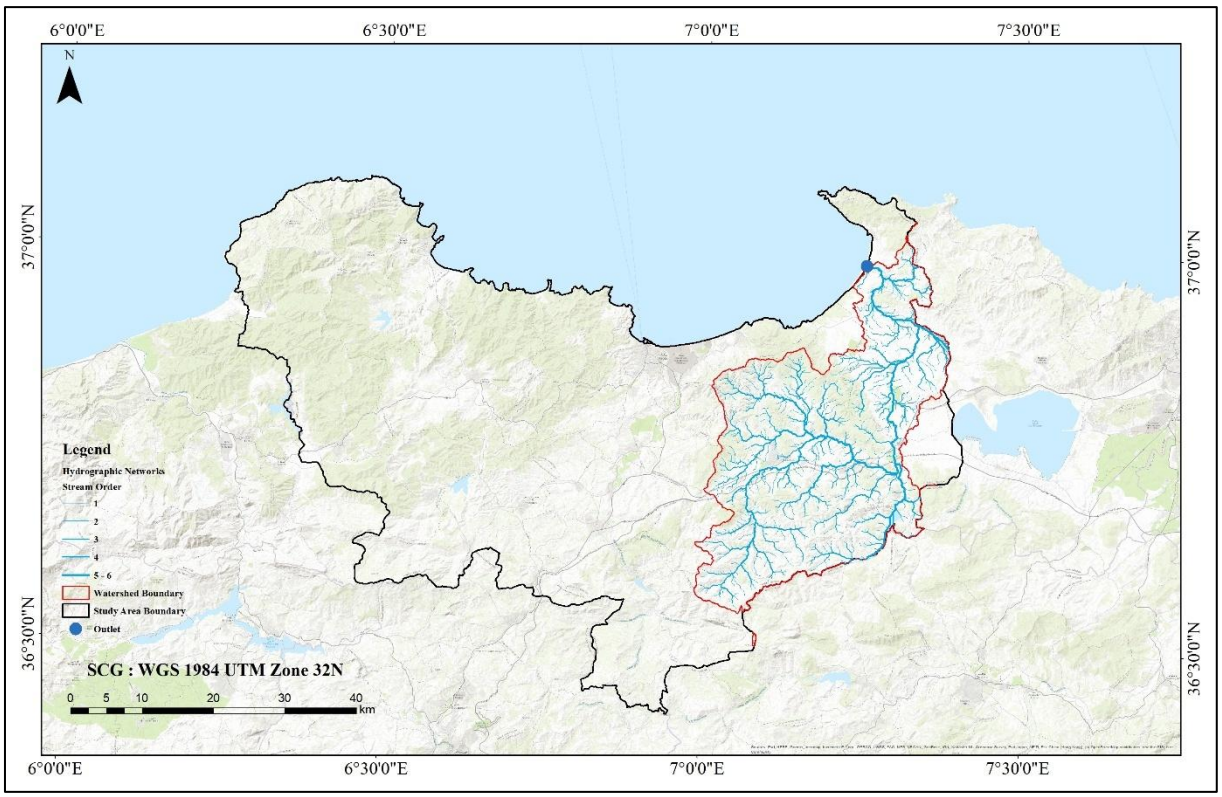


Figure 4: Watershed Map of Oued El Kebir.

Located in the east of the gulf, mainly drains the Bennazzouz plain. Its watershed covers an area of 994,5 km², and it flows into the Mediterranean Sea at La Marsa after a course of

approximately 100 km. The main oued length is 57.60 km, which influences the basin's hydrological behavior.

The Horton Index (KHK_HKH) for Oued El Kebir Ouest is 0.30, calculated using the formula:

Equation 1

$$KH = \frac{\text{Watershed Area}}{(\text{Main River Length})^2}$$

This value indicates a moderate elongation of the basin, affecting how water is concentrated and discharged into the Mediterranean.

**Oued Saf-Saf**

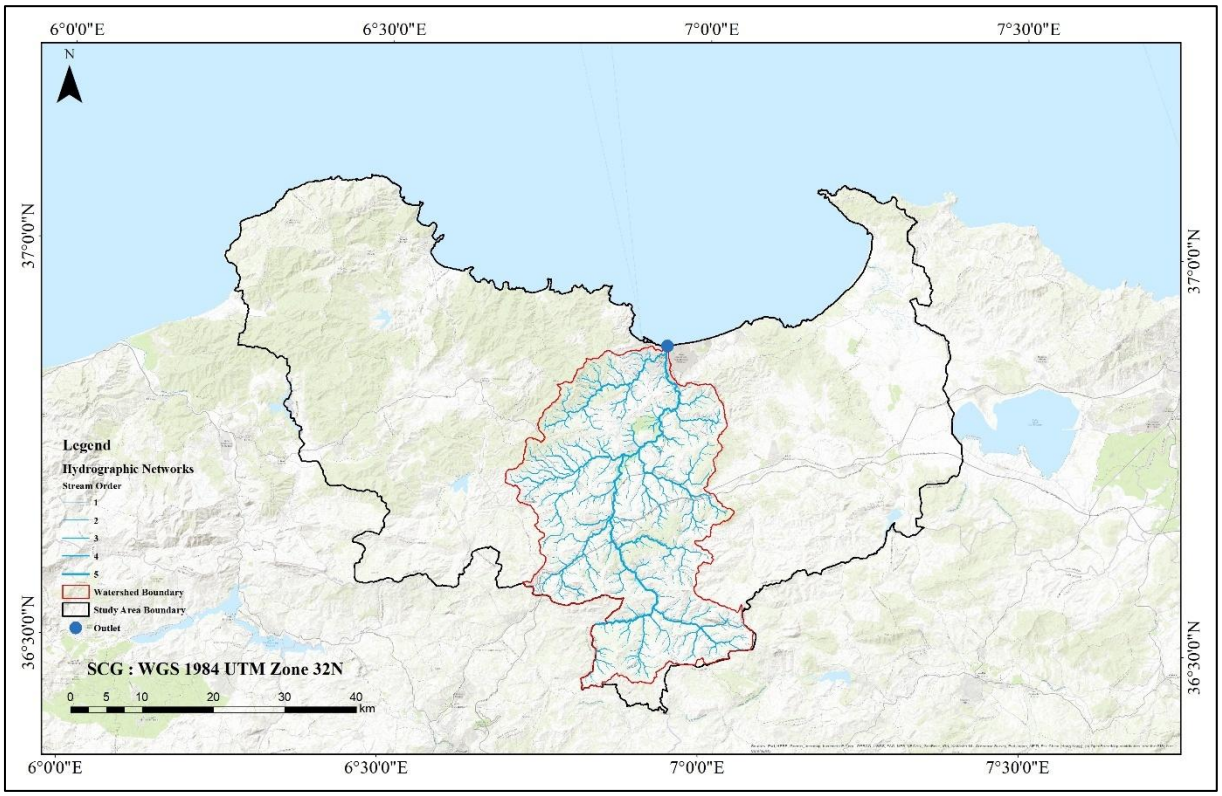


Figure 5: Watershed Map of Oued Saf-Saf.

The most significant wadi in the studied area, has a watershed of 1155 km². It originates in the south of the Numidian chain, specifically in the Djebel El Ouahch region (Constantine), and follows a north-south path over a length of 62 km before reaching the Mediterranean Sea.

The Horton Index (KHK_HKH) for Oued Saf-Saf is 0.26, this value suggests a relatively elongated basin, meaning that water is channeled efficiently through the main oued course. However, due to its geomorphological configuration, the alluvial plain located downstream of Oued Saf-Saf is particularly prone to flooding during heavy rainfall. The low slope of the terrain and increasing urbanization promote water accumulation, thereby increasing the risk of flooding and its associated damages.

In this study, we will specifically focus on Oued Saf-Saf, as the available data allow for an in-depth analysis of its hydrology and the infuence of floods in this region.

**Oued El Guebli**

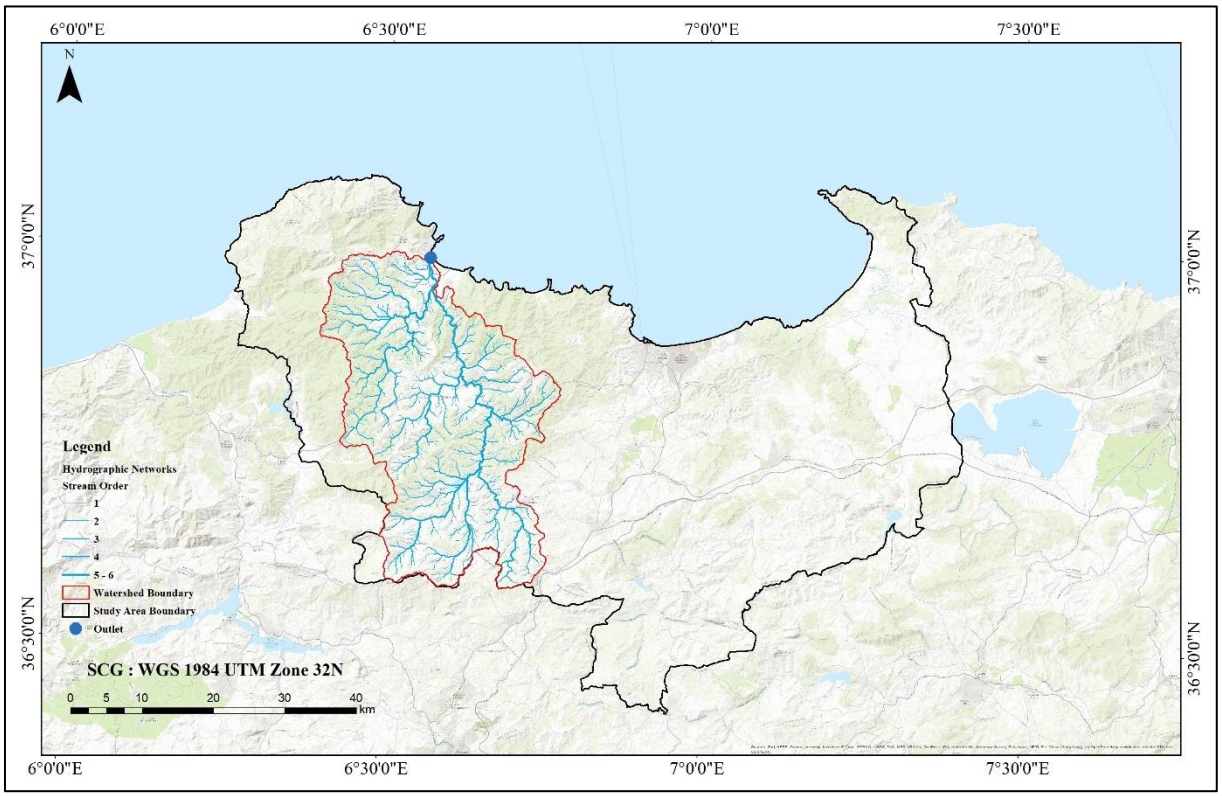


Figure 6: Watershed Map of Oued El Guebli.

Situated in the west of the gulf, has a watershed area of 977 km² and is almost entirely within the administrative boundaries of the Skikda province. The main watercourse has a length of 62.55 km, influencing the hydrological characteristics of the region.

The Horton Index (KHK_HKH) for Oued El Guebli is 0.25, this value suggests that Oued El Guebli's basin is relatively elongated, leading to a more concentrated flow along the main oued course. This can contribute to rapid water accumulation during heavy rains, increasing the risk of flooding in the downstream areas.

## II.4 Climatic Framework

### II.4.1 Precipitation

**Annual precipitation**

According to the results of Figure 7, it is observed that; Over the period from 2015 to 2024, annual precipitation in Skikda has shown significant variability, with notable fluctuations in rainfall levels. The highest recorded precipitation occurred in 2015, reaching 106 mm, while the lowest was observed in 2022, with only 13 mm. Another peak was recorded in 2019, with 101 mm of rainfall, but this was followed by a marked decline starting in 2020, where precipitation dropped to 67 mm and continued decreasing until it reached its lowest point in

2022. Although there was a slight rise in 2023, with 20 mm of rainfall, the 2024 figure remains low at 18 mm, indicating a persistent precipitation deficit. This decline in rainfall can be attributed to rising temperatures, which enhance water evaporation and hinder condensation, ultimately limiting precipitation. As a result, Skikda is experiencing a progressively drier climate.

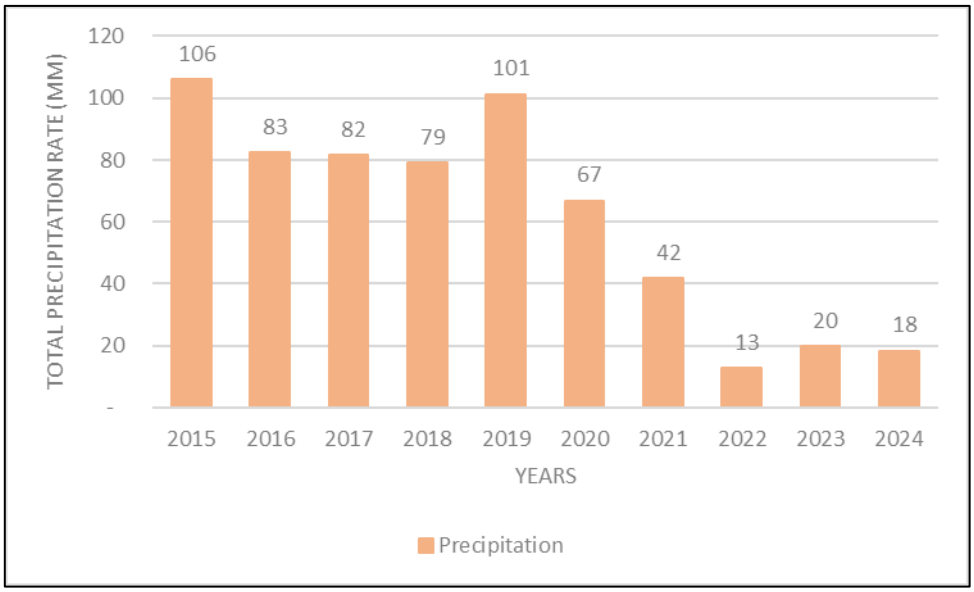


Figure 7: The annual precipitation in the Skikda region from 2015 to 2024 (Source: Historique-Météo 15/03/2025).

**Monthly precipitation**

According to the observations in Figure 8, it is noted that:

- Winter (89.37 mm) and autumn (77.67 mm) are the wettest seasons, with significant precipitation in November, December, and January.
- Summer (16.4 mm) is the driest season, with a sharp decline in precipitation, particularly in July (3.3 mm)
- The annual monthly average is 62.73 mm, confirming an uneven distribution of precipitation, characterized by a dry season and a wet season

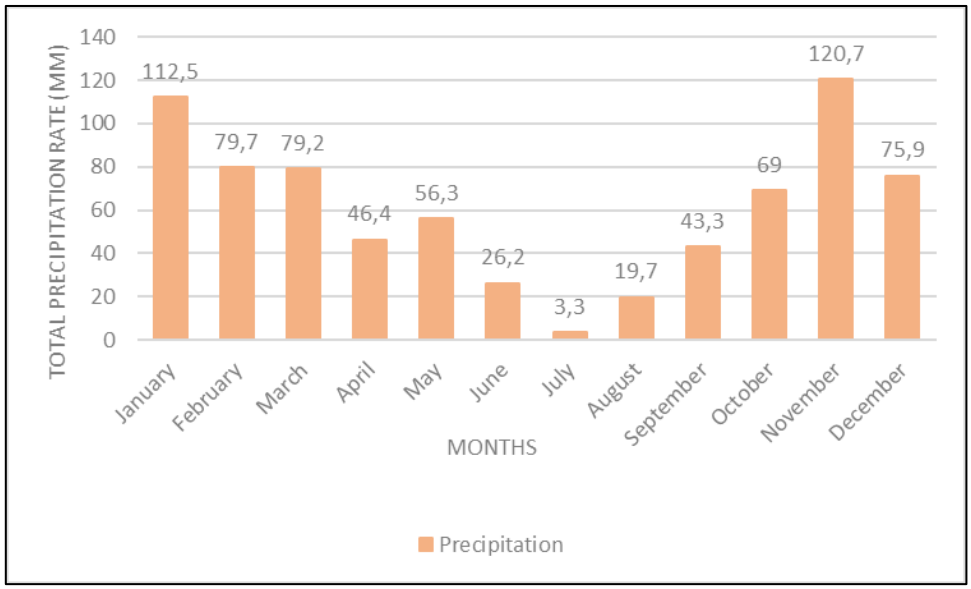


Figure 8: The monthly average precipitation in the Skikda region from 2015 to 2024 (Source: Historique-Météo 15/03/2025).

### II.4.2 Temperature

**Annual Temperature**

Over the years, temperature data in the region shows a gradual growth with minor fluctuations, suggesting a potential warming trend, likely influenced by climate change. The maximum temperature, despite some variations, generally rises between 2020 and 2022, reaching its peak in 2022. Although a slight decrease is observed in 2023 and 2024, the recorded values remain higher than in previous years. Similarly, the average temperature follows an upward trajectory, particularly after 2020, indicating an overall warming pattern that affects both daytime and nighttime temperatures. The minimum temperature remains relatively stable, showing only a slight increase over time, with notable dips in 2019 and 2023, which could be attributed to temporary cooling phases or natural climatic variability. The consistent rise in maximum and average temperatures suggests increasingly hotter summers and milder winters, while the stability of minimum temperatures may indicate a reduction in extreme cold conditions during winter and that what we see in Figure 9.

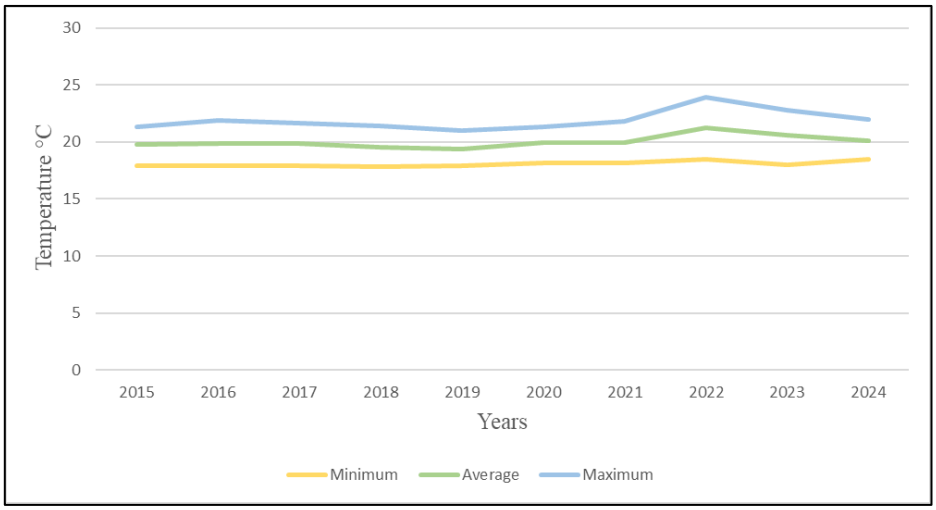


Figure 9: Annual temperature variations in the Skikda region from 2015 to 2024 (Source: Historique-Météo 15/03/2025).

**Monthly Temperature**

According to the results of Figure 10, it is observed that; Temperature patterns in the region follow a typical Mediterranean climate, characterized by hot summers and mild, humid winters. From January onward, temperatures gradually rise, reaching their peak during the summer months of July and August before decreasing toward December. According to the graph, July stands out as the hottest month, with maximum temperatures exceeding 30°C and an average ranging between 27 and 28°C. In contrast, January is the coldest month, with minimum temperatures dropping close to 5°C and an average between 10 and 12°C. The transition between seasons is gradual, with a steady rise in temperatures from March to June, followed by a decline from September to December.

This seasonal trend reflects the influence of the Mediterranean Sea, which moderates temperature variations and contributes to the region's coastal climate.

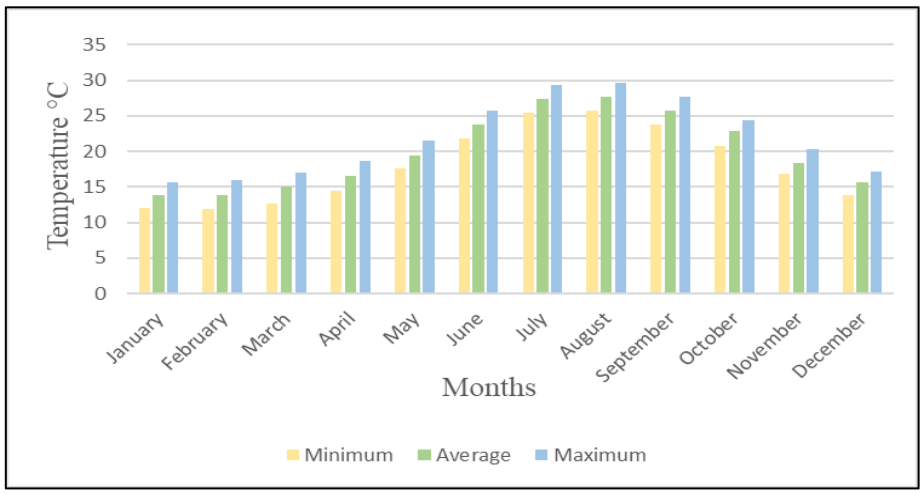


Figure 10: Monthly temperature variations in the Skikda region from 2015 to 2024 (Source: Historique-Météo 15/03/2025).

### II.4.3 The Wind

Wind plays an important role in the dynamics of the coastline as well as in erosion, marine submersion, and flooding processes. The analysis of wind patterns in the Skikda region was conducted using data from the online database Wave Climate (www.waveclimate.com), covering the period from 1992 to 2022. Information on wind speed and direction is graphically represented as wind roses in the Figure 11.

The annual wind rose (Figure 11) indicates that the winds blowing offshore in the Skikda region are predominantly from two main directions: the West (W) and the North-Northwest (NNW), which account for the highest percentages of the recorded winds. The peak wind speed observed reached 7 km/h, originating from the North-Northwest sector.

To better understand the seasonal variability of wind patterns in the region, a detailed analysis was conducted for each season:

- Autumn: During autumn, the wind rose analysis highlights the predominance of two main sectors: the West (W) and the West-Northwest (WNW), with a maximum recorded speed of 7.1 km/h and a frequency of 11.83%.
- Winter: In winter, the analysis reveals that the dominant wind sector is the West (W), generating the strongest winds with a speed of 10 km/h and a frequency of 15.63%. The West-Northwest (WNW) sector follows, with a speed of 9.2 km/h and a percentage of 14.22%. Notably, the highest wind speed was recorded during the winter season.
- Spring: In spring, the wind rose also shows a dominance of the West (W), with a frequency of 12.45% and an average speed of 7.1 km/h. The second most frequent direction is the West-Northwest (WNW), with a speed of 7.5 km/h and a frequency of 13.16%. Wind speeds appear to be relatively balanced, indicating a season without significant extreme events.
- Summer: The analysis of summer wind patterns reveals a clear dominance of the North-Northeast (NNE) sector, with a speed of 8.7 km/h and a frequency of 13.38%. However, the East (E) sector also shows frequent winds during this season, with a frequency of 11.96% and a speed of 7.6 km/h.

The study of the wind rose in the Skikda region thus highlights seasonal variability in dominant wind directions, with the highest wind intensity observed during winter.

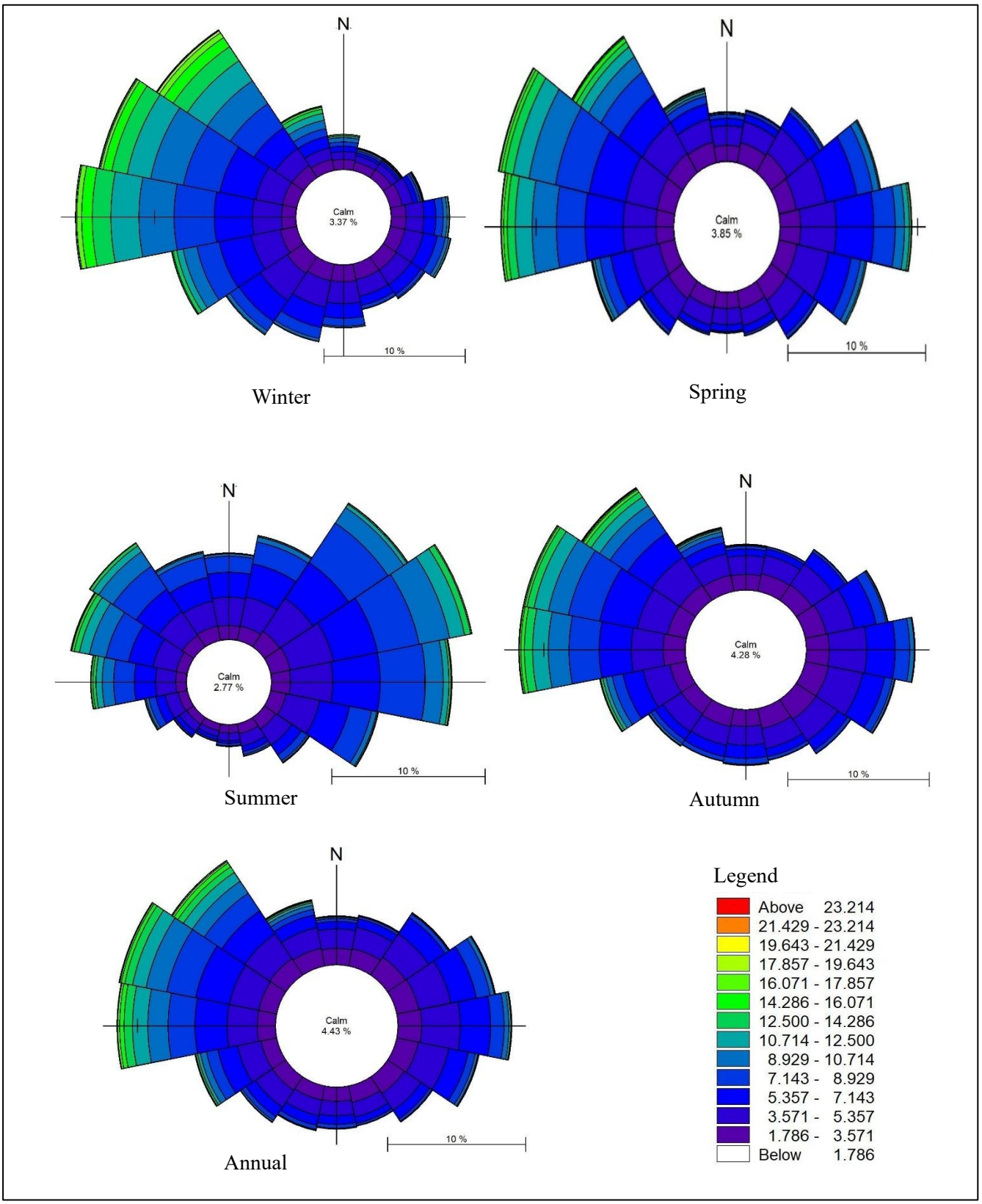


Figure 11: Annual and Seasonal Wind Roses of Skikda (1992-2022) (Source: Wave Climate).

## II.5 Oceanographic Framework

### II.5.1 Wave

In all coastal zone studies, the analysis of wave is particularly important due to its direct or indirect outcomes on shoreline mobility. The analysis of wave characteristics in the Skikda region was carried out using data from the online database Wave Climate (www.waveclimate.com), covering the period from 1992 to 2022. Information on wave height, period, and direction is graphically represented in Figure 12.

The annual wave rose (Figure 12) reveals that two predominant wave directions are observed in the Skikda region: North-Northwest (NNW), accounting for approximately 23.24% of recorded waves, and West-Northwest (WNW), with an occurrence rate of 15.88%.

The seasonal wave rose (Figure 12) indicates:

- Autumn: The autumn wave rose indicates the dominance of two main directions with varying intensities: North-Northwest (NNW), with a frequency of 22.35%, and West-Northwest (WNW), appearing in 17.06% of recorded cases.
- Winter: The winter wave analysis highlights the prevalence of two sectors, though with different intensities. The most dominant direction is North-Northwest (NNW), occurring 23.53% of the time, followed by West-Northwest (WNW), which accounts for 15.59% of recorded waves.
- Spring: The spring wave rose analysis also reveals two predominant directions: North-Northwest (NNW), representing 22.56% of the recorded waves, and West-Northwest (WNW), which appears in approximately 17.18% of cases.
- Summer: During summer, the wave analysis shows the dominance of two different directions: North-Northwest (NNW), which is the most frequent at 21.67%, followed by East-Northeast (ENE), appearing with a frequency of 19.58%.

The wave analysis in the Skikda region thus indicates a strong predominance of the North-Northwest (NNW) direction throughout the year, with the highest wave intensity recorded during the summer season.

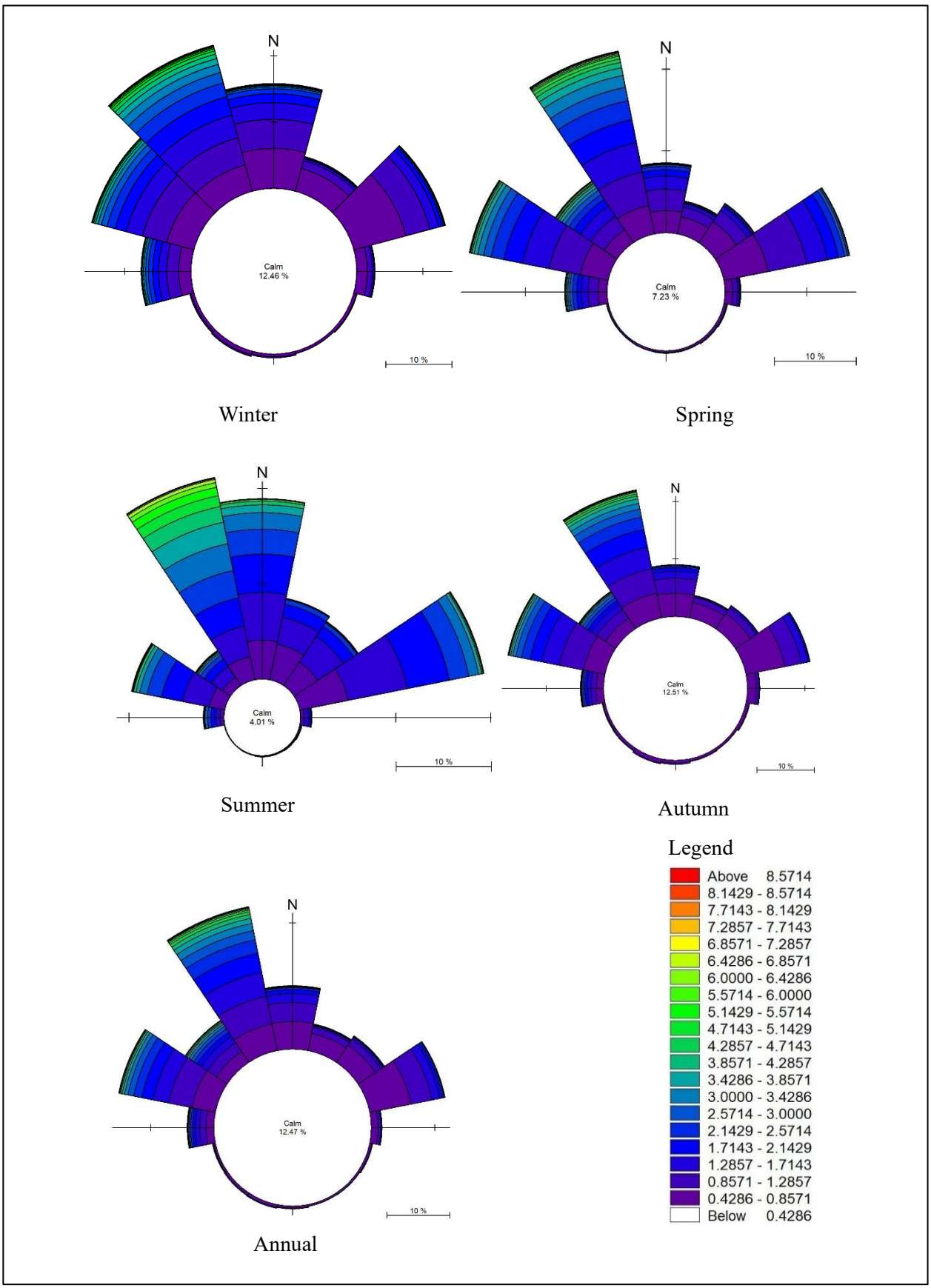


Figure 12: Annual and Seasonal Wave Roses of Skikda (1992-2022) (Source: Wave Climate).

### II.5.2 Tides

Skikda, a coastal city in northeastern Algeria, experiences semi-diurnal tides, meaning it has two high tides and two low tides per day. These tides are mainly influenced by the gravitational forces of the Moon and the Sun, as well as the Earth's rotation. The tidal range in Skikda is relatively small, which is typical for the Mediterranean Sea, where tides are generally less pronounced compared to open ocean systems.

Tidal patterns in Skikda follow a predictable rhythm. High tides occur approximately every 12 hours and 25 minutes, and according to the online database Tide Forecast (Tide-Forecast.com), the height of high tides can reach up to 0.5m. Similarly, low tides follow the same semi-diurnal cycle, with the lowest tides receding to around 0.2m, according to data from Tides For Fishing (Tides4Fishing.com).

# Chapter III: Spatiotemporal Shoreline Evolution

# III.1 Introduction

The coastline represents a dynamic interface between land and sea, subject to natural and human-induced processes that continually alter its morphology. Among these processes, coastal erosion has become a major global concern, effecting coastal ecosystems, infrastructures, and economic activities.

The Bay of Skikda, located on the northeastern coast of Algeria, is a strategic area due to its port, tourism, and industrial activities. Over the past decades, this region has experienced significant shoreline changes, resulting from both natural dynamics (waves, marine currents, extreme weather events) and human interventions (port construction, coastal urbanization, shoreline developments).

In this context, analyzing shoreline evolution in Skikda is essential to understand the extent of erosion, identify vulnerable zones, and propose appropriate management strategies. This study intends to analyze the shoreline changes in the Bay of Skikda over a 30-year period (1993–2023), using Landsat satellite data and spatial analysis tools such as the Digital Shoreline Analysis System (DSAS).

# III.2 Methodology

## III.2.1 Data collection

For this study, the primary data required includes the shoreline and a reference baseline; all additional parameters will be computed using the Digital Shoreline Analysis System (DSAS).

**Baseline**

The baseline, used as a reference for DSAS, is essential for generating transects and for the statistical calculation of shoreline evolution. It is digitized as a polyline and positioned at a maximum distance of 1000m from the shorelines in order to facilitate the visualization of transects on the maps.

**transects**

The transects were generated using the DSAS dialog window. For this study, the spacing between transects was set at 250m, resulting in 674 transects with a maximum length of 1000m.

**Shorelines**

In order to effectively monitor the evolution of the shoreline of Skikda Bay, four shoreline positions were extracted at regular 10-year intervals, corresponding to the years 1993, 2003, 2013, and 2023. These shorelines were generated from Landsat 5, 7, and 8 satellite images using Python scripts developed on the Google Earth Engine platform, ensuring a precise and consistent extraction of the coastal lines. This choice was motivated by the desire to observe long-term evolution trends, reduce the effects of seasonal variations, adapt to the availability of satellite images, and capture the significant impacts of natural and anthropogenic dynamics on coastal morphology. Using a fixed 10-year period between shoreline positions was also favored to ensure consistency in the temporal analysis, facilitate statistical processing, minimize biases related to variable intervals, and adhere to methodological standards in scientific studies. This constant time step thus makes it possible to better represent major shoreline evolution trends,

independently of seasonal or exceptional variations, and to guarantee the reliability of the results obtained.

Table 3: Shorelines resolution.

| Shoreline Period (Year) | 1993 | 2003 | 2013 | 2023 |
|---|---|---|---|---|
| Resolution (m) | 30 | 30 | 30 | 30 |

### III.2.2 Shoreline uncertainty

The uncertainty associated with these shoreline positions was estimated using the root sum of squares (RSS) method, following the guidelines provided by the "Guide to the Expression of Uncertainty in Measurement" and error sources were identified and total positional uncertainty was calculated following methods adapted from **(Hapke et al., 2011)**, who outlined the principal components affecting shoreline mapping accuracy in historical satellite and aerial datasets.

Equation 2

$$Unc = \sqrt{Es^2 + Etd^2 + Ed^2 + Er^2 + Ep^2}$$

The uncertainty of each shoreline position is presented in the following table

Table 4: Estimation of the uncertainty associated with each shoreline data source.

| Error Estimation (m) | 1993 | 2003 | 2013 | 2023 |
|---|---|---|---|---|
| Seasonal error (Es) | 5 | 5 | 5 | 5 |
| Tidal fluctuation (Etd) | 0,5 | 0,5 | 0,5 | 0,5 |
| Georeferencing error (Er) | 10 | 7 | 5 | 5 |
| Digitization error (Ed) | 3 | 3 | 3 | 3 |
| Pixel error (Ep) | 0,25 | 0,25 | 0,15 | 0,15 |
| Total error (Et) | 11,59 | 9,13 | 7,7 | 7,7 |

The total uncertainty is calculated using the following formula

Equation 3

$$Total\ Uncertainty = \sqrt{\frac{Unc_1^2 + Unc_2^2 + \cdots + Unc_n^2}{n}}$$

With n is the number of shorelines

Table 5: Total Shoreline Change Uncertainty Over Time Periods.

| Shoreline Period (year) | 1993 To 2003 | 2003 To 2013 | 2013 To 2023 | 1993 To 2023 |
|---|---|---|---|---|
| Total uncertainty (m) | 10.4 | 8.4 | 7.7 | 9.2 |

In this case study, we will analyze the combined shorelines from 1993 to 2023.

## III.3 Results of the shoreline evolution

To analyze shoreline dynamics over the study period, two key indicators were calculated: the End Point Rate (EPR) and Net Shoreline Movement (NSM). The EPR provides the rate of shoreline change between the oldest and most recent shoreline positions, while the NSM represents the total distance between these two shorelines, measured in meters.

An uncertainty value was also calculated using the root sum of squares (RSS) method for both indicators to account for positional errors in shoreline delineation.

**EPR uncertainty**

The EPR uncertainty is 0.61m/year and it is calculated using the following formula

$$E_{EPR} = \frac{\sqrt{Unc_1^2 + Unc_2^2 + \cdots + Unc_n^2}}{Date_n - Date_1}$$

**NSM uncertainty**

The NSM uncertainty is 18.33 m and it is calculated using the following formula

$$E_{NSM} = \sqrt{Unc_1^2 + Unc_2^2 + \cdots + Unc_n^2}$$

The following maps and graphs illustrate the spatial distribution of these shoreline changes and present the detailed results for each transect across the study area.

**Results of the EPR analysis**

**Interpretation**

The evolution of the shoreline between 1993 and 2023 shows contrasting coastal dynamics between the western and eastern sectors, highlighting the significant influence of coastal environments and processes of erosion or accretion see Figures 13 and 17.

**Eastern Sector: Sandy Coastline with Evolving Beaches**

The eastern sector (Figures 14 and 18) is largely composed of sandy beaches, making it much more vulnerable to erosion and coastal dynamics. The maps reveal higher Net Shoreline Movement (NSM) values in this area, indicating both significant shoreline retreat and, in some cases, localized accretion phases.

This sector shows higher End Point Rate (EPR) values. Several zones exhibit clear shoreline retreat, particularly during periods likely marked by storms or rising sea levels. This retreat can reach several meters, highlighting pronounced coastal erosion linked to the natural mobility of beaches and the absence of effective coastal protection structures in certain locations.

However, some parts of the eastern sector also show signs of accretion or stabilization, sometimes associated with human interventions such as artificial beach nourishment or the construction of coastal defense structures.

**Western Sector: Predominantly Rocky and Stable Coastline**

In contrast, the western sector (Figures 15 and 19) consists largely of rocky coasts and displays

low shoreline mobility over the studied period. The resistant nature of the coastal rocks limits the impact of marine dynamics, resulting in low NSM values. Erosion in this area is moderate or even non-existent in many locations.

End Point Rate (EPR) phenomena in this sector are limited, although some short segments may show signs of localized retreat, often due to the occasional effect of wave action, weather events, or natural geological faults. Overall, this sector remains relatively stable throughout the 1993–2023 period.

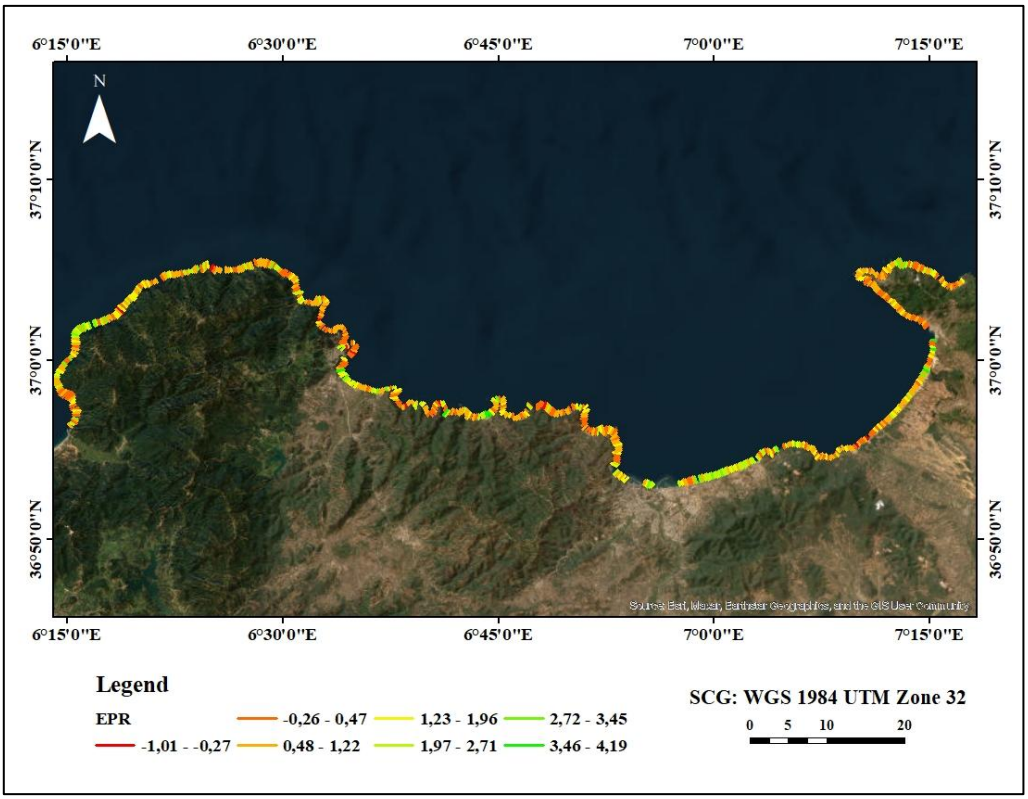


Figure 13: EPR Results Map for the Wilaya of Skikda between 1993 and 2023.

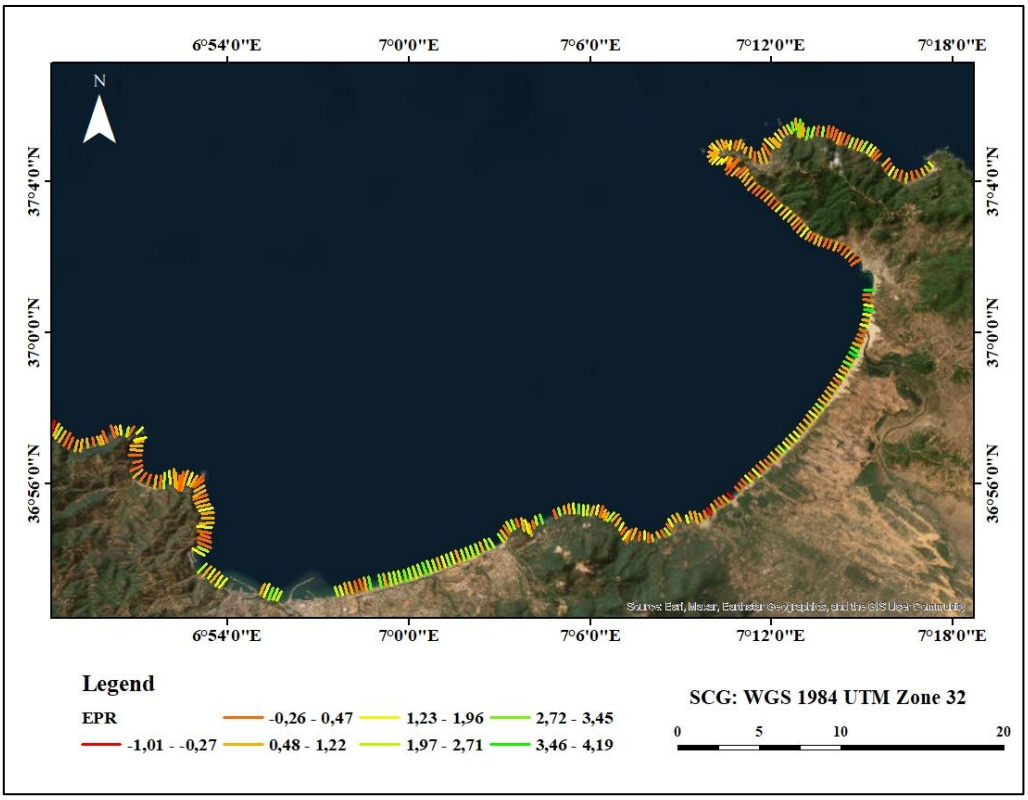


Figure 14: EPR Results Map for the Eastern Part of the Wilaya of Skikda between 1993 and 2023.

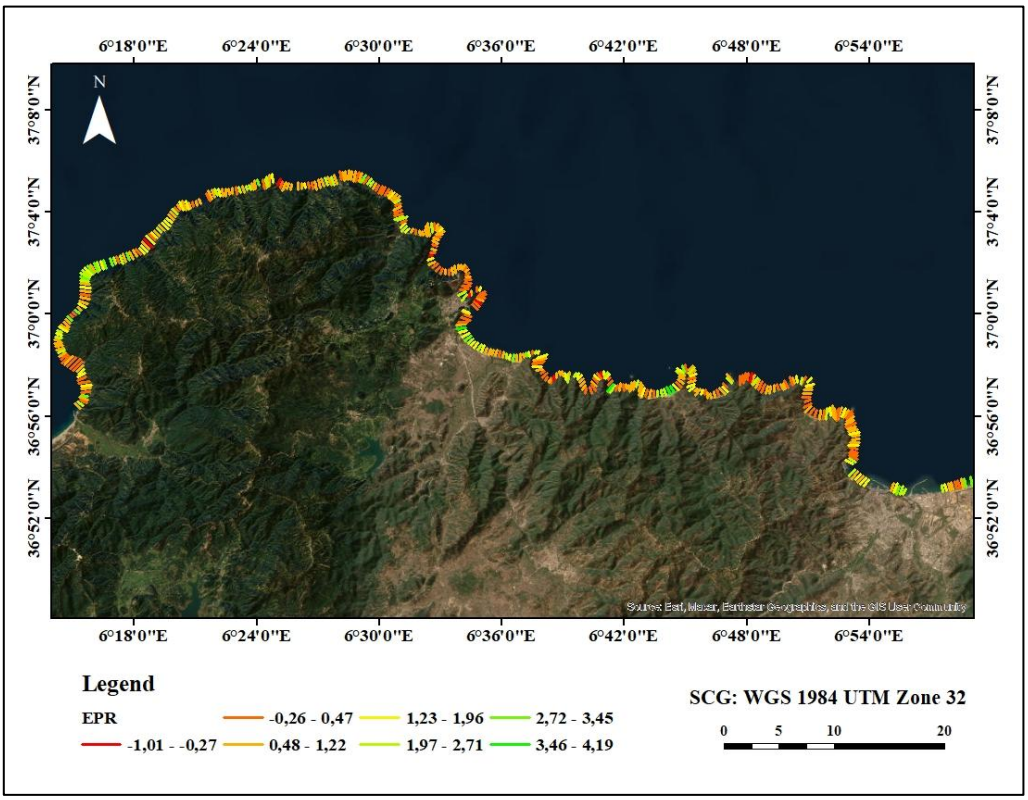


Figure 15: EPR Results Map for the Western Part of the Wilaya of Skikda between 1993 and 2023.

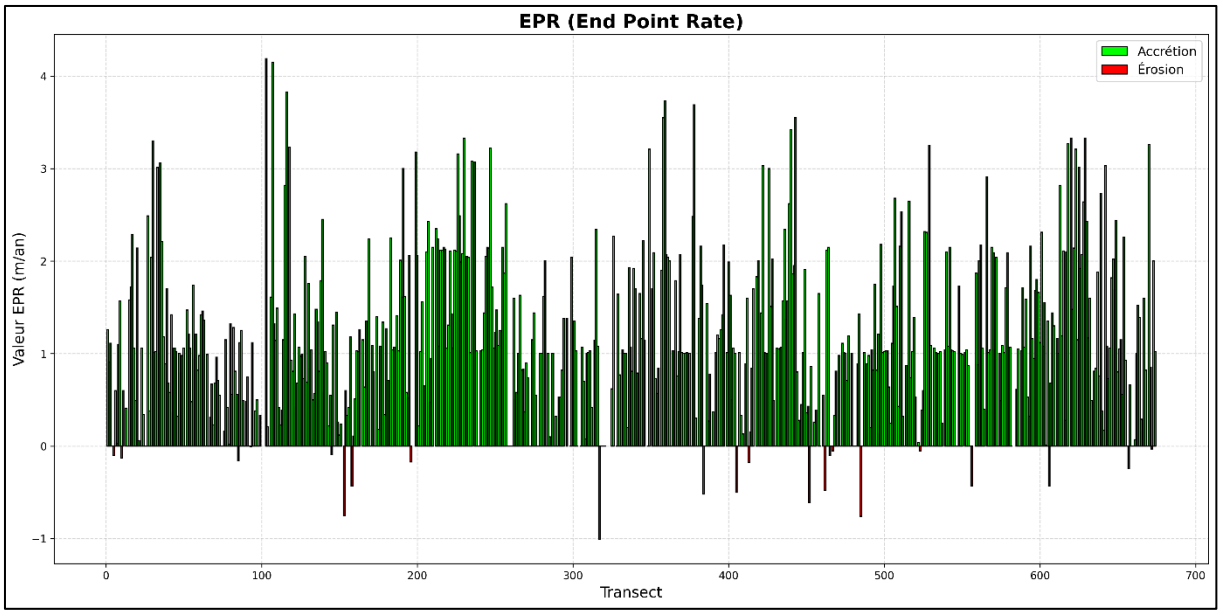


Figure 16: EPR Results Graph for the Wilaya of Skikda between 1993 and 2023.

## Results of the NSM analysis

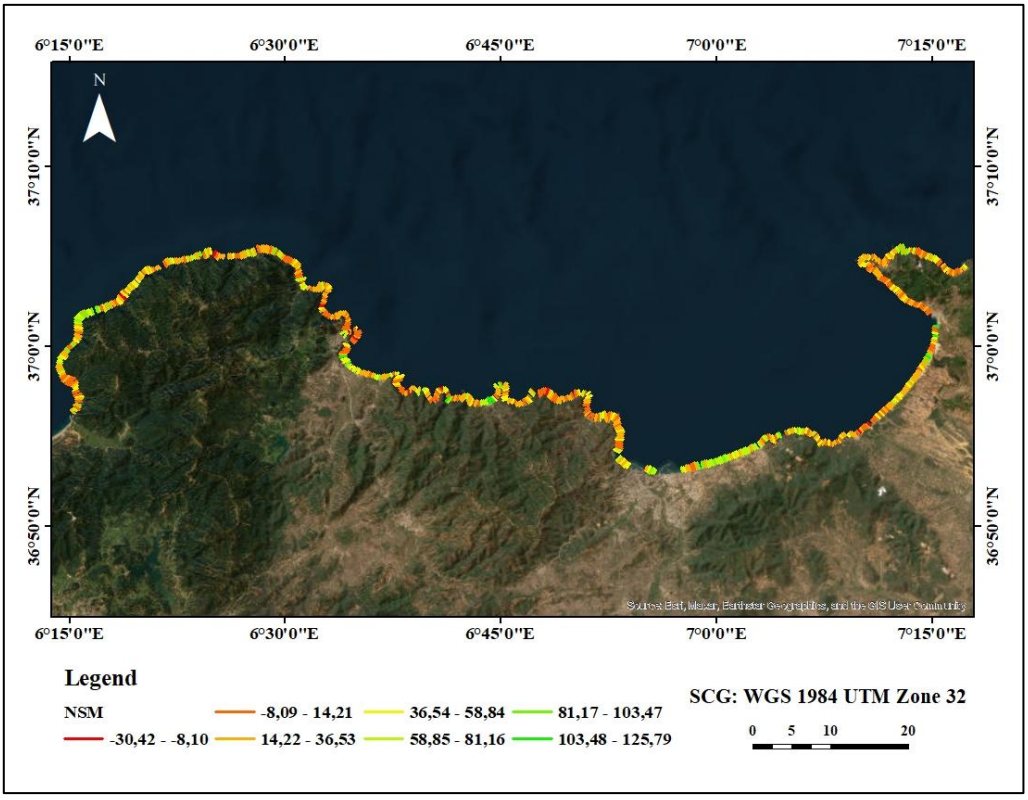


Figure 17: NSM Results Map for the Wilaya of Skikda between 1993 and 2023.

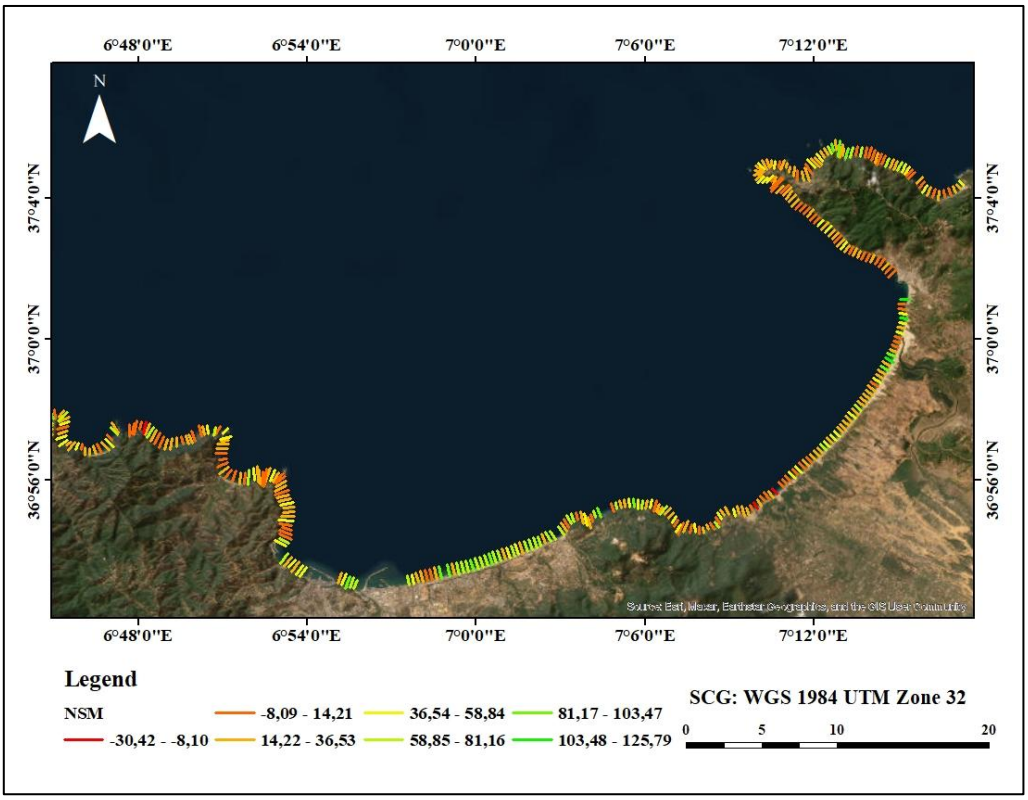


Figure 18: NSM Results Map for the Eastern Part of the Wilaya of Skikda between 1993 and 2023.

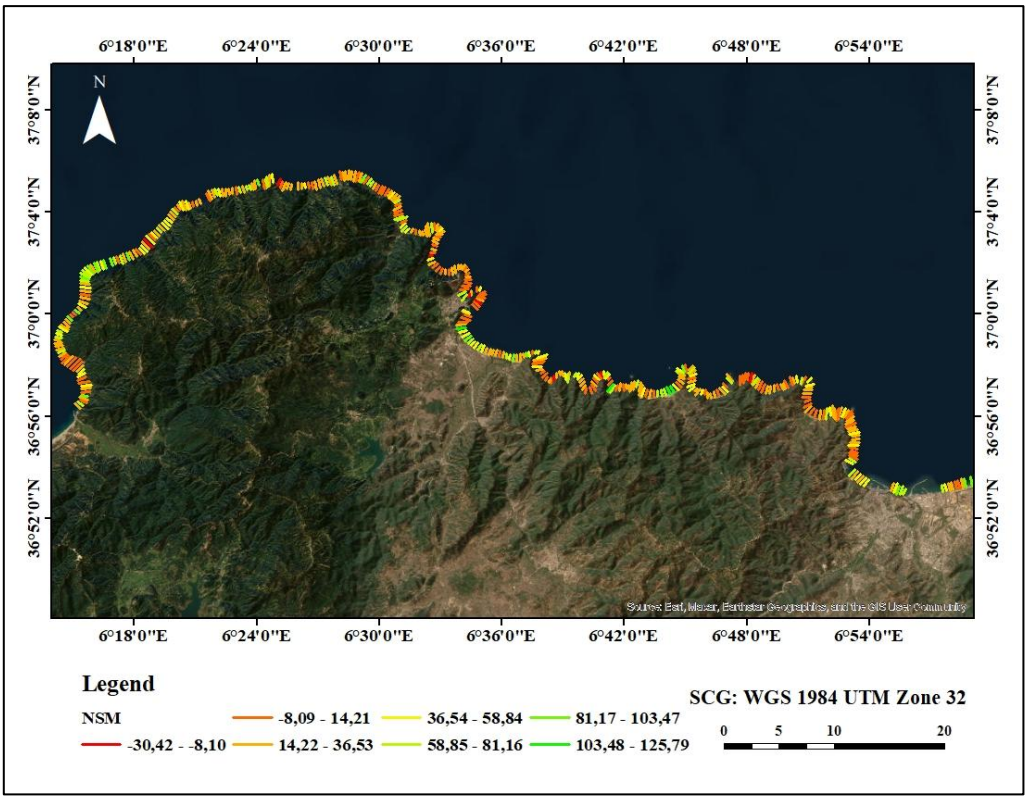


Figure 19: NSM Results Map for the Western Part of the Wilaya of Skikda between 1993 and 2023.

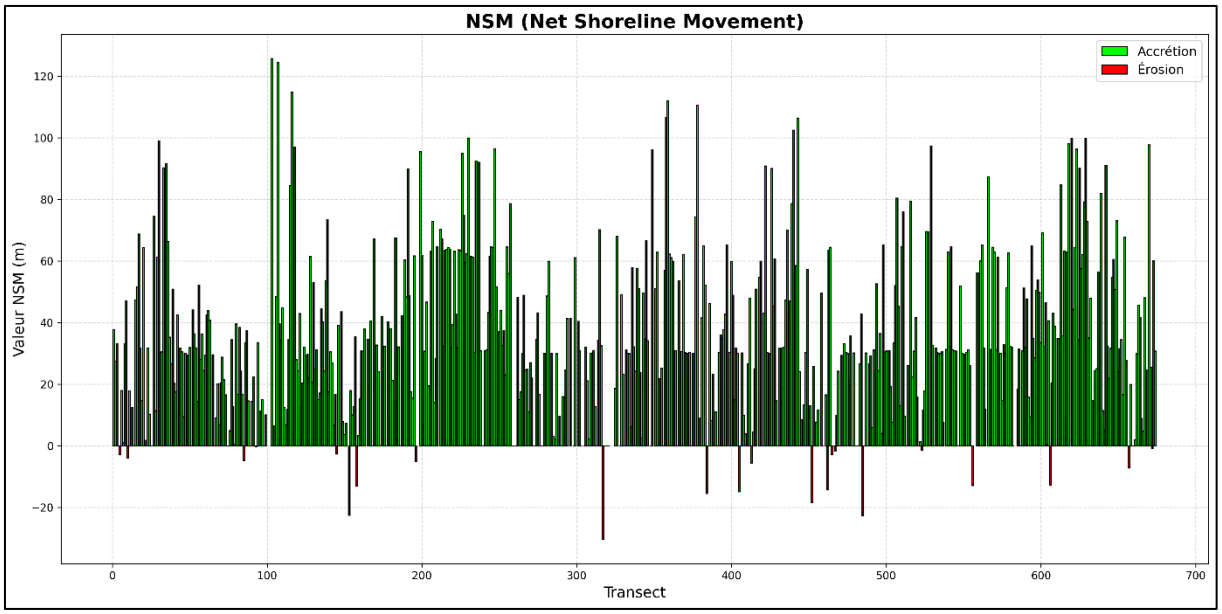


Figure 20: NSM Results Graph for the Wilaya of Skikda between 1993 and 2023.

To better analyze coastal dynamics, shoreline evolution was analyzed using the End Point Rate (EPR) indicator for three successive periods: 1993–2003, 2003–2013, and 2013–2023. The map displays these results as color-coded segments between each shoreline pair, allowing for a spatial visualization of erosion zones and accretion zones over time.

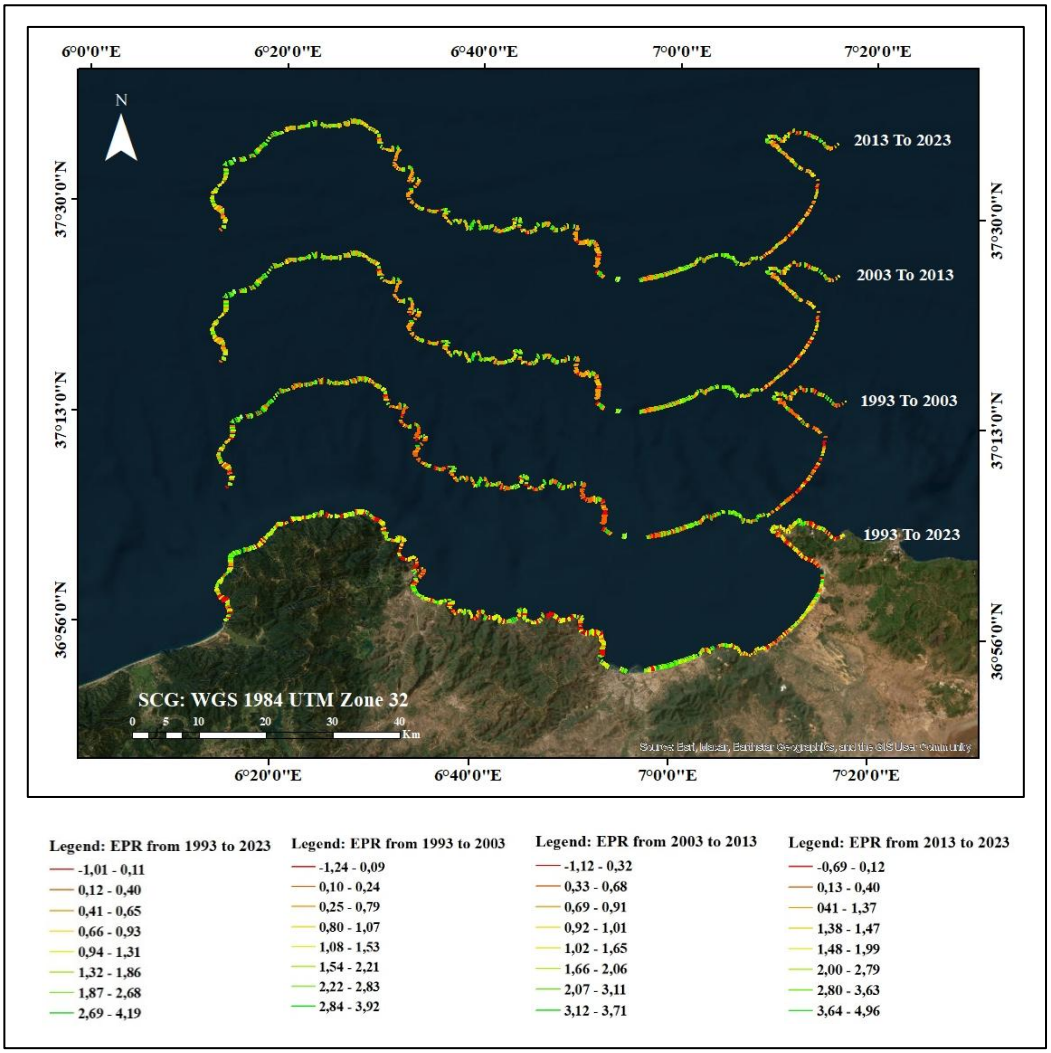


Figure 21: Spatial Evolution of Coastal Erosion and Accretion by Periods.

## III.4 The Shoreline Evolution Forecast

To analyze the potential future changes of the shoreline, two forecast scenarios were conducted using the Digital Shoreline Analysis System (DSAS): a 10-year and a 20-year forecast. These forecasts were carried out to estimate how the shoreline might evolve over the selected timeframes. For both cases, the previously generated forecast line features were used as baselines within DSAS. The primary statistical methods applied for the analysis were the End Point Rate (EPR) and the Net Shoreline Movement (NSM), allowing for a quantitative comparison of shoreline displacement between the forecast periods and the baseline condition.

### III.4.1 Results of the Shoreline Evolution Forecast for 10 Years

**Results of the EPR analysis**

**Interpretation**

**Eastern Sector**

In the forecast period (2023–2033) shown in Figures 23 and 27, the eastern sector, composed mainly of sandy beaches, shows a continued trend of shoreline retreat. The maps indicate moderate to high Net Shoreline Movement (NSM) values and more active End Point Rate

(EPR) across several zones. These results point to ongoing erosion, particularly in areas that are unprotected or exposed to prevailing wave action.

The sandy composition of this sector makes it especially vulnerable to coastal processes, and forecasts suggest that erosion could continue at a steady pace over the next decade. However, a few localized stretches may experience slight accretion or stabilization, possibly due to sediment redistribution or minor human interventions. Despite these exceptions, shoreline retreat remains the dominant trend in the eastern sector for the 2023–2033 period.

**Western Sector**

In contrast, the western sector shown in Figures 24 and 28, characterized by its predominantly rocky shoreline, continues to show strong stability. The forecast maps reflect very limited changes, with consistently low NSM values and minimal EPR variations. This indicates that shoreline mobility remains negligible, as the resistant nature of the rocky coast effectively absorbs marine energy and reduces the likelihood of erosion.

Although a few localized areas may display slight retreat, these changes appear to be minor and likely the result of isolated influences such as wave concentration in specific inlets or small-scale geological weaknesses. Overall, the sector remains remarkably stable, consistent with its behavior during the 1993–2023 historical period.

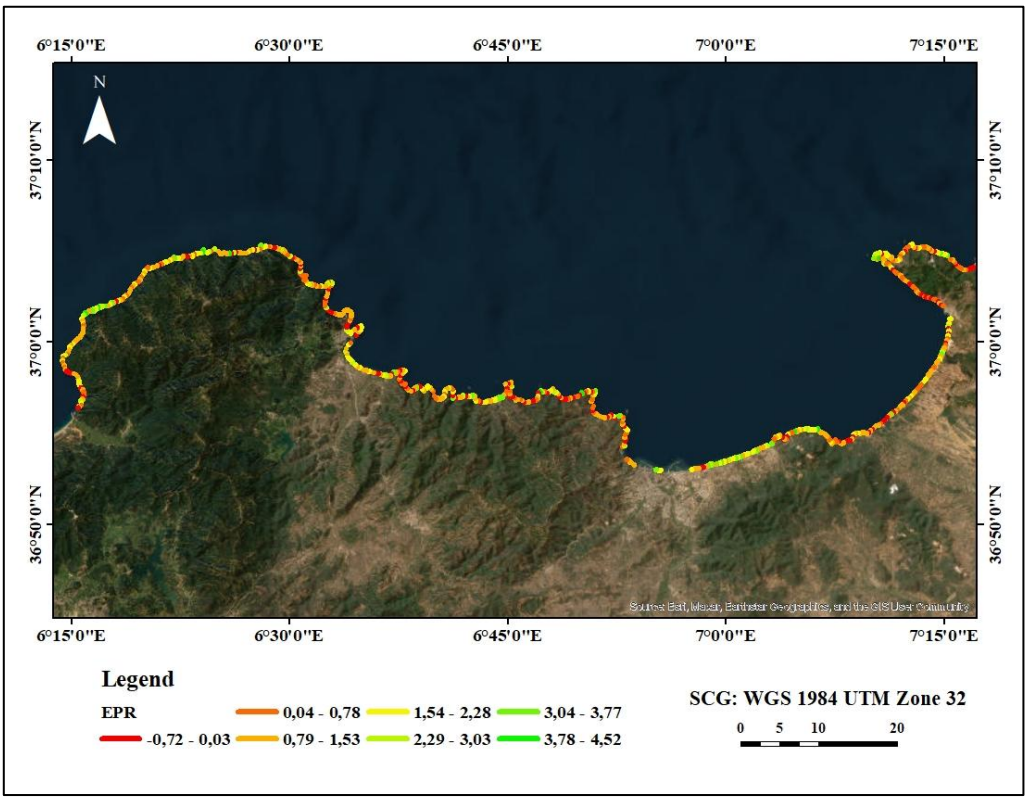


Figure 22: EPR Results Map of the 10-Year Shoreline Evolution Forecast for the Wilaya of Skikda.

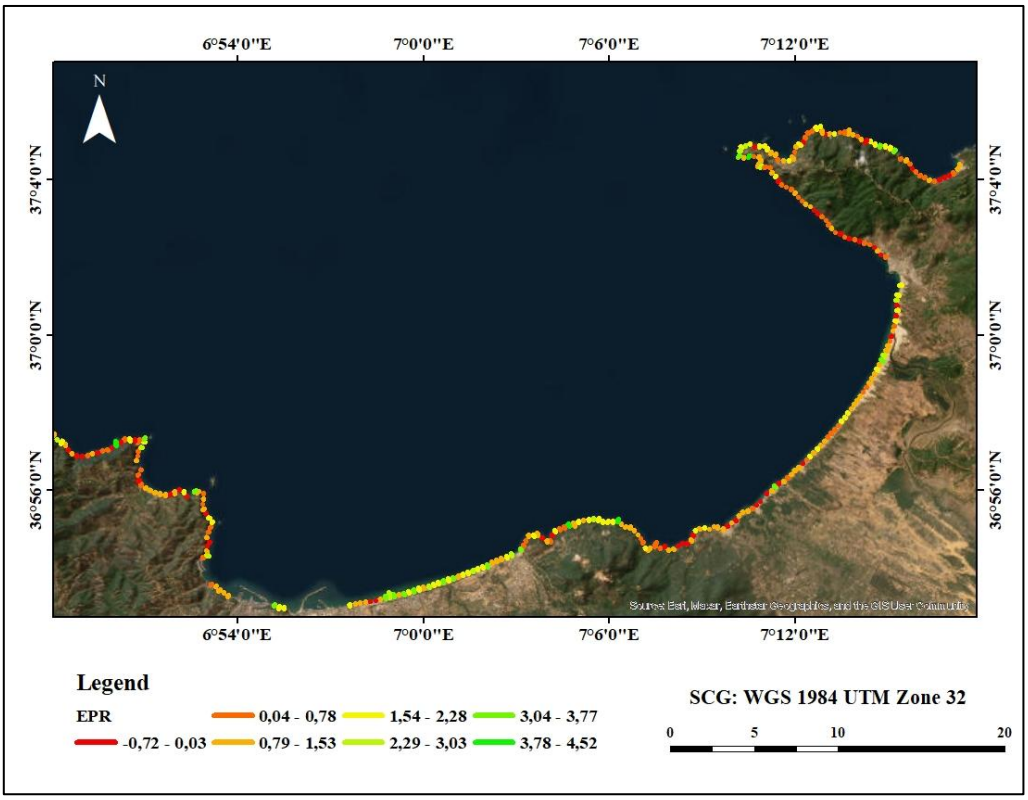


Figure 23: EPR Results Map of the 10-Year Shoreline Evolution Forecast for the Eastern Part of the Wilaya of Skikda.

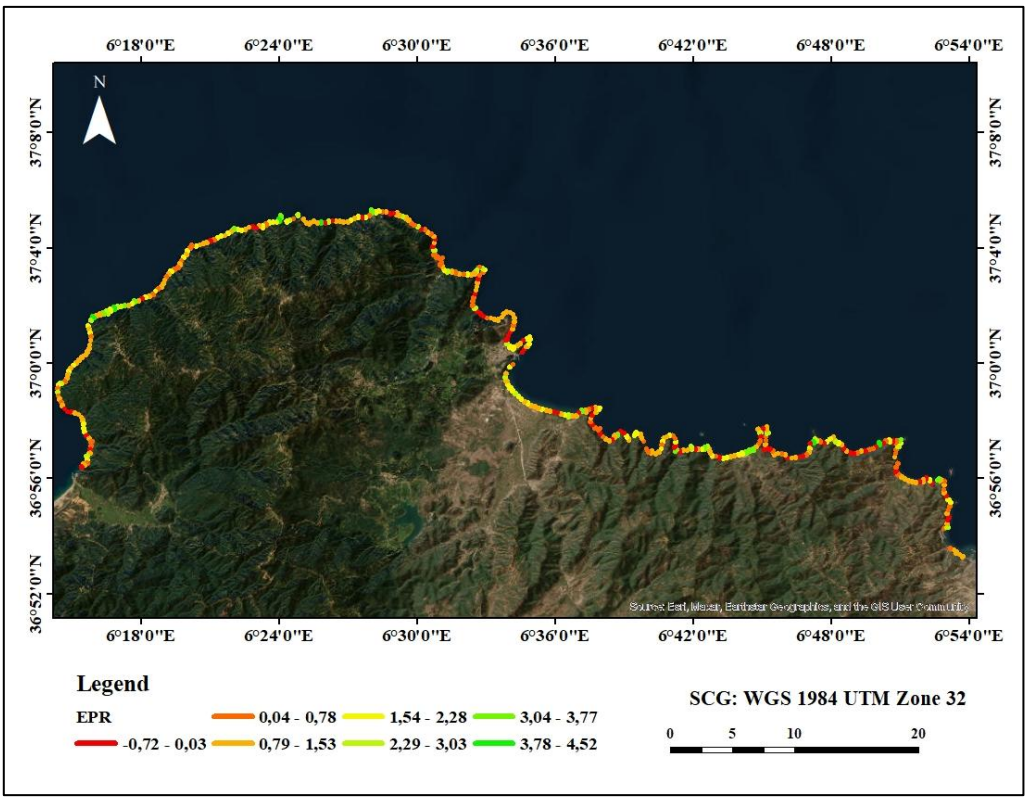


Figure 24: EPR Results Map of the 10-Year Shoreline Evolution Forecast for the Western Part of the Wilaya of Skikda.

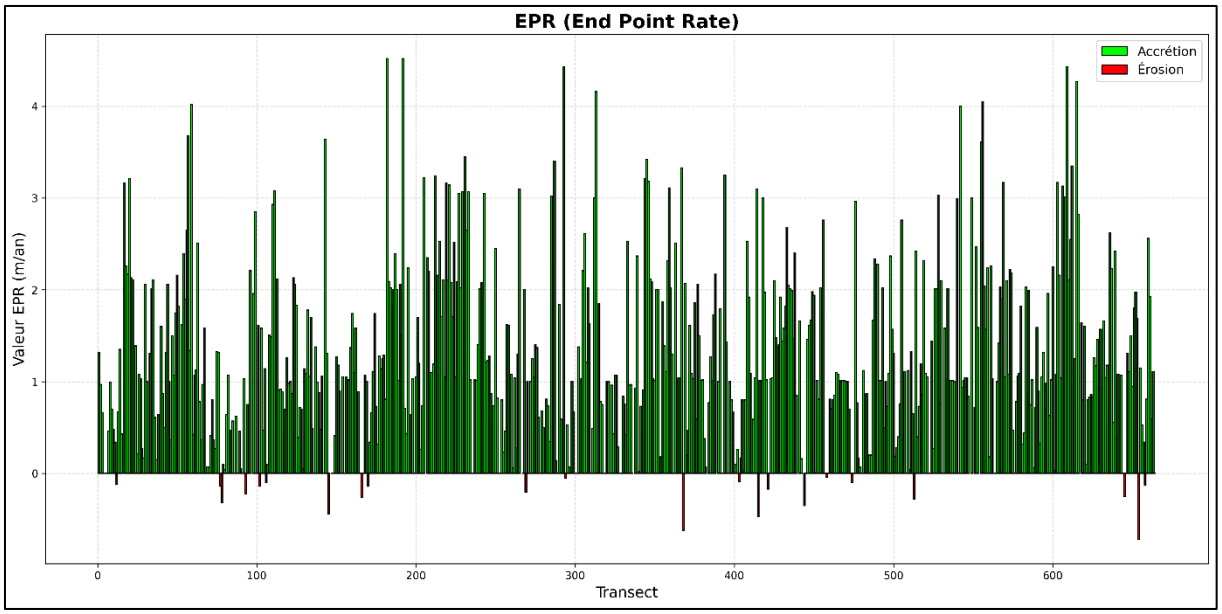


Figure 25: EPR Results Graph of the 10-Year Shoreline Evolution Forecast for the Wilaya of Skikda.

## Results of the NSM analysis

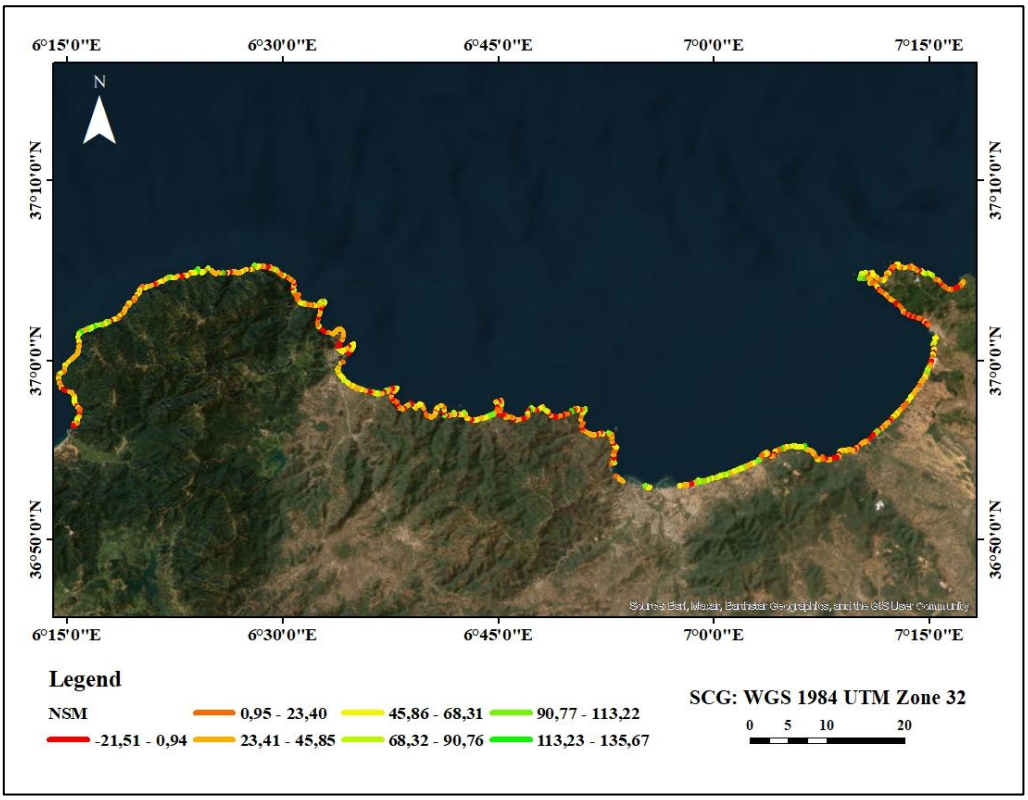


Figure 26: NSM Results Map of the 10-Year Shoreline Evolution Forecast for the Wilaya of Skikda.

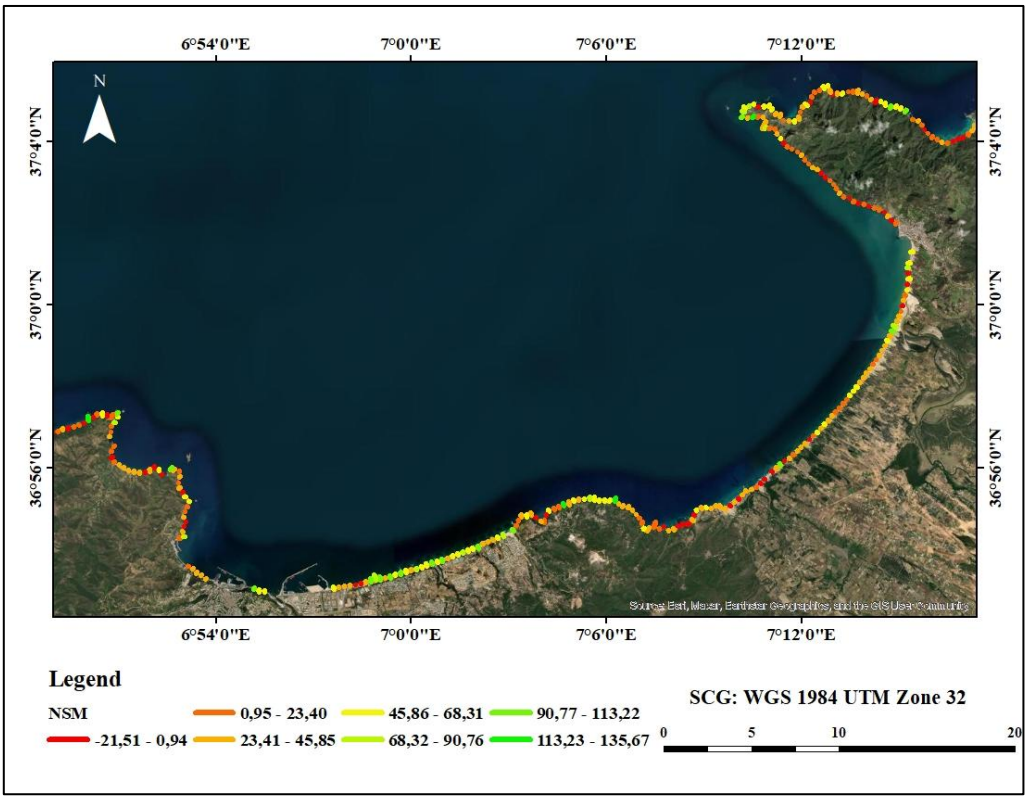


Figure 27: NSM Results Map of the 10-Year Shoreline Evolution Forecast for the Eastern Part of the Wilaya of Skikda.

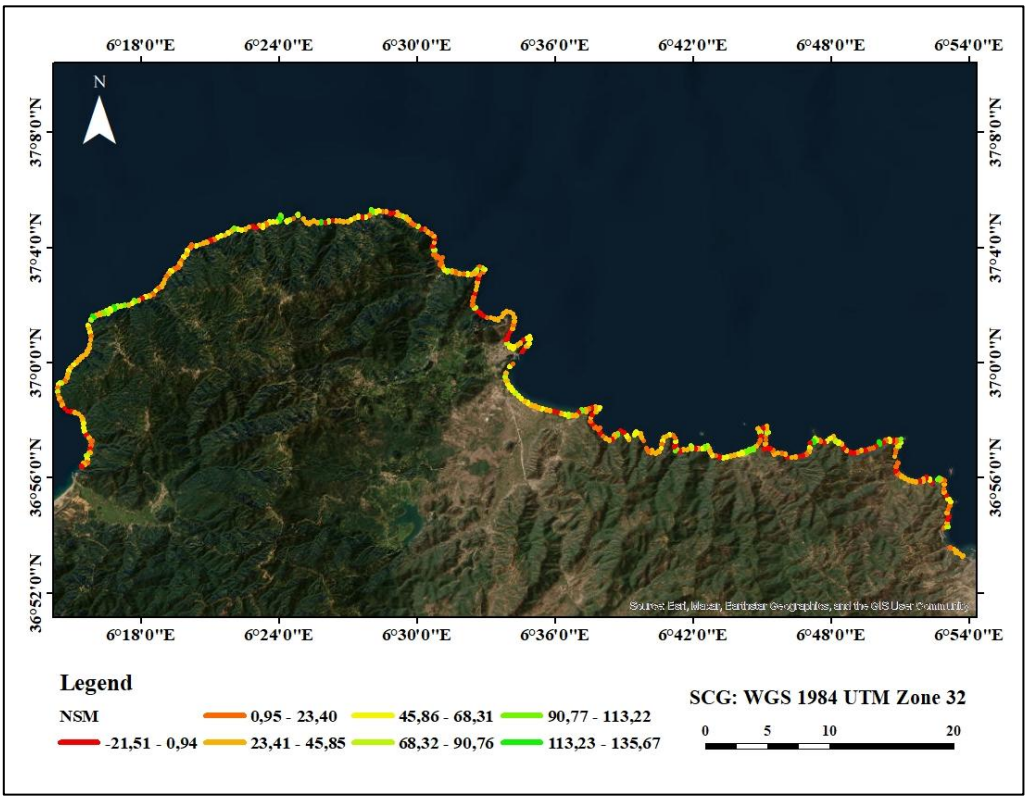


Figure 28: NSM Results Map of the 10-Year Shoreline Evolution Forecast for the Western Part of the Wilaya of Skikda.

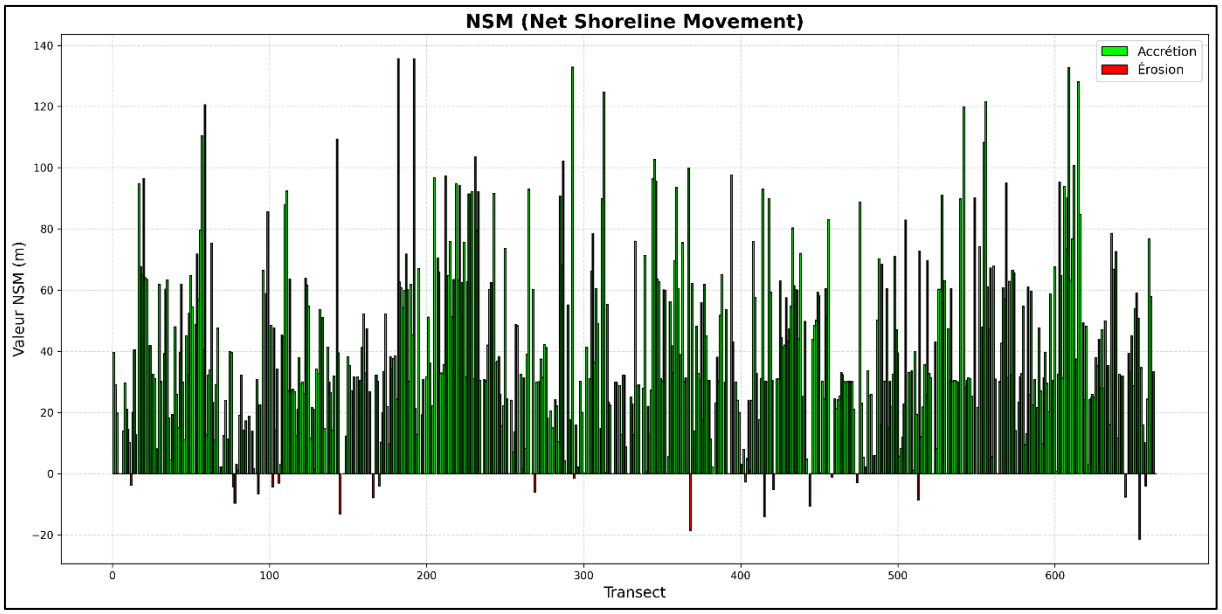


Figure 29: NSM Results Graph of the 10-Year Shoreline Evolution Forecast for the Wilaya of Skikda.

### III.4.2 Shoreline Evolution Forecast for 20 Years

**Results of the EPR analysis**

**Interpretation**

**Eastern Sector (Accelerated Erosion)**

Over a 20-year horizon (2023–2043), the eastern sector (Figures 31 and 35) shows a more intensified pattern of retreat. The maps reveal increasing Net Shoreline Movement (NSM) values and more significant End Point Rate (EPR) trends, indicating that erosion processes are likely to accelerate without substantial intervention. The retreat becomes more widespread, particularly along unprotected beaches and sediment-rich stretches of the coastline.

Some areas may show signs of temporary accretion due to natural sediment transport or the effects of local protective measures, but these are relatively limited in extent. Overall, the eastern sector is projected to continue losing ground at a growing rate, making it a priority for future coastal management and adaptation efforts.

**Western Sector (Long-Term Stability)**

In contrast, the 20-year forecast reinforces the long-term stability of the western sector (Figures 32 and 36). NSM values remain consistently low, and EPR indicates very little shoreline displacement, even over the extended timeframe. The rocky structure of the coast continues to offer natural protection, limiting the influence of waves and reducing erosion risks.

Where changes are projected, they remain minimal and highly localized, possibly linked to occasional storm effects or small-scale geological variations. Overall, the western sector is expected to maintain its current form with very limited shoreline change between 2023 and 2043.

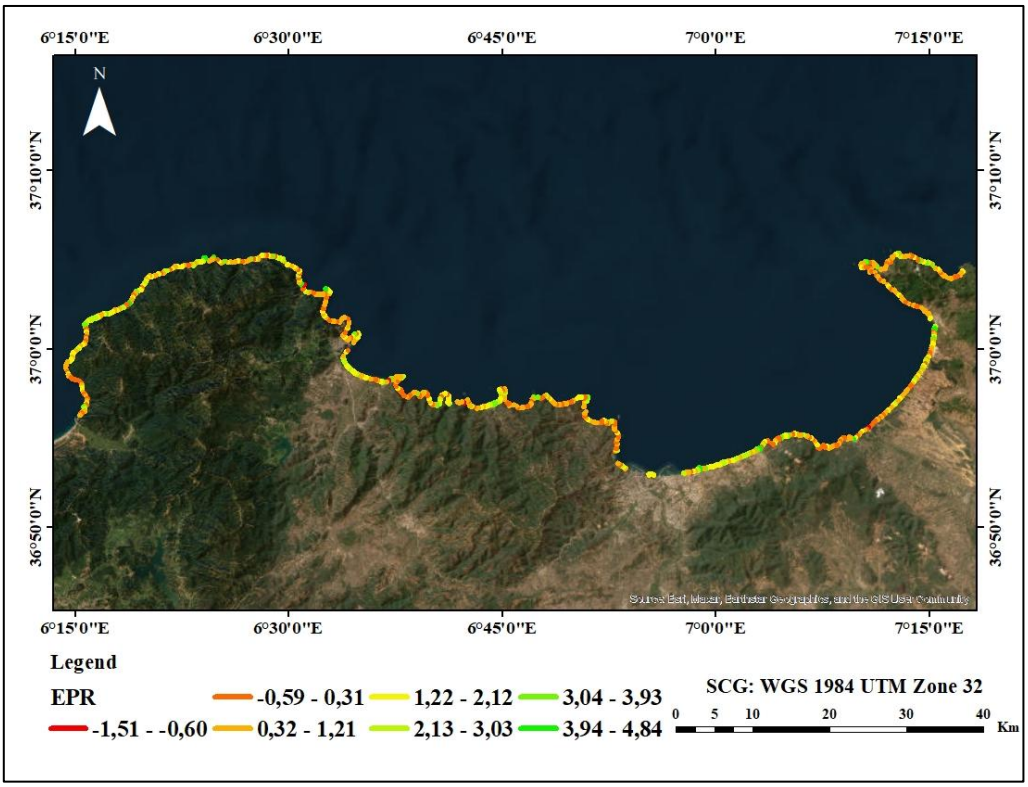


Figure 30: EPR Results Map of the 20-Year Shoreline Evolution Forecast for the Wilaya of Skikda.

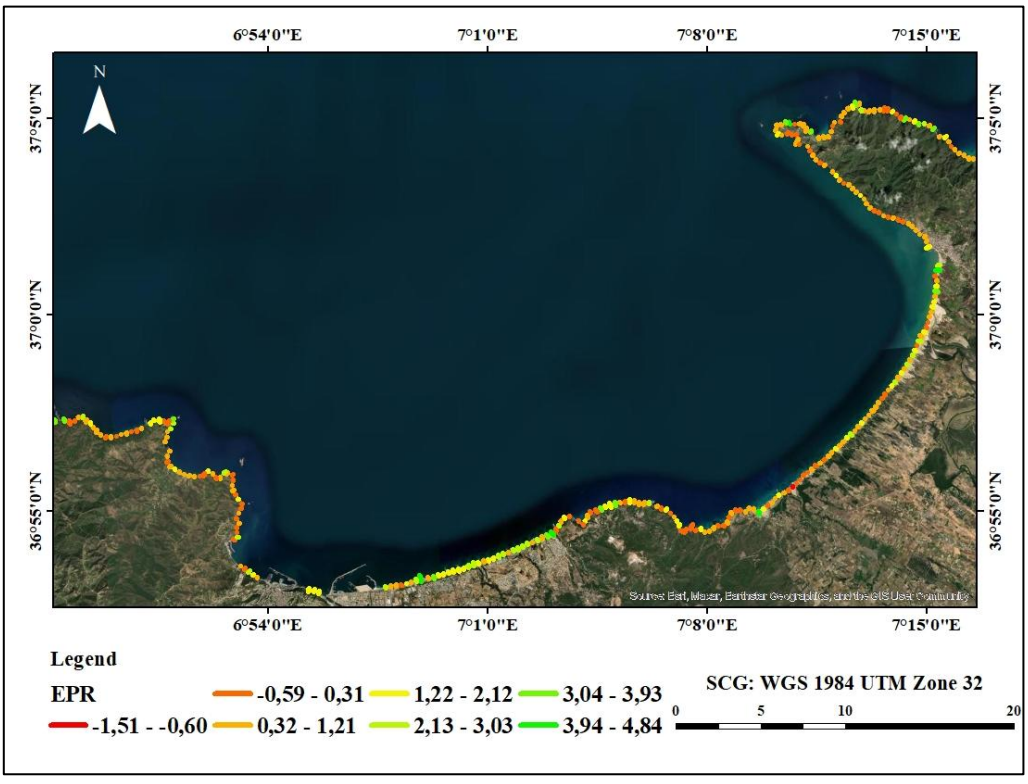


Figure 31: EPR Results Map of the 20-Year Shoreline Evolution Forecast for the Eastern Part of the Wilaya of Skikda.

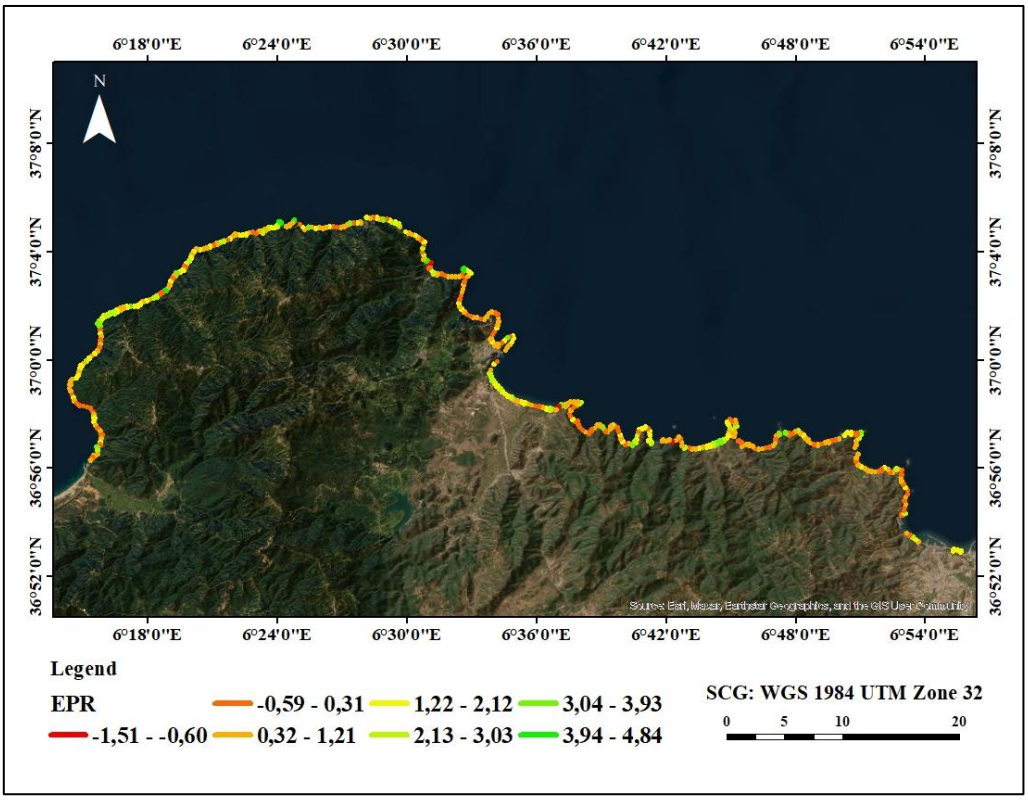


Figure 32: EPR Results Map of the 20-Year Shoreline Evolution Forecast for the Western Part of the Wilaya of Skikda.

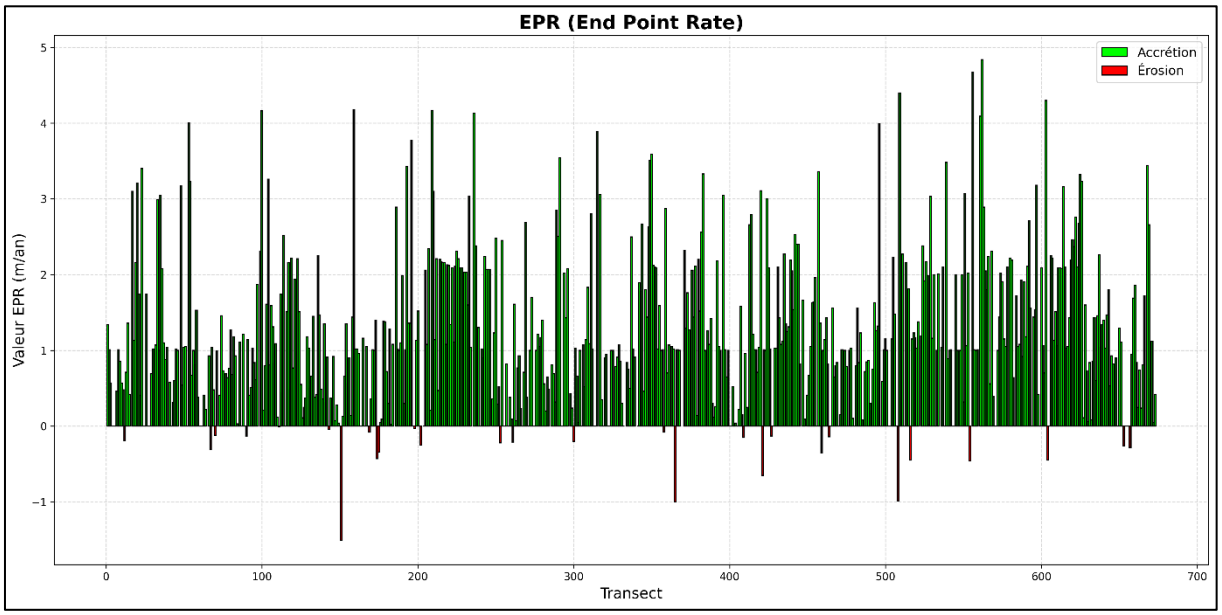


Figure 33: EPR Results Graph of the 20-Year Shoreline Evolution Forecast for the Wilaya of Skikda.

## Results of the NSM analysis

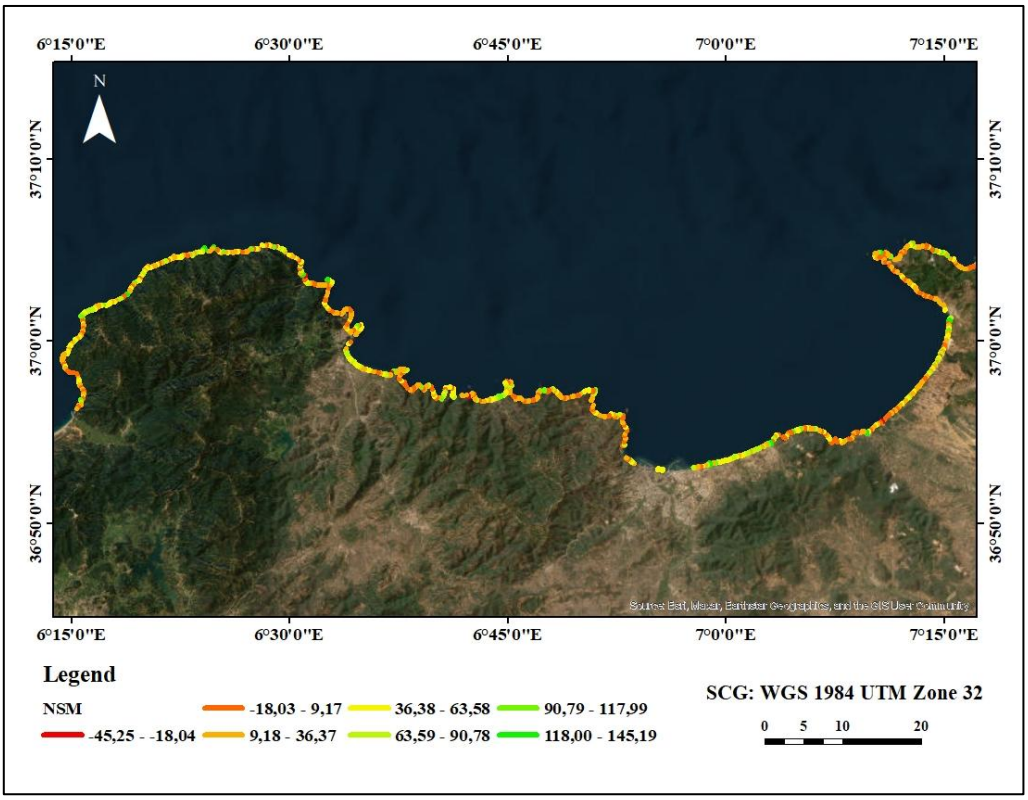


Figure 34: NSM Results Map of the 20-Year Shoreline Evolution Forecast for the Wilaya of Skikda.

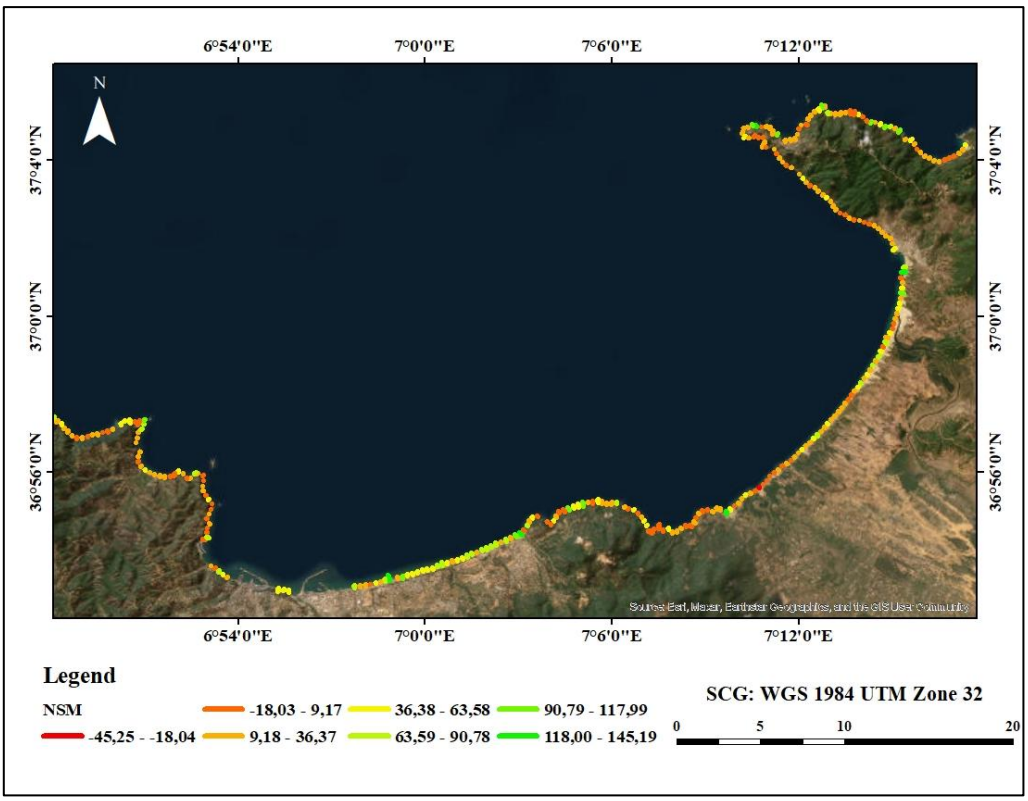


Figure 35: NSM Results Map of the 20-Year Shoreline Evolution Forecast for the Eastern Part of the Wilaya of Skikda.

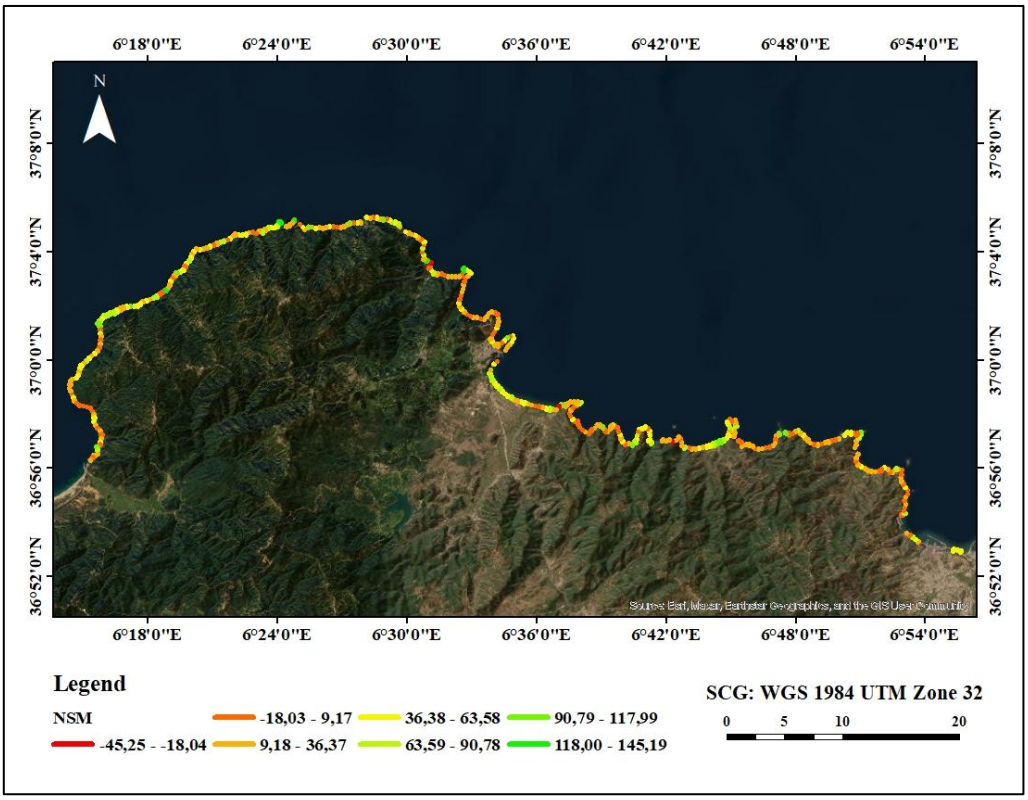


Figure 36: NSM Results Map of the 20-Year Shoreline Evolution Forecast for the Western Part of the Wilaya of Skikda.

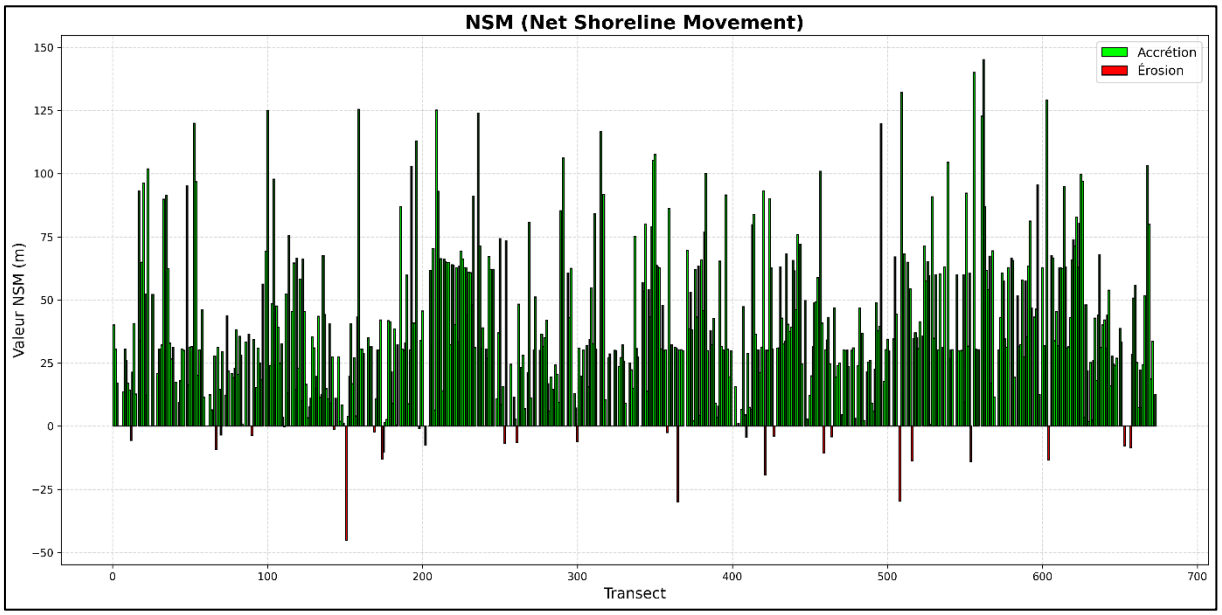


Figure 37: NSM Results Graph of the 20-Year Shoreline Evolution Forecast for the Wilaya of Skikda.

## Conclusion

Looking at the shoreline changes from 1993 all the way through the forecasts for 2033 and 2043, there's a clear difference between how the western and eastern parts of the coast are evolving and it mostly comes down to the nature of the coastline itself.

On the western side, where the coast is mostly rocky, things have stayed very stable. The data from the past 30 years show barely any movement of the shoreline, and the forecasts suggest that this won't change much over the next 10 to 20 years. The rocks in this area do a good job resisting the force of waves and storms, so erosion is minimal and usually only happens in small, isolated spots.

In contrast, the eastern sector, which is made up of sandy beaches, is much more active and vulnerable. Between 1993 and 2023, the shoreline has both retreated and advanced in different places, but overall, it shows more movement than the west. The future forecasts suggest that erosion is likely to continue and even get worse in some areas especially where the beaches are unprotected. There are still some zones where sand is accumulating or where the shoreline seems stable, but these are limited and don't outweigh the broader trend of retreat.

In short, the west is holding steady and doesn't need much attention, while the east is at greater risk and will probably need more careful management in the future to deal with erosion and protect the coast.

# Chapter IV: Extreme Events Analysis

## IV.1 Introduction

The vulnerability of coastal areas to extreme phenomena, such as erosion and marine submersion, is a major concern in the context of climate change and the increasing urbanization of coastal regions. The need to anticipate these events and adapt protective infrastructures is essential to mitigate environmental, economic, and social impacts. Numerical simulations play a key role in this process by helping predict the evolution of risks over different time scales. These models are generally designed to estimate the return levels of extreme events over a defined period, often 100 years, to optimize the design of coastal defense structures. However, these forecasts involve uncertainties that must be accurately quantified, in this context, the use of advanced statistical methods, particularly extreme value theory, proves to be an effective approach for analyzing and characterizing rare and intense events. By combining these tools with oceanographic and meteorological data, it becomes possible to improve the understanding of extreme phenomena and effectively adapt coastal risk management strategies. So, the object of this study is to analyze extreme events affecting the coastline, focusing on modeling approaches and their implications for protecting vulnerable areas.

## IV.2 Extreme Value Theory

Extreme value theory focuses on the exceptional values of an event and seeks to identify trends or estimate extreme quantiles. By definition, these events are rare and located at the tails of the distribution. Often, such observations are considered outliers and are ignored. However, understanding their distribution can be valuable.

In environmental sciences, this applies to phenomena such as rainfall patterns, floods, or heatwaves. To model these events, it is relevant to measure variables such as rainfall amounts, river flow rates, or temperature over a certain period and infer the distribution of extreme values. This helps to better understand their frequency of occurrence and intensity **(VALIQUETTE, 2020).**

In statistics, two main methods are used to define extreme values. The first is the Block Maxima approach, which involves dividing the study period into several blocks and selecting the most extreme value from each block for further analysis. The second method is based on exceedances over a chosen threshold (u) and is known as the Peaks Over Threshold (POT) method.

A disadvantage of the block maxima approach is that it only considers a single maximum within each block. This creates the risks of omitting significant data. The POT method, on the other hand, eliminates this risk by taking all values greater than the selected threshold into consideration **(STANDER, 2015).**

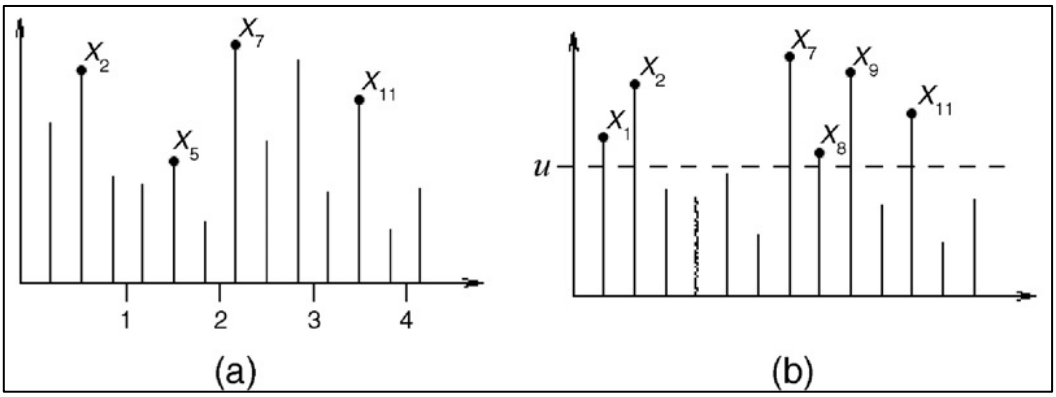


Figure 38: Representative diagram of the Block Maxima and POT methods **(BHATTACHARYYA et al., 2006)**.

### IV.2.1 Analysis of Wave Parameters: HS, TP and D

The analysis of Figure 39, based on recorded data from 1992 to 2022, indicates that the significant wave height (Hs) varies between 0.02 m and 8.76 m, with an average value of 1.28 m. The majority of recorded wave heights fall within the range of 0.5 to 3 m, likely representing the typical wave state in the region. Although extreme events where Hs exceeds 5 m are relatively rare, they have been observed recurrently throughout the analyzed period, highlighting the potential for occasional high-energy wave activity.

Similarly, the recorded wave periods span a relatively broad range, from 2.62 seconds to 13.49 seconds. Most values fall between 4 and 11 seconds, which is characteristic of typical swell conditions in a coastal environment. A high peak period exceeding 10 seconds is generally associated with long-period swells, often originating from distant storms. In contrast, shorter periods below 6 seconds usually indicate locally generated swells or wind-driven seas, reflecting more immediate and short-lived wave activity.

In terms of wave direction, three critical sectors dominate: West-Northwest (WNW), Northwest (NW), and North-Northwest (NNW). These frequently observed directions have a significant impact on the region, influencing coastal erosion and sediment dynamics. The density of recorded data suggests a notable seasonal and interannual variability, which may indicate shifting climatic patterns or long-term changes in wave dynamics.

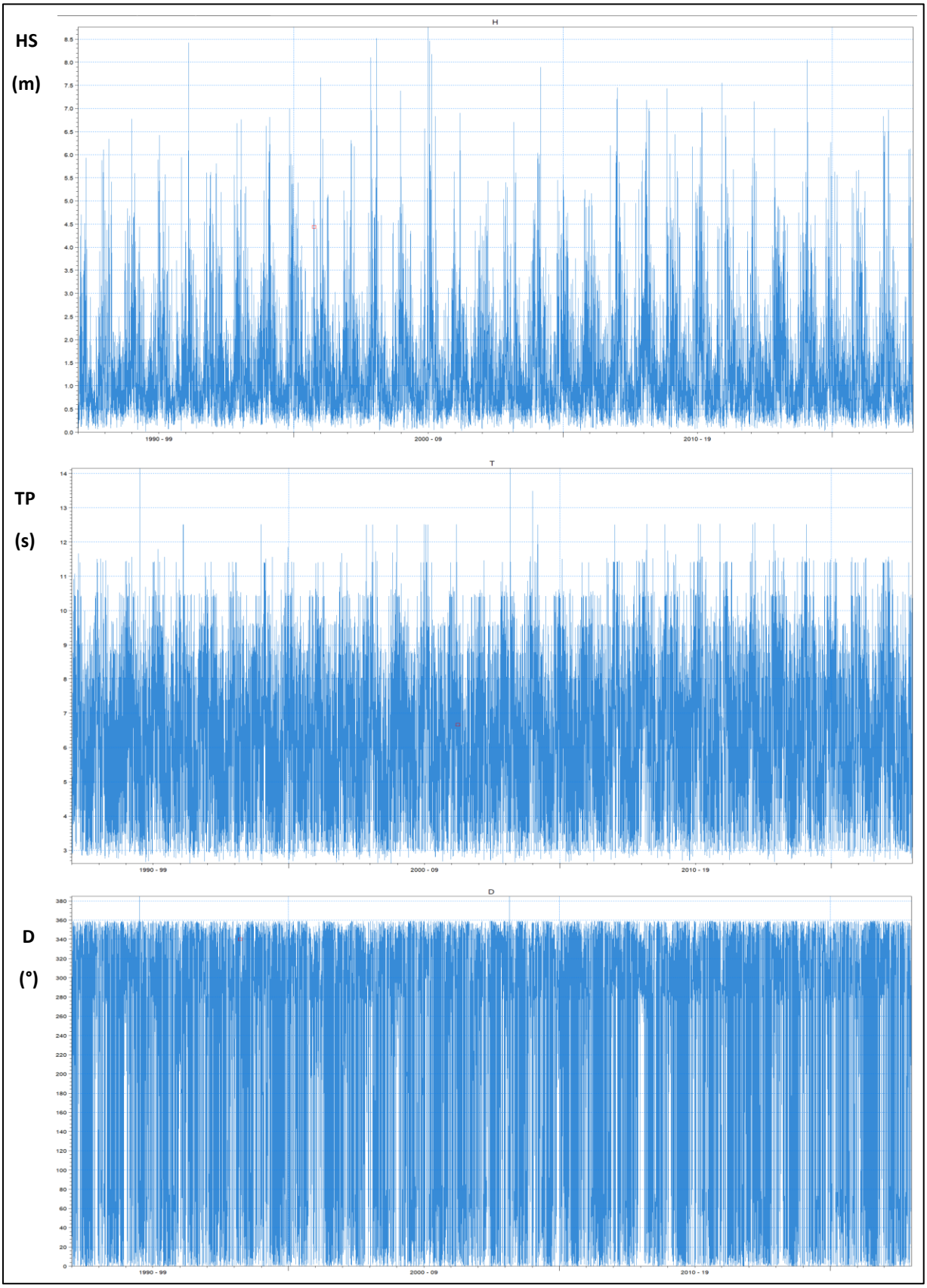


Figure 39: Representation of the Wave Parameters Spectrums.

## IV.3 Peaks Over Threshold (POT) Method

Introduced by **de Haan & Rootzen (1993)**. Let "$u$" be a real number that is "sufficiently large" and less than the terminal point "($u$ <ω ($F$))", called the threshold. The excess method relies on an approximation of the distribution of exceedances above the threshold "$u$" of the real-valued random variable "$X$", meaning the conditional distribution of the positive real-valued random variable "$X - u$", given that "$X > u$" **(GARRIDO, 2002)**. The cumulative distribution function of exceedances beyond the threshold "$u$" is defined as

Equation 4

$$F_u(y) = P(X - u \leq y | X > u) = \begin{cases} \frac{F(u+y)+F\{u\}}{1-F(u)} & for\ y \geq 0 \\ 0 & if\ y < 0 \end{cases}$$

Before setting the threshold, we calculated the mean residual using Python and the pyextreme library to analyze its variations and determine the most appropriate threshold. The threshold should lie on the straight-line segment before any fluctuations in the mean residual.

The chosen threshold was set at 4.8 m for the study area, as shown in Figure 40:

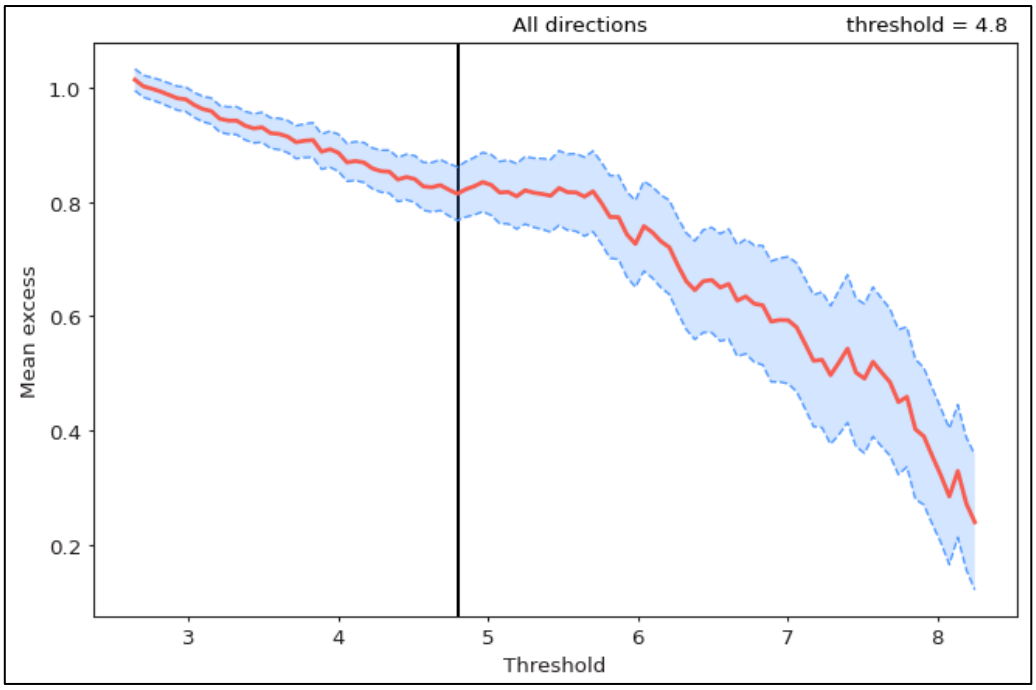


Figure 40: Residual mean of the omnidirectional height series from the recording in the Wilaya of Skikda.

The set of selected points for the calculation is shown in Figures 41:

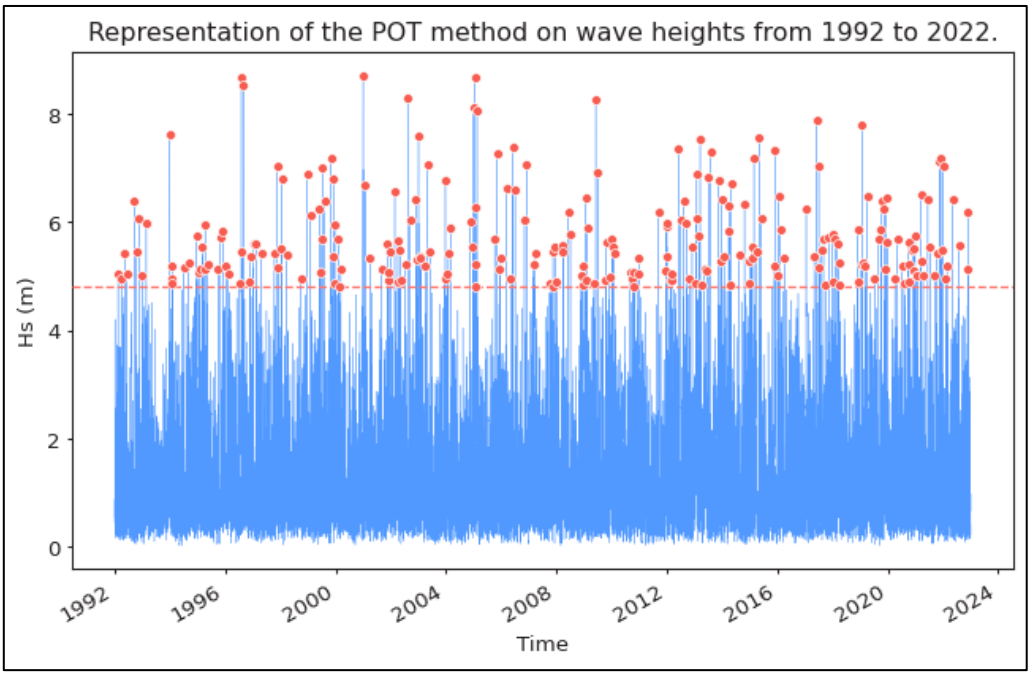


Figure 41: Representation of the POT method applied to wave heights from 1992 to 2022 for omnidirectional.

The coming Figures demonstrate that the threshold is correct. Additionally, these plots validate the effectiveness of the POT method in modeling extreme wave heights for the given dataset. The return value plot provides estimates for future extreme events, while the Q-Q and P-P plots confirm the model's reliability:

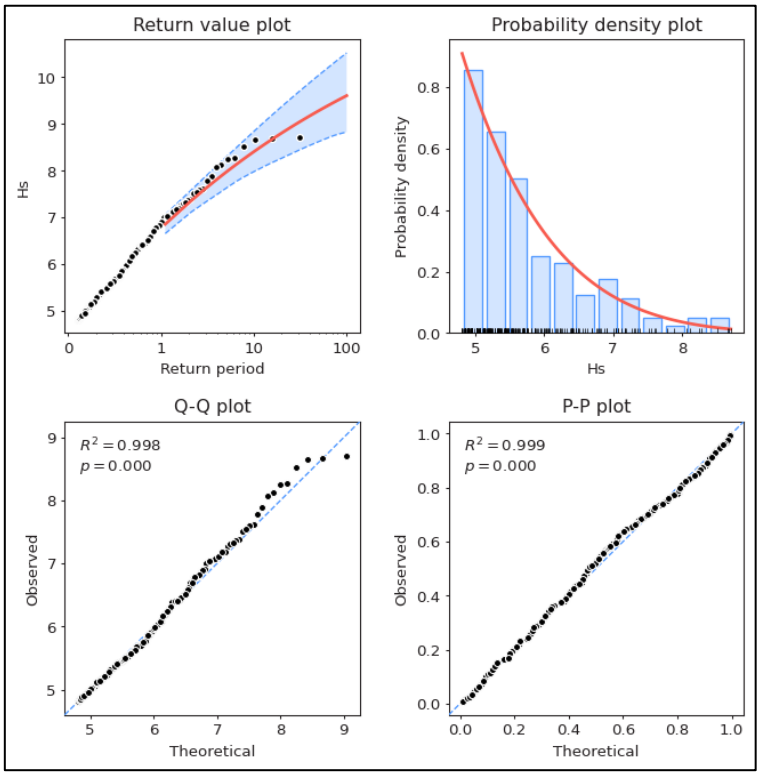


Figure 42: Validation of Extreme Wave Height Modeling Using the POT Method for omnidirectional.

Since the peak selection step is complete, the next step is the calculation of wave heights and their return periods using the same pyextreme library in Python. The obtained results are shown in the following Figures:

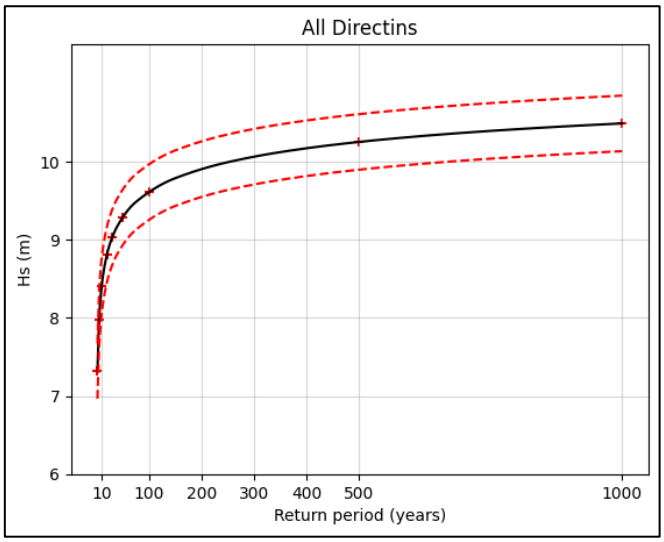


Figure 43: Estimation of extreme events using the POT method for omnidirectional.

The results displayed in Figure 43 illustrate the estimated wave heights for different return periods, with red lines representing the acceptable error margin of 5%. The red crosses indicate the wave heights corresponding to return periods of 2, 5, 10, 20, 30, 50, 100, and 1000 years.

These markers provide a clear visualization of the trend and reliability of the applied model. The proximity of the estimated values to the error limits confirms the accuracy of the method. This approach will be extended to other directions to ensure a comprehensive analysis of wave height variations across different directions as it is shown in Figure 44.

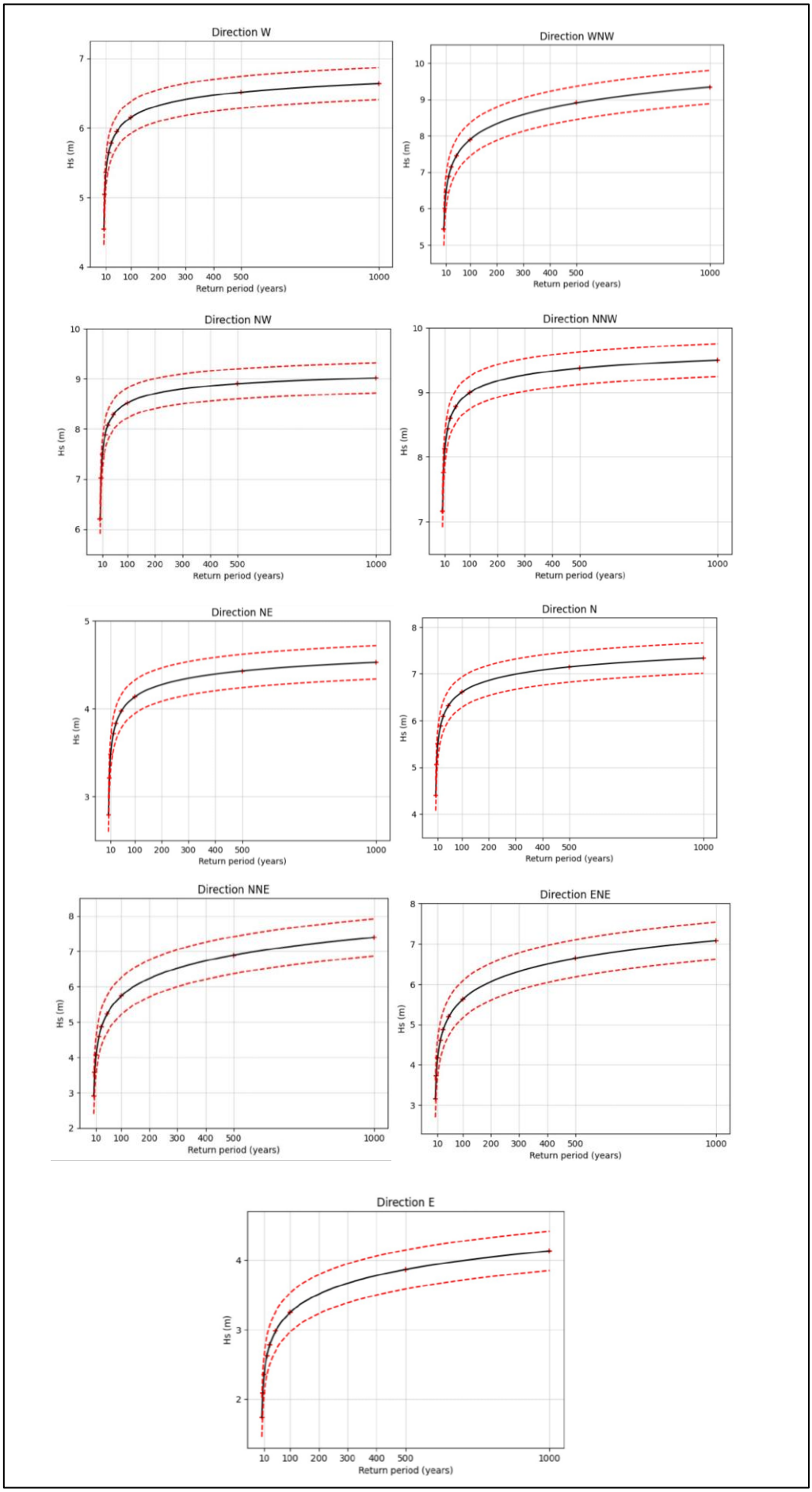


Figure 44: Estimation of extreme events using the POT method for each direction.

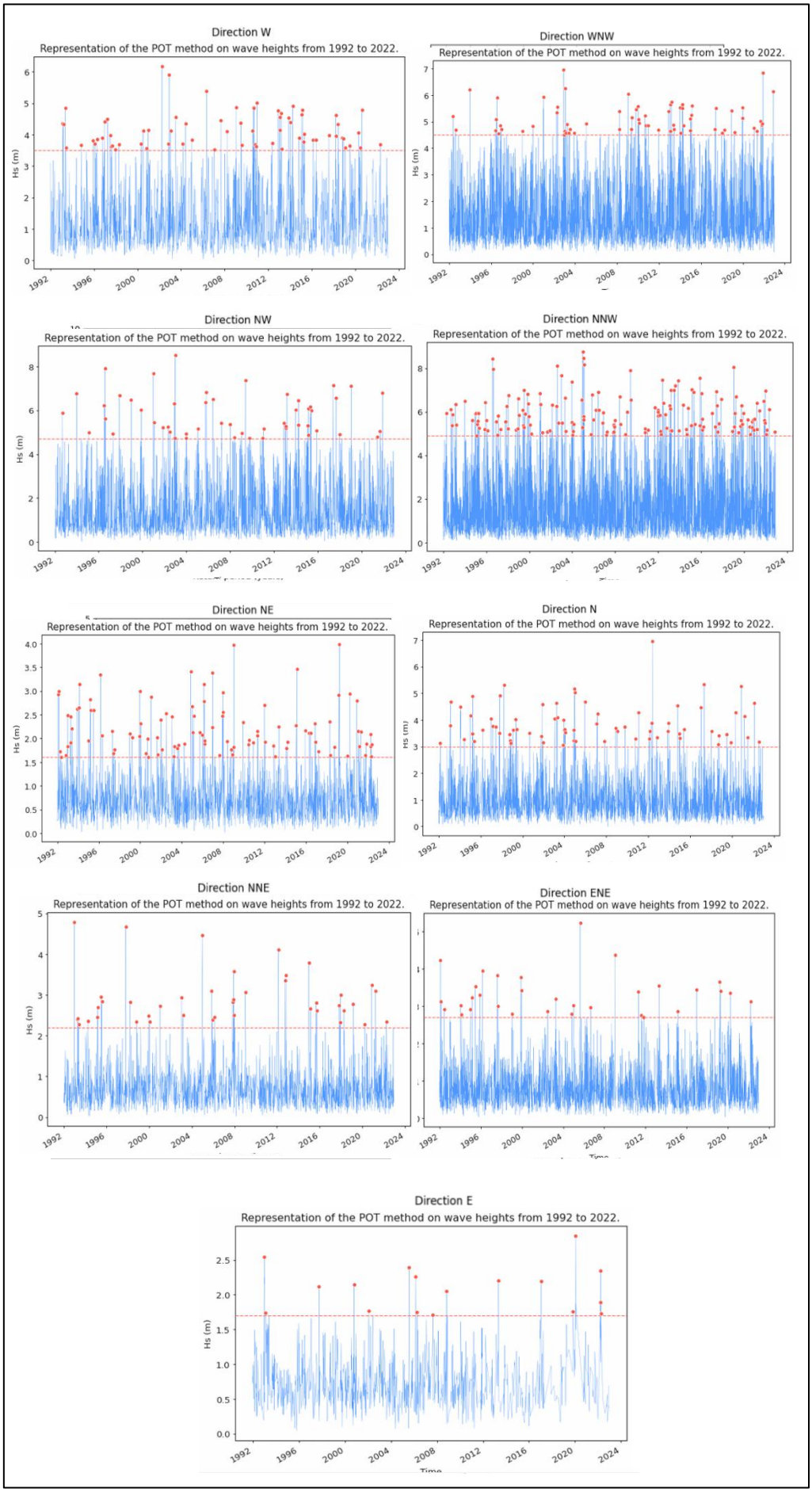


Figure 45: Representation of the POT method applied to wave heights from 1992 to 2022 for all the directions.

For a better interpret of the results obtained using the POT method, the following table summarizes all the extreme wave heights estimated for different return periods. These values provide insights into the occurrence of extreme wave events in the future, helping to estimate the potential risks associated with wave activity over time. By analyzing these results, we can better understand the frequency and magnitude of extreme waves and use this information for coastal planning, risk mitigation, and infrastructure resilience.

Table 6: Table summarizing all the results obtained using the POT method.

| POT | | | | | | | | | | |
|---|---|---|---|---|---|---|---|---|---|---|
| | Wave height by direction (m) | | | | | | | | | |
| **Return period (year)** | **W** | **WNW** | **NW** | **NNW** | **N** | **NNE** | **NE** | **ENE** | **E** | **omni** |
| **2** | 4.54 | 5.43 | 6.2 | 7.16 | 4.39 | 2.91 | 2.78 | 3.15 | 1.73 | 7.32 |
| **5** | 5.04 | 6.01 | 7.01 | 7.75 | 5.06 | 3.57 | 3.21 | 3.73 | 2.08 | 7.97 |
| **10** | 5.36 | 6.44 | 7.49 | 8.12 | 5.59 | 4.07 | 3.48 | 4.17 | 2.35 | 8.41 |
| **20** | 5.64 | 6.88 | 7.88 | 8.43 | 5.88 | 4.57 | 3.71 | 4.6 | 2.62 | 8.81 |
| **30** | 5.78 | 7.13 | 8.07 | 8.59 | 6.08 | 4.86 | 3.83 | 4.86 | 2.77 | 9.03 |
| **50** | 5.94 | 7.45 | 8.28 | 8.78 | 6.32 | 5.23 | 3.96 | 5.18 | 2.97 | 9.29 |
| **100** | 6.14 | 7.89 | 8.51 | 8.99 | 6.6 | 5.73 | 4.13 | 5.62 | 3.24 | 9.61 |
| **1000** | 6.63 | 9.33 | 9.01 | 9.49 | 7.33 | 7.38 | 4.52 | 7.07 | 4.13 | 10.49 |

The analysis of predicted wave heights using the POT method, as presented in Table 6, highlights significant variations depending on the wave direction. The East direction appears to be the least prone to generating extreme wave events, while the Northwest (NW), North-Northwest (NNW), and West-Northwest (WNW) directions exhibit the highest potential for extreme wave heights.

Furthermore, the omnidirectional wave height analysis provides the most extreme values, as it considers the maximum recorded heights within the dataset. This indicates that the model captures the most significant wave events, offering a comprehensive understanding of potential extreme conditions in the study area.

# Chapter V: Hydrodynamic Modeling

# V.1 Introduction

Marine numerical models rely on mathematical equations to simulate and analyze the movement of fluids, including water and air, across the Earth's surface. These models also account for biogeochemical processes, such as nutrient cycling and ecosystem dynamics, as well as complex sea ice behavior, including its formation, melting, and drift. By integrating these various components, numerical models provide essential insights into ocean circulation, climate interactions, and environmental changes over time.

Moreover, numerical modeling plays a fundamental role in predicting tidal patterns, ocean currents, and coastal phenomena. It enables researchers and decision-makers to analyze the potential consequences of coastal infrastructure projects and environmental modifications. As a result, numerical modeling has become an indispensable tool for informed decision-making in maritime region management, infrastructure planning, and the protection of fragile coastal ecosystems. Through continuous advancements in computational techniques and data assimilation, these models continue to enhance our understanding of marine dynamics and contribute to sustainable coastal development.

# V.2 Model Presentation

## V.2.1 MIKE 21

MIKE 21 is an advanced software suite developed by DHI for simulating and analyzing water flow, currents, wave conditions, and processes in marine and coastal environments. It offers robust visualization tools and data management capabilities, enabling users to effectively interpret simulation results. The software is widely utilized by engineers, scientists, and environmental professionals in fields such as coastal engineering, water resource management, evaluating environmental impacts, and climate change adaptation planning.

MIKE 21 specialises in two-dimensional (2D) modelling, offering precise simulations of water flow and movement in coastal areas, estuaries, and rivers. It enables accurate predictions of water levels, currents, temperature variations, and flood occurrences, excelling in managing intricate bathymetry and external forces like wind effects **(DHI, 2014).**

## V.2.2 Mesh Generator

The flexible mesh is generated by using the mesh generator which creates detailed digital mesh for use in the MIKE Zero flexible mesh (FM). Within two-dimensional model the elements would be considered as triangles and quadrilateral elements. The mesh file that yielded by mesh generator is an ASCII file which includes information of the geographical position and water depth at each node point in the mesh, **(NOVICO et al., 2012).**

Creating an effective mesh for marine numerical modeling involves several essential steps. First, selecting an appropriate coordinate system tailored to the study area is so important; in this case, the WGS 84 UTM Zone 32 system. Next, accurately integrating the coastline and bathymetry data is vital, with these datasets ideally provided in an XYZ file format to ensure a faithful representation of the study area. Finally, generating a mesh with varying cell sizes is necessary to balance result precision and computational efficiency, enabling precise simulations

while optimizing computational resources. These steps are fundamental to ensuring the quality and reliability of hydrodynamic simulations in marine and coastal environments.

### V.2.3 The Hydrodynamic Module: MIKE 21 HD

The MIKE 21 Hydrodynamic (HD) module is designed to simulate water level variations and flow patterns in marine and coastal environments. It solves the classical two-dimensional Saint-Venant equations under the Boussinesq assumption, employing both finite volume methods on flexible meshes and finite difference methods on rectangular grids **(DHI, 2014).**

The module accounts for various physical factors, including bottom friction, wind influence, atmospheric pressure gradients, the Coriolis effect, different turbulence representations, and temporal changes in domain geometry, such as areas that flood and dry during tidal variations. Additionally, it can simulate coastal currents by considering wave-induced radiation stresses in surf zones.

**Flow and Water level variation equations**

The following equation, the conservation of mass and momentum integrated over the vertical, describe the flow and water level variations **(DHI, 2017)**:

Equation 5

$$\frac{\partial \zeta}{\partial t}+\frac{\partial p}{\partial x}+\frac{\partial q}{\partial y}=\frac{\partial d}{\partial t}$$

Equation 6

$$\frac{\partial p}{\partial t}+\frac{\partial}{\partial x}\left(\frac{p^2}{h}\right)+\frac{\partial}{\partial y}\left(\frac{pq}{h}\right)+gh\frac{\partial \zeta}{\partial x}+\frac{gp\sqrt{p^2+q^2}}{c^2h^2}-\frac{1}{\rho_w}\left[\frac{\partial}{\partial x}(h\tau_{xx})+\frac{\partial}{\partial y}(h\tau_{xy})\right]-\Omega_q - fVV_x+\frac{h}{\rho_w}\frac{\partial p_a}{\partial x}=0$$

Equation 7

$$\frac{\partial q}{\partial t}+\frac{\partial}{\partial y}\left(\frac{q^2}{h}\right)+\frac{\partial}{\partial x}\left(\frac{pq}{h}\right)+gh\frac{\partial \zeta}{\partial y}+\frac{gp\sqrt{p^2+q^2}}{c^2h^2}-\frac{1}{\rho_w}\left[\frac{\partial}{\partial y}(h\tau_{yy})+\frac{\partial}{\partial x}(h\tau_{xy})\right]+\Omega_p - fVV_y+\frac{h}{\rho_w}\frac{\partial p_a}{\partial y}=0$$

The following symbols are used in these equations:

- $\boldsymbol{h\,(x, y, t)}$: Water depth (m)
- **d** $\boldsymbol{(x, y, t)}$: Temporal variation of water depth (m)
- $\boldsymbol{\zeta\,(x, y, t)}$: Surface elevation (m)
- **p, q** $\boldsymbol{(x, y, t)}$: Flow densities in the x and y directions ($m^3/s/m$)
- **C** $\boldsymbol{(x, y)}$: Chezy coefficient (m^ (1/2) /s)

- **g**: Gravitational acceleration (m/s²)
- **f(V)**: Wind friction factor
- **V, $V_x$, $V_\gamma(x, y, t)$**: Wind velocity components in the x and y directions (m/s)
- **$\Omega(x, y)$**: Coriolis parameter ($s^{-1}$)
- **$P_a(x, y, t)$**: Atmospheric pressure (kg/m/s²)
- **$\rho w$**: Water density (kg/m³)
- **$\tau_{xx}$, $\tau_{x\gamma}$, $\tau_{\gamma\gamma}$**: Components of the effective shear stress

### V.2.3 The Spectral Wind Wave Module: MIKE 21 SW

MIKE 21 SW is a new generation spectral wind-wave model based on unstructured meshes. The model simulates the growth, decay and transformation of wind-generated waves and swell waves in offshore and coastal areas.

MIKE 21 SW includes the following physical phenomena:

- Wave growth by action of wind
- Non-linear wave-wave interaction
- Dissipation due to white-capping
- Dissipation due to bottom friction
- Dissipation due to depth-induced wave breaking
- Refraction and shoaling due to depth variations
- Wave-current interaction
- Effect of time-varying water depth

MIKE 21 SW is used for the evaluation of wave climates in offshore and coastal areas - in hindcast and forecast mode **(DHI, 2017).**

**Wave Action conservation equations**

In horizontal Cartesian coordinates, the conservation equation for wave action can be written as:

Equation 8

$$\frac{\partial N}{\partial t} + \nabla \cdot (\vec{v} N) = \frac{S}{\sigma}$$

where $N(\vec{x}, \sigma, \theta, t)$ the action density, t is the time, $\vec{x} = (x, y)$ is the Cartesian coordinates, v = $(cx, cy, c\sigma, c\theta)$ is the propagation velocity of a wave group in the four-dimensional phase space $\vec{x}$, σ, θ, and S is the source term for the energy balance equation. ∇ is the four-dimensional differential operator in the $\vec{x}$, σ, θ space.

The four characteristic propagation speeds are given by:

Equation 9

$$(c_x, c_y) = \frac{d\vec{x}}{dt} = \overrightarrow{c_g} + \vec{U}$$

Equation 10

$$c_\sigma = \frac{d\sigma}{dt} = \frac{\partial\sigma}{\partial d}\left[\frac{\partial d}{\partial t} + \vec{U}\cdot\nabla_x d\right] - \vec{k}\cdot\frac{\partial\vec{U}}{\partial s}$$

Equation 11

$$c_\theta = \frac{d\theta}{dt} = -\frac{1}{k}\left[\frac{\partial\sigma}{\partial d}\frac{\partial d}{\partial m} + \vec{k}\cdot\frac{\partial\vec{U}}{\partial s}\right]$$

Here, s is the space coordinate in wave direction θ, and m is a coordinate perpendicular to s. $\nabla\vec{x}$ is the two-dimensional differential operator in the $\vec{x}$space.

## V.3 Work Methodology

### V.3.1 Bathymetric data for the generation of the Mesh

The study area extends over a regional scale of approximately 250.19 km. To ensure a more accurate simulation of this area, we included Oued Saf-Saf and the El Marsa fishing harbor. The bathymetric data used in this study is a combination of field data, NAVIONICS, and VERT ET BLEU, stored in a (.xyz) file.

The bathymetry of the study area and the coastline were obtained through the digitization of the NAVIONICS Sonar Chart™ map, 2024 edition, at a scale of 1:250,000, with a resolution ranging from 100 m offshore to 0.5 m near the coast. For the El Marsa fishing harbor, the bathymetric data was obtained via EURL VERT ET BLEU.

The mesh generation was performed using an embedded triangular mesh, providing enhanced spatial accuracy to better represent the local characteristics of both ports. This approach selectively adjusts the mesh density based on specific needs, ensuring more precise results in areas of interest while optimizing computational resources. The mesh generation is followed by an interpolation process, with two available methods for triangular elements:

Nearest neighbor interpolation: assigns the value of the closest grid node (or vertex) to each interpolated point.

Linear interpolation: calculates the value at any given point as a linear combination of the values of the triangle's vertices. (DHI, 2014).

In our case, the nearest neighbor interpolation method was chosen.

### V.3.2 Mesh and Bathymetry

**Mesh**

The mesh consists of 6,565 nodes and 10,878 triangular elements, with a varying resolution: 50,000 m near the Oued, 5,000 m near the port, and 10,000 km offshore. A mesh refinement (degradation) was applied in two specific areas, as illustrated in Figures 46, 47 and 48.

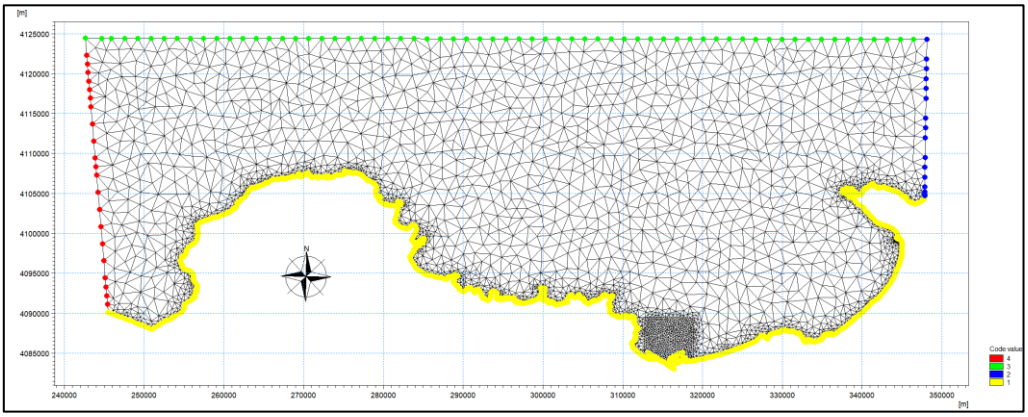

Figure 46: Mesh grid at the scale of the Skikda Bay.

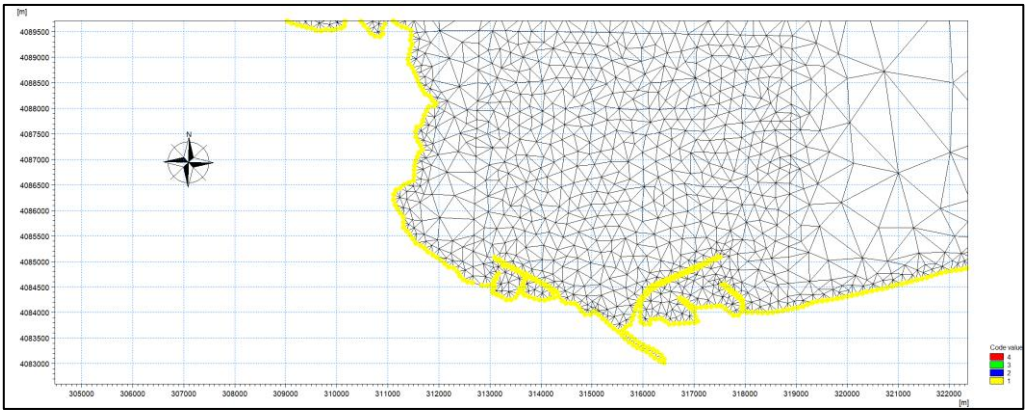

Figure 47: Mesh grid at the scale of the Oued Saf-Saf.

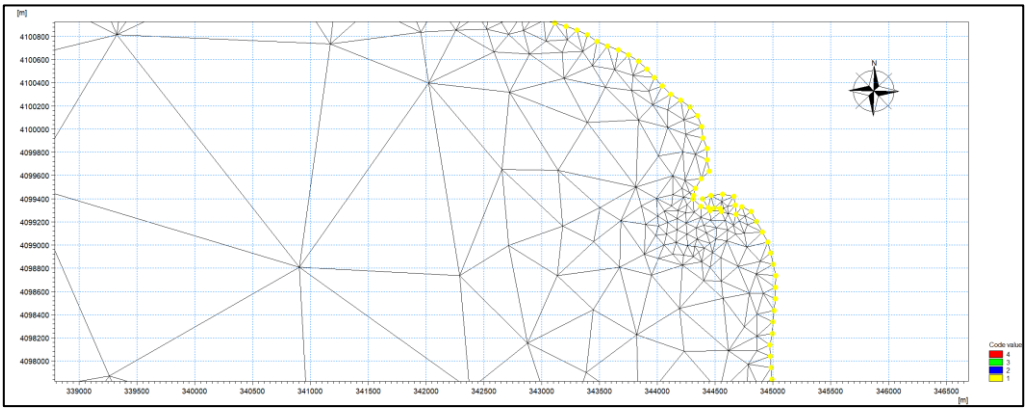

Figure 48: Mesh grid at the scale of the El Marsa fishing harbor.

### Bathymetry

After the interpolation of the mesh, a bathymetry of the study area is obtained, extending to the abyssal plain of the Mediterranean as illustrated in Figures 49.

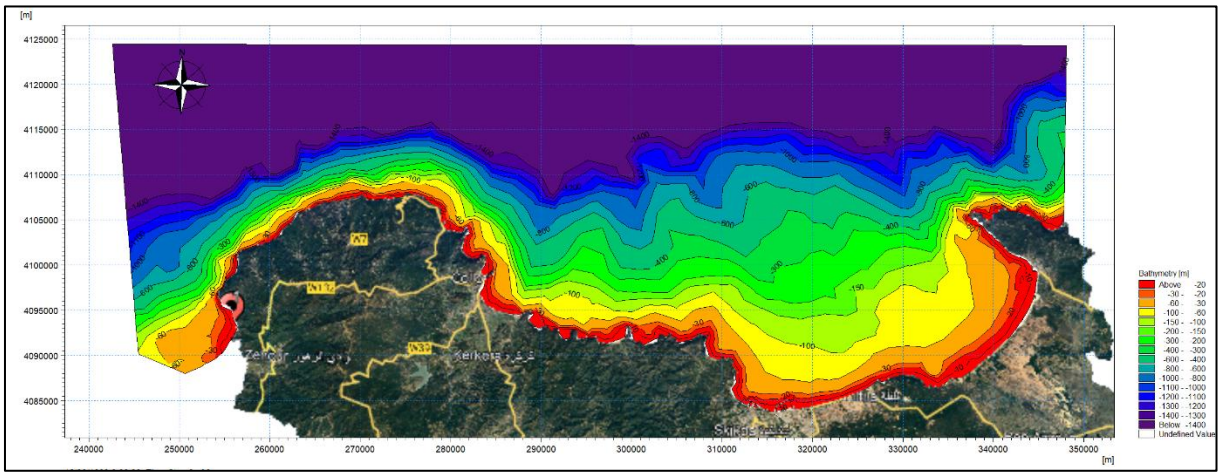


Figure 49: Bathymetric map of Skikda Bay.

### Analysis of Bathymetric Zones

The analysis of the bathymetric map reveals three distinct zones within the Bay of Skikda:

**The coastline and nearshore areas**: Along the coast, the bathymetry highlights a rapid transition from shallow waters to deeper areas. The presence of rocky formations and headlands results in steep slopes, particularly in the western and eastern parts of the bay. These areas are subject to intense hydrodynamic activity, which can promote coastal erosion and sediment accumulation in sheltered parts.

**The central part of the bay:** This zone is characterized by a gentler slope from 20 to 30m of depth, indicating the presence of soft sediment deposits. These sea-beds are influenced by terrigenous inputs from nearby rivers and by a more moderate marine dynamic compared to areas exposed to headlands. Bathymetric variations are less pronounced here, suggesting a more stable environment in terms of sedimentation and particle transport.

**The offshore zone and transition to deep waters:** Moving away from the shore, about 200m of depth, there is a gradual increase in depth until the end of the continental shelf. This transition is marked by a tightening of isobaths, indicating a steeper slope leading to the Mediterranean abyss. This zone is subject to deep hydrodynamic processes and plays a key role in sediment exchange between the continental shelf and the deep-sea floor.

## V.4 Simulation scenarios

Since the penalizing directions are detected and the extreme events calculated, the chosen method is to associate the significant wave height and peak period for three different return periods with each wind direction. This approach also takes into account Algerian General Level (NGA) it is essential to add it to ensure consistency between bathymetric data and the sea

level; therefore, the depths are adjusted relative to the NGA, allowing for accurate linking of bathymetric values to a recognized general reference level. It's important to note that all simulations use a constant wind speed for each direction, with average wind speed and direction being obtained from a dataset spanning from 1992 to 2022, based on the WaveClimat database in the study area. However, coupling wind and wave events from the same return period results in highly overestimated scenarios. To address this, the proposed solution is to determine the probability of occurrence for wind-wave pairs rather than directly coupling return periods, providing more realistic scenarios.

Table 7: Simulation inputs for all return periods (10, 30, and 100 years) for the Bay of Skikda.

| | **Return period of 10 years** | | | | **Sea level** |
|---|---|---|---|---|---|
| **Wave Parameters** | Wave height (m) | Peak Period (s) | Wind speed (m/s) | Wind direction (°) | |
| **Directions** | | | | | **NGA= ZH+0.34** |
| **WNW** | 6.44 | 10.67 | 13 | 292,5 | **NGA = 0.34** |
| **NW** | 7.49 | 11.73 | 13 | 315 | |
| **NNW** | 8.12 | 12.35 | 13 | 337,5 | |
| | **Return period of 30 years** | | | | **Sea level** |
| **Wave Parameters** | Wave height (m) | Peak Period (s) | Wind speed (m/s) | Wind direction (°) | |
| **Directions** | | | | | **NGA= ZH+0.34** |
| **WNW** | 7.13 | 11.38 | 13 | 292,5 | **NGA = 0.34** |
| **NW** | 8.07 | 12.30 | 13 | 315 | |
| **NNW** | 8.59 | 12.79 | 13 | 337,5 | |
| | **Return period of 100 years** | | | | **Sea level** |
| **Wave Parameters** | Wave height (m) | Peak Period (s) | Wind speed (m/s) | Wind direction (°) | |
| **Directions** | | | | | **NGA= ZH+0.34** |
| **WNW** | 7.89 | 12.12 | 13 | 292,5 | **NGA = 0.34** |
| **NW** | 8.51 | 12.72 | 13 | 315 | |
| **NNW** | 8.99 | 13.16 | 13 | 337,5 | |

# V.5 Simulation results

## V.5.1 Wave conditions

### Interpretation

#### Case of West-Northwest (WNW) Wave Direction

In the case of a wave coming from the west-northwest, the highest wave heights, exceeding 4.7m, are mainly observed offshore and directly impact the western coast of the Skikda wilaya. This region, characterized by rocky coasts and steep bathymetry about 100m nearshore, acts as a natural barrier. It largely blocks the propagation of waves toward the center of the bay. As a result, areas further east, particularly the bay center and the Skikda region, are relatively protected. Wave heights there remain moderate, often below 2m of height at 10m of depth, thanks to the dissipative effect of the coastal nature and sea depth.

#### Case of Northwest (NW) Wave Direction

When the wave direction shifts toward the northwest, its propagation becomes more frontal with respect to the bay's opening. This allows wave energy to penetrate more effectively inward, partially bypassing the natural barrier formed by the rocky western coast where the depth is about 100m. Consequently, the central areas of the bay, particularly around Kerkera and Skikda, begin to experience higher wave heights, which can exceed 3.5m in certain areas at 10m of depth. The protective influence of the western coast thus becomes less effective, allowing more room for wave development within the bay.

#### Case of North-Northwest (NNW) Wave Direction

With a north-northwest wave direction, the waves arrive almost perpendicularly to the coast, significantly increasing the extent of the exposed shoreline. The barrier effect offered by the rocky western coast is greatly diminished, and the waves affect both the central and eastern parts of the wilaya. Although the bathymetry still partially reduces (less then 10m of depth) wave intensity, wave heights still exceed 2.5m in areas that are usually sheltered from more oblique wave directions. Therefore, shoreline exposure becomes widespread when the wave direction shifts closer to the north.

It is observed that despite the rise in the return period (from 10 to 100 years), wave heights increase only slightly as they approach the coast. This is mainly due to the stable bathymetry, which remains unchanged in all three cases, playing an important role in limiting the propagation of wave energy toward the shore. Thus, even for extreme events, wave heights increase slightly offshore, but the effect near the coast remains moderate.

The coming figures (Figures 50 to 58) visually support this analysis, illustrating the spatial distribution of wave heights and their variation under different wave directions and return periods. They highlight the contrast in wave exposure between the western rocky coast and the more vulnerable central and eastern zones.

## Return period of 10 years

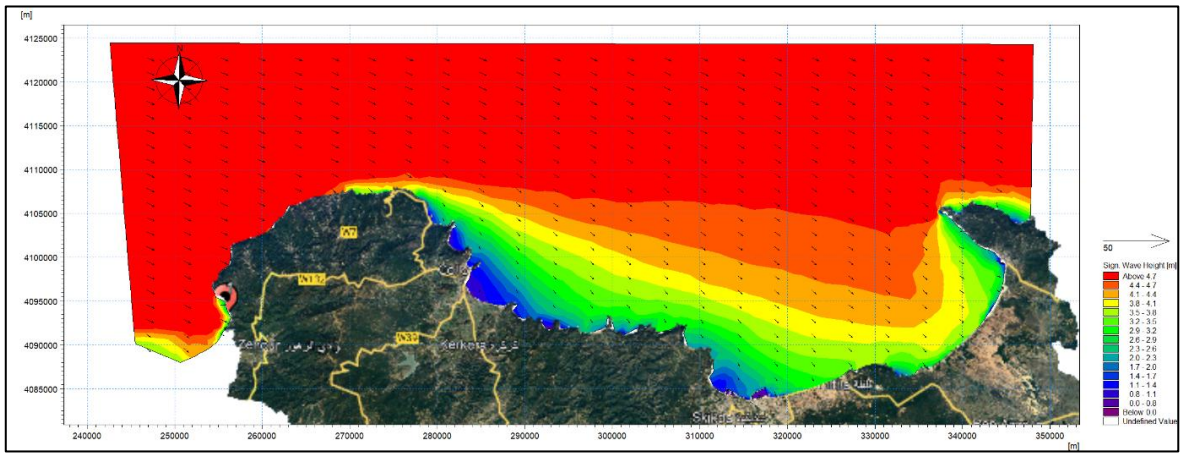

Figure 50: Wave conditions in the Bay of Skikda for the WNW direction (10).

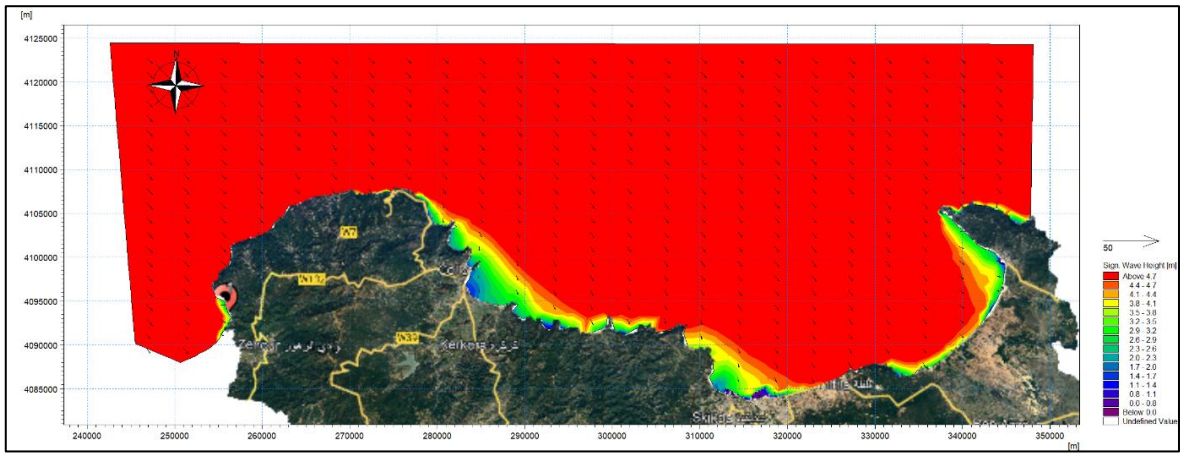

Figure 51: Wave conditions in the Bay of Skikda for the NW direction (10).

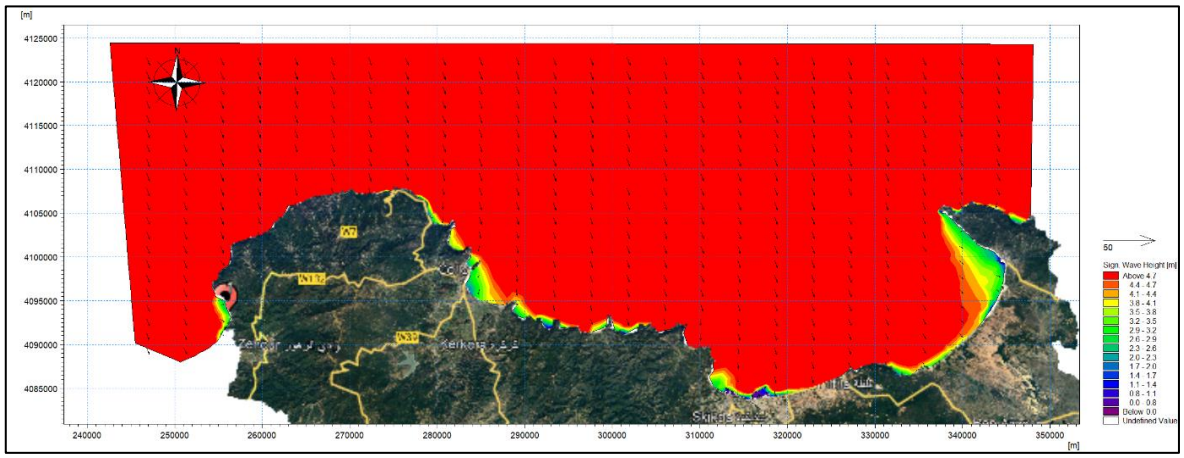

Figure 52: Wave conditions in the Bay of Skikda for the NNW direction (10).

## Return period of 30 years

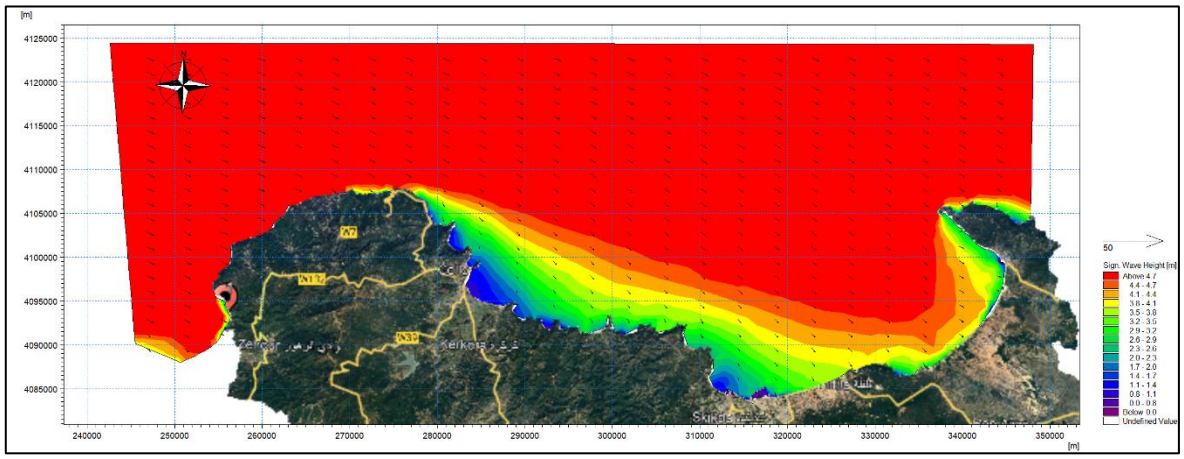

Figure 53: Wave conditions in the Bay of Skikda for the WNW direction (30).

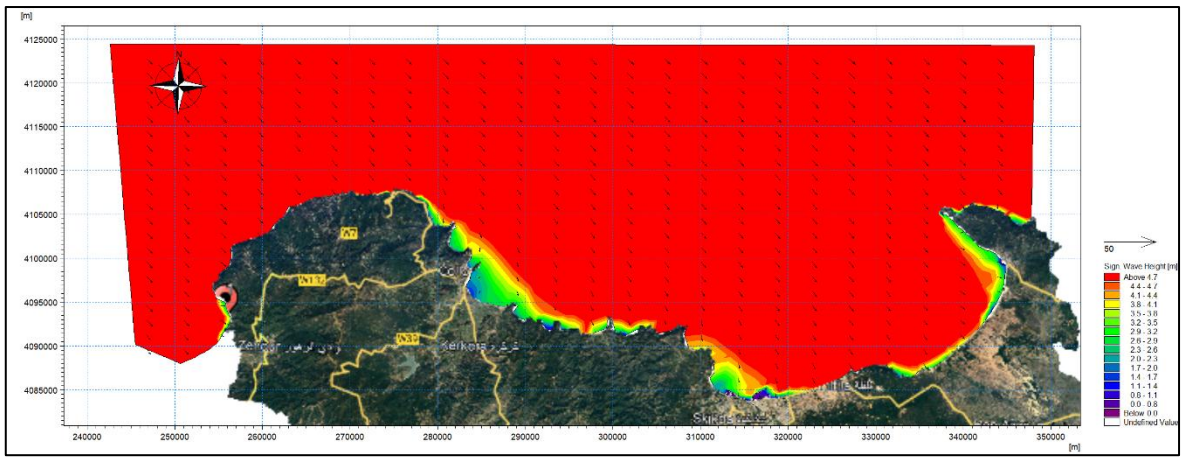

Figure 54: Wave conditions in the Bay of Skikda for the NW direction (30).

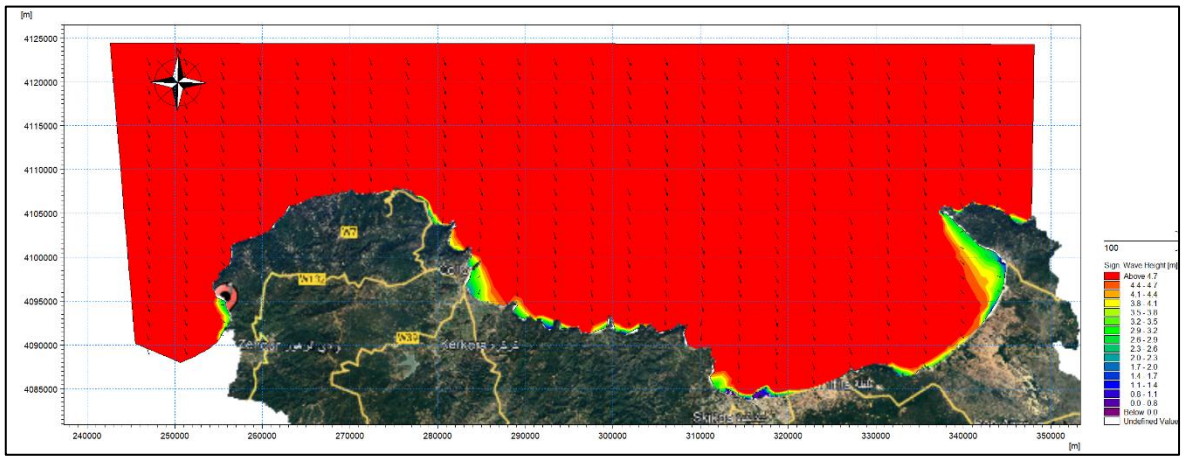

Figure 55: Wave conditions in the Bay of Skikda for the NNW direction (30).

## Return period of 100 years

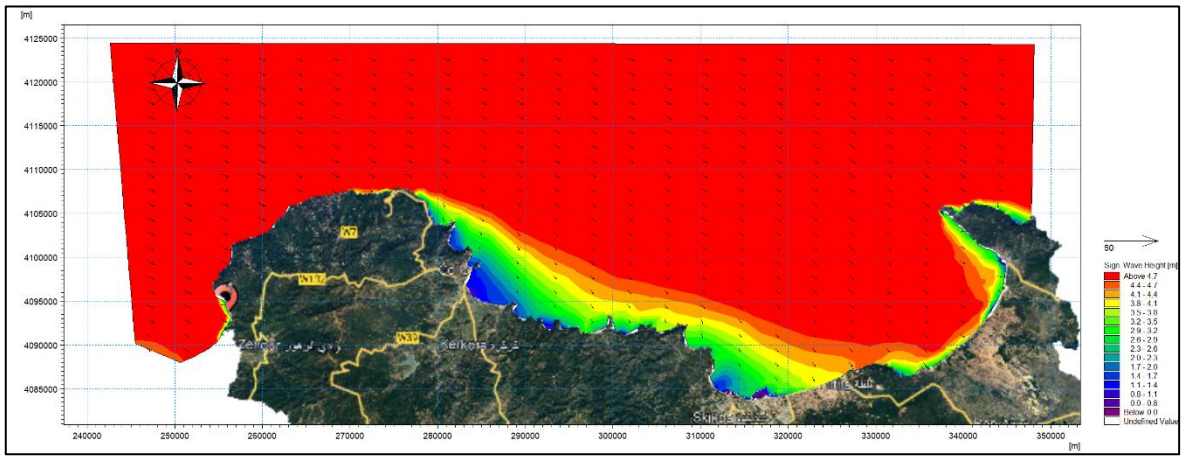


Figure 56: Wave conditions in the Bay of Skikda for the WNW direction (100).

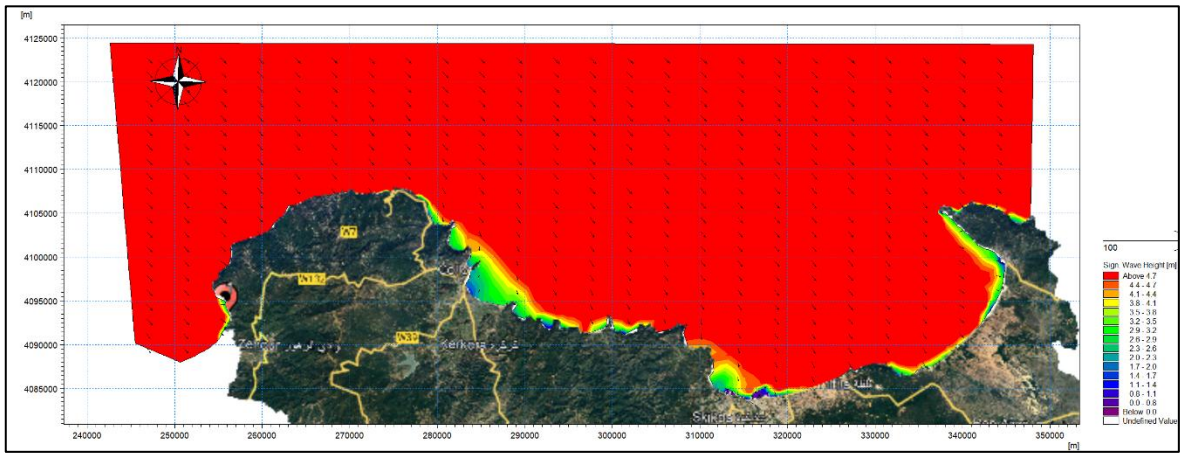


Figure 57: Wave conditions in the Bay of Skikda for the NW direction (100).

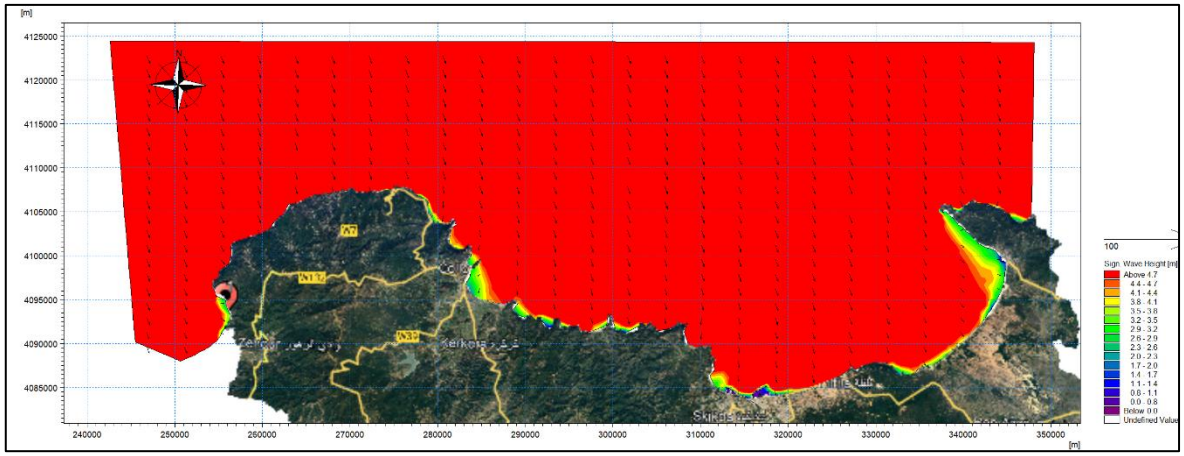


Figure 58: Wave conditions in the Bay of Skikda for the NNW direction (100).

### V.5.2 Current conditions in the Bay of Skikda

**Interpretation**

The simulation results reveal a complex current dynamic in the Bay of Skikda, influenced by wind direction, bathymetry, and coastal structures. In offshore areas, the currents are relatively uniform, with moderate to high velocities depending on exposure to the dominant swell.

As they approach the coastline, the currents are subject to significant modifications. In certain areas, particularly near headlands and channels where the speed reaches to 1.8m/s, current velocity increases due to the reduction of hydrodynamic flows caused by coastal morphology and depth variations. Conversely, in more sheltered bays or within port infrastructures, velocities decrease due to energy dissipation and recirculation effects.

The maps also highlight the effects of diffraction and longshore drift, with currents aligning parallel to the coast in some areas, transporting water masses and sediments over varying distances. Zones of current convergence and divergence are also observed, particularly around port structures and irregular sea-beds, which can influence erosion and sedimentation processes.

In conclusion, current circulation in the Bay of Skikda is not uniform and varies according to coastal configuration and hydrodynamic conditions. Some areas experience accelerated currents, while others show stagnation zones or low velocities.

The following figures (Figures 59 to 67) illustrate these patterns in detail, showing the spatial variation of current velocities and directions under different scenarios. They provide a clear visualization of flow concentration zones, divergence points, and the interactions between hydrodynamics and coastal features.

**Return period of 10 years**

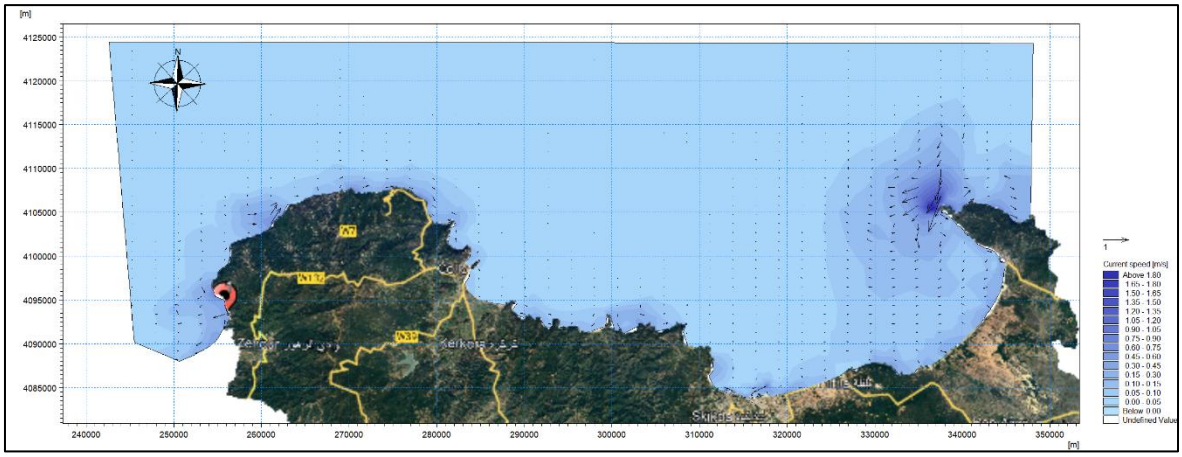


Figure 59: Current conditions in the Bay of Skikda for the WNW direction (10).

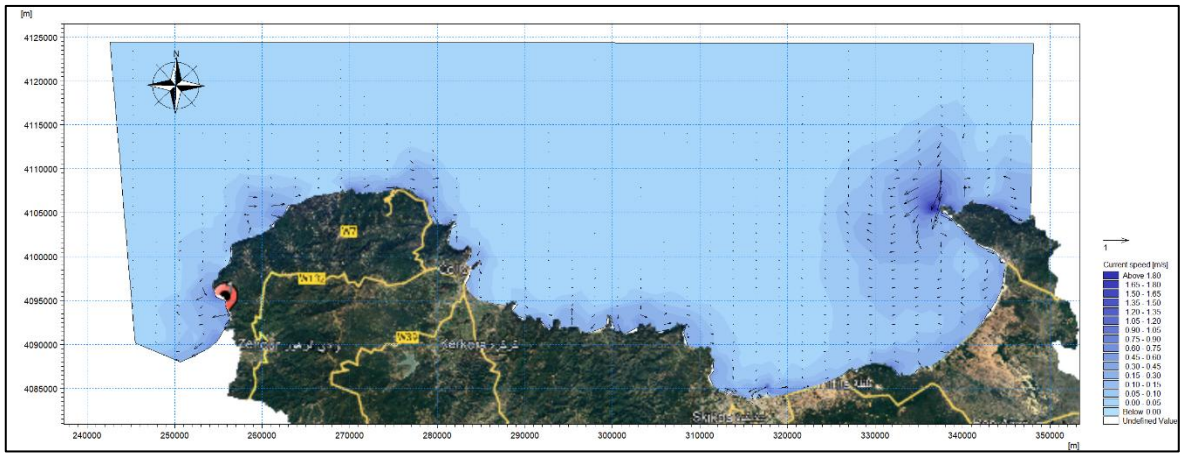

Figure 60: Current conditions in the Bay of Skikda for the NW direction (10).

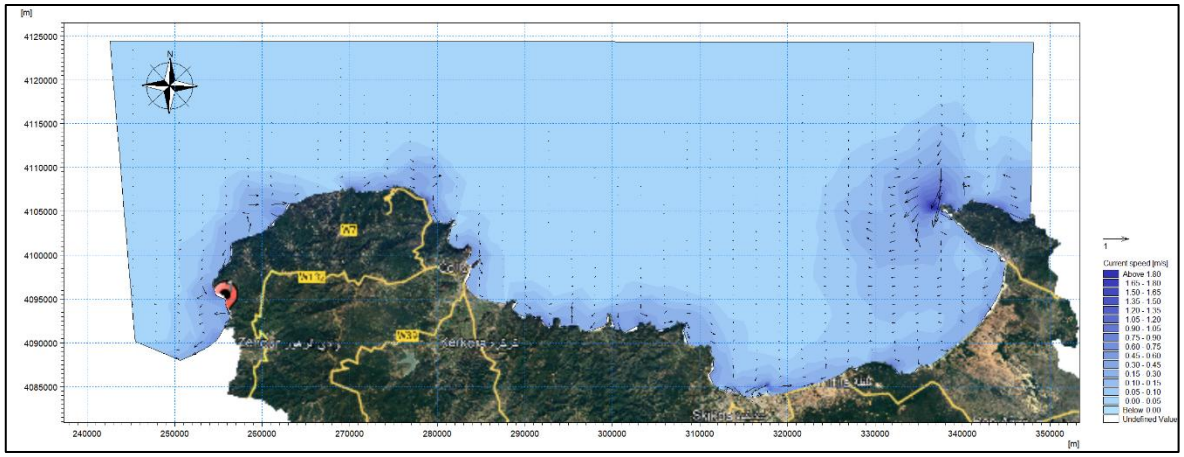

Figure 61: Current conditions in the Bay of Skikda for the NNW direction (10).

## Return period of 30 years

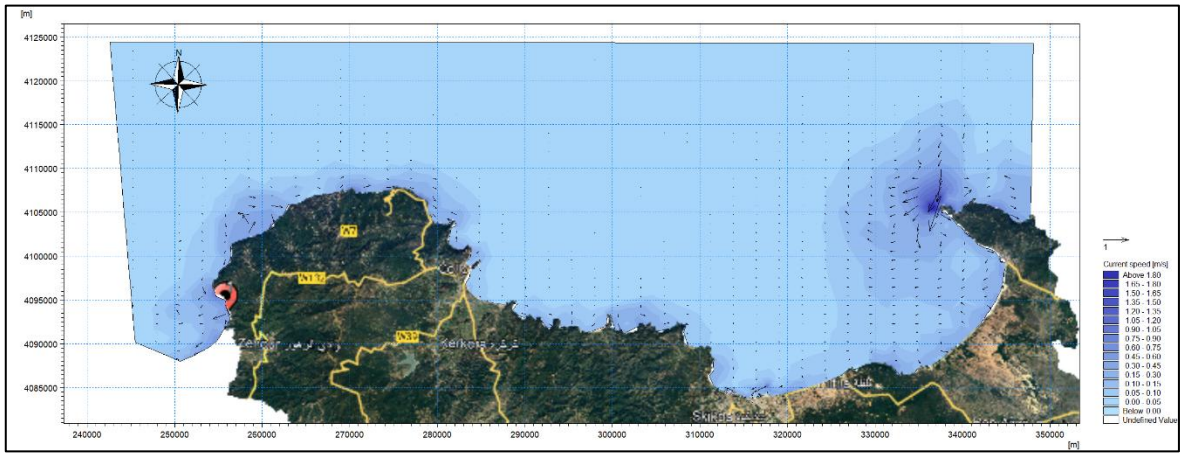

Figure 62: Current conditions in the Bay of Skikda for the WNW direction (30).

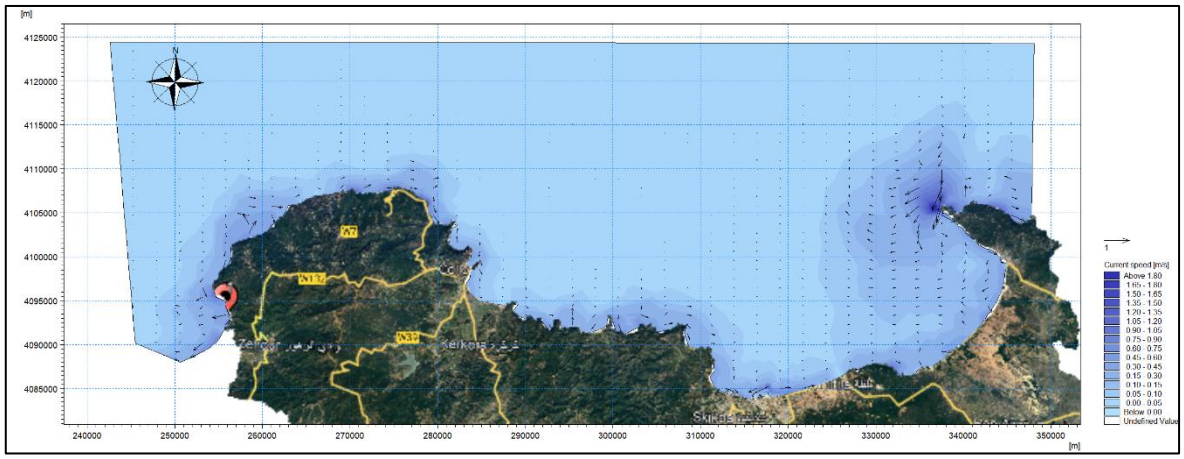

Figure 63: Current conditions in the Bay of Skikda for the NW direction (30).

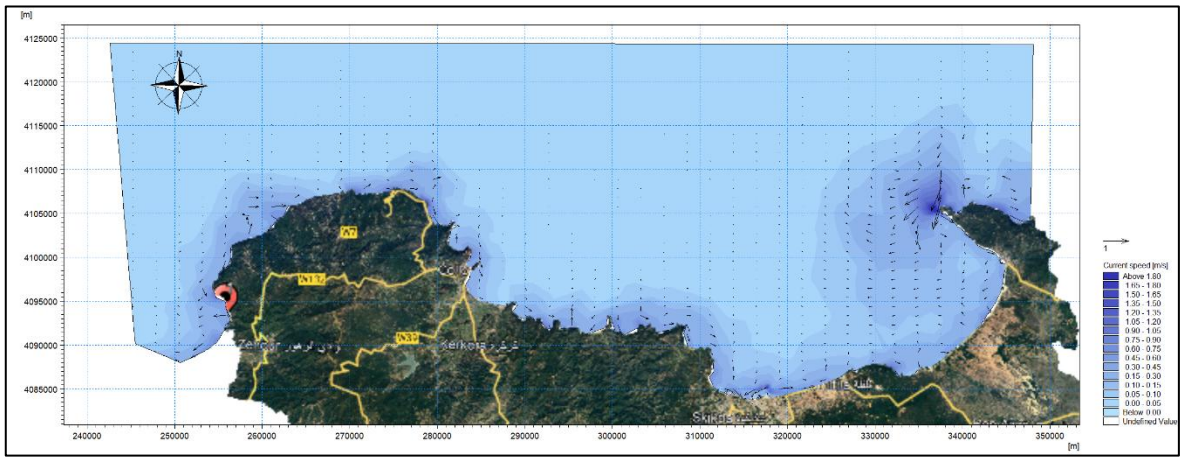

Figure 64: Current conditions in the Bay of Skikda for the NNW direction (30).

## Return period of 100 years

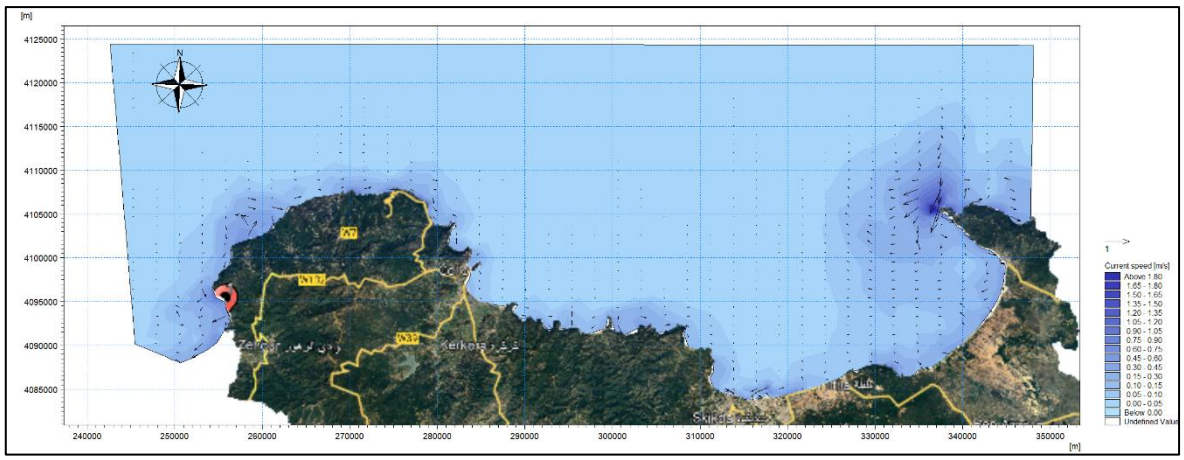

Figure 65: Current conditions in the Bay of Skikda for the WNW direction (100).

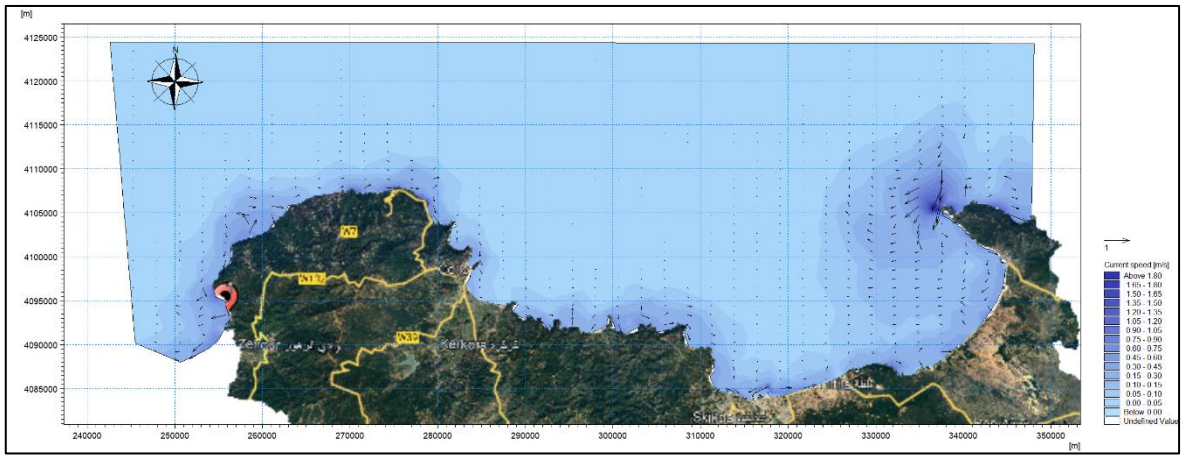


Figure 66: Current conditions in the Bay of Skikda for the NW direction (100).

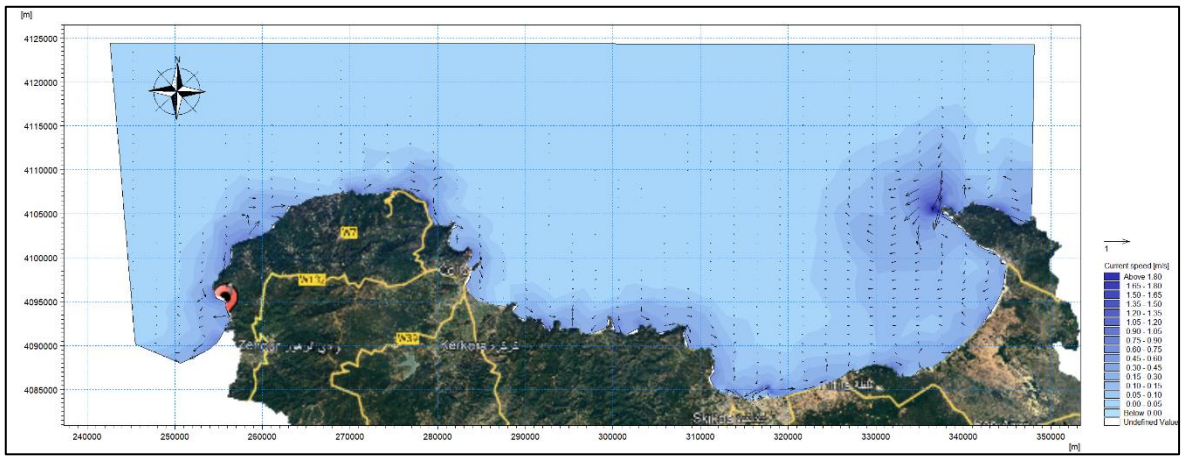


Figure 67: Current conditions in the Bay of Skikda for the NNW direction (100).

### V.5.3 Current conditions in Oued Saf-Saf

**Interpretation**

The circulation of currents in the Oued Saf-Saf area is highly heterogeneous (see Figures 68 to 76), influenced by the coastal configuration and prevailing oceanographic and meteorological conditions. Across different return periods, certain sectors, particularly near narrow passages or areas of hydrodynamic constriction, experience accelerated current velocities, while others, especially in more sheltered regions, exhibit reduced flow speeds, leading to stagnation zones or areas of low hydrodynamic activity.

## Return period of 10 years

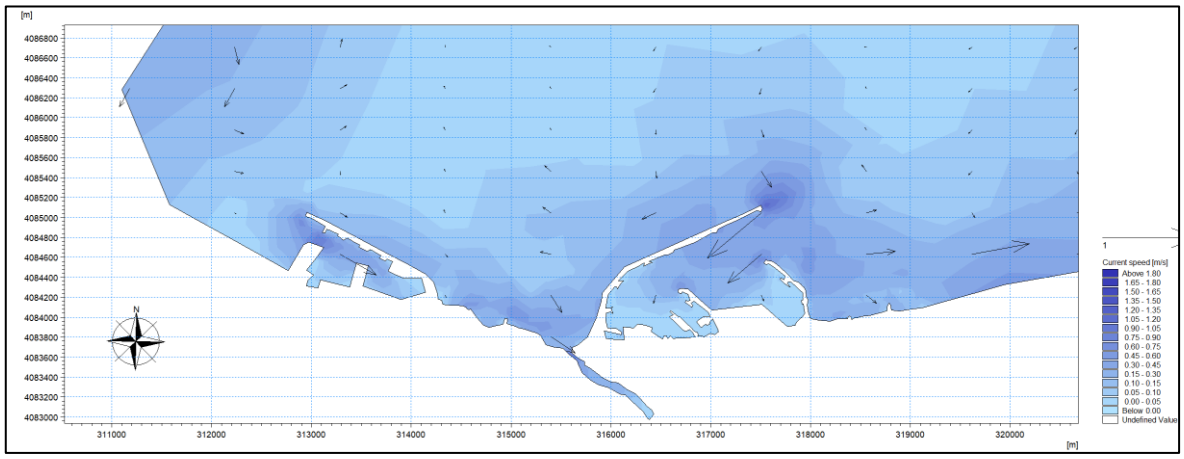


Figure 68: Current conditions in Oued Saf-Saf for the WNW direction (10).

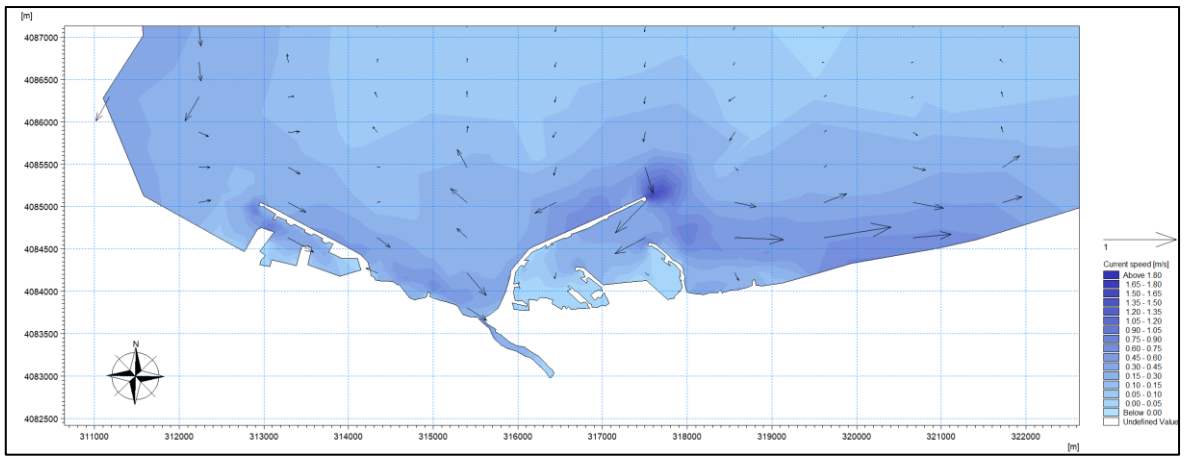


Figure 69: Current conditions in Oued Saf-Saf for the NW direction (10).

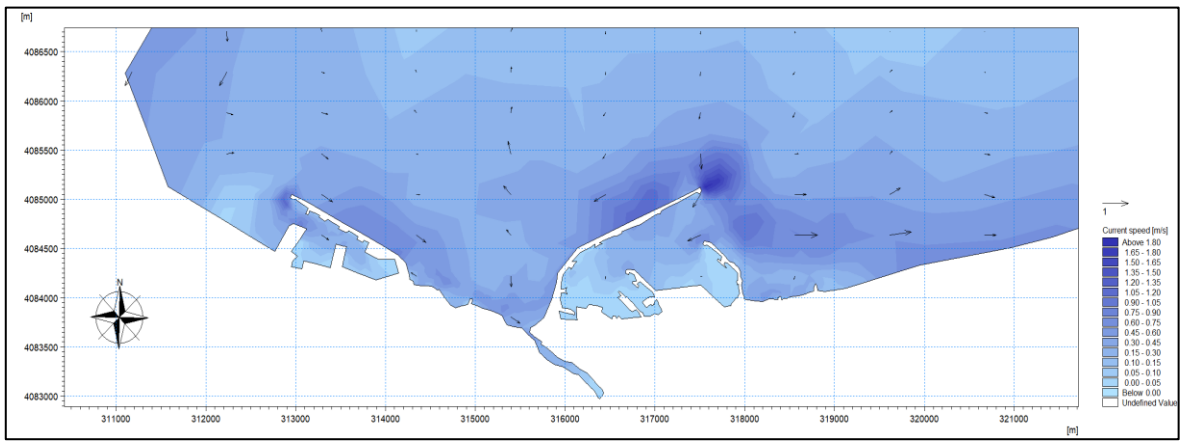


Figure 70: Current conditions in Oued Saf-Saf for the NNW direction (10).

## Return period of 30 years

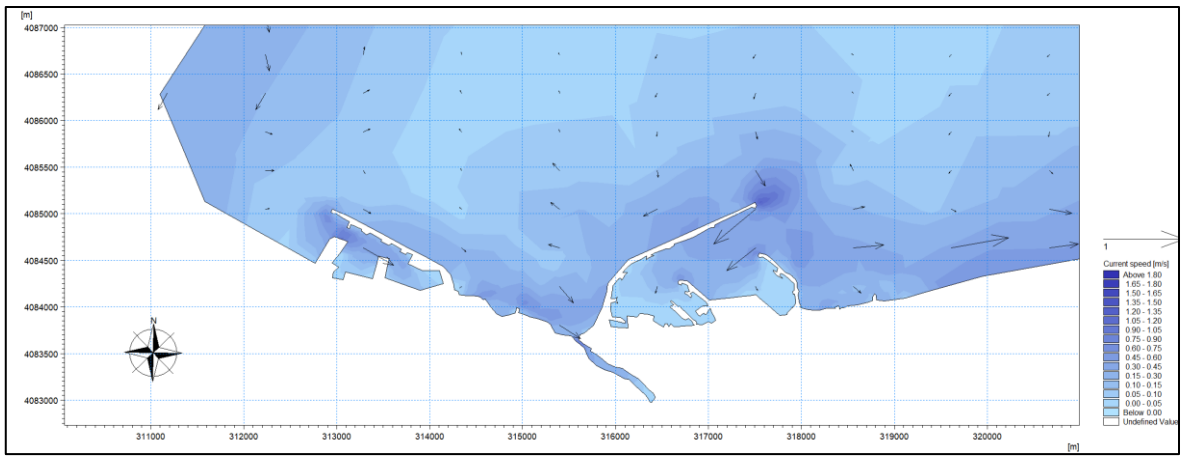


Figure 71: Current conditions in Oued Saf-Saf for the WNW direction (30).

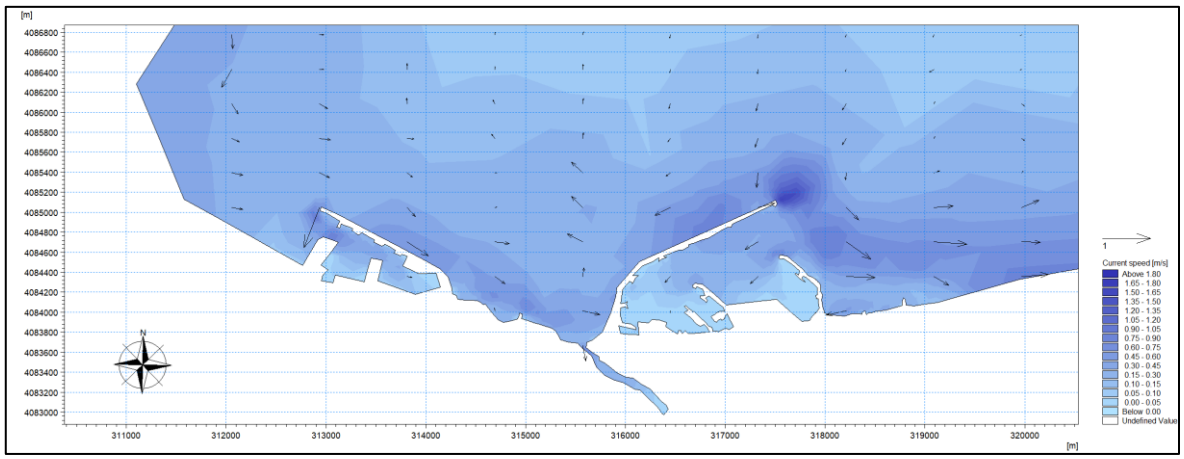


Figure 72: Current conditions in Oued Saf-Saf for the NW direction (30).

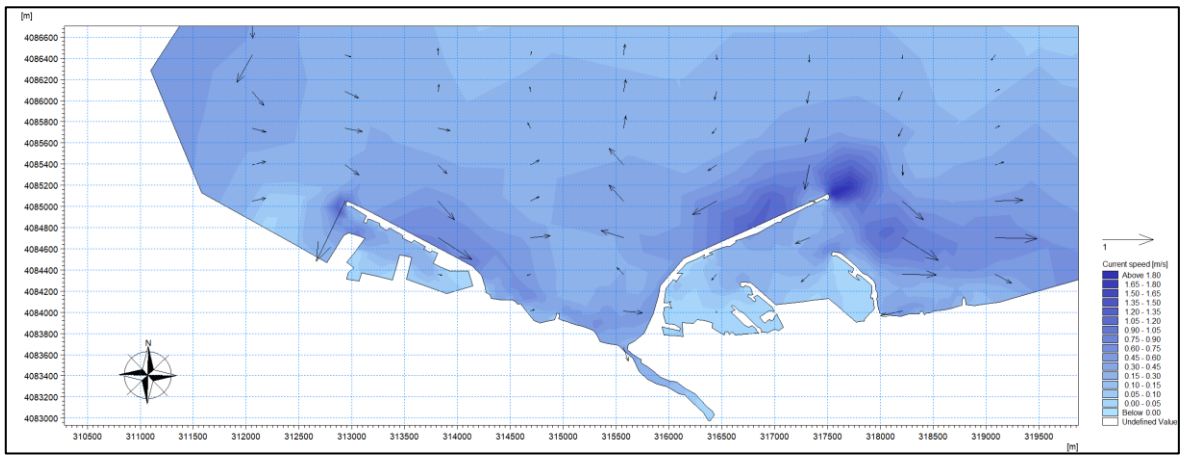


Figure 73: Current conditions in Oued Saf-Saf for the NNW direction (30).

## Return period of 100 years

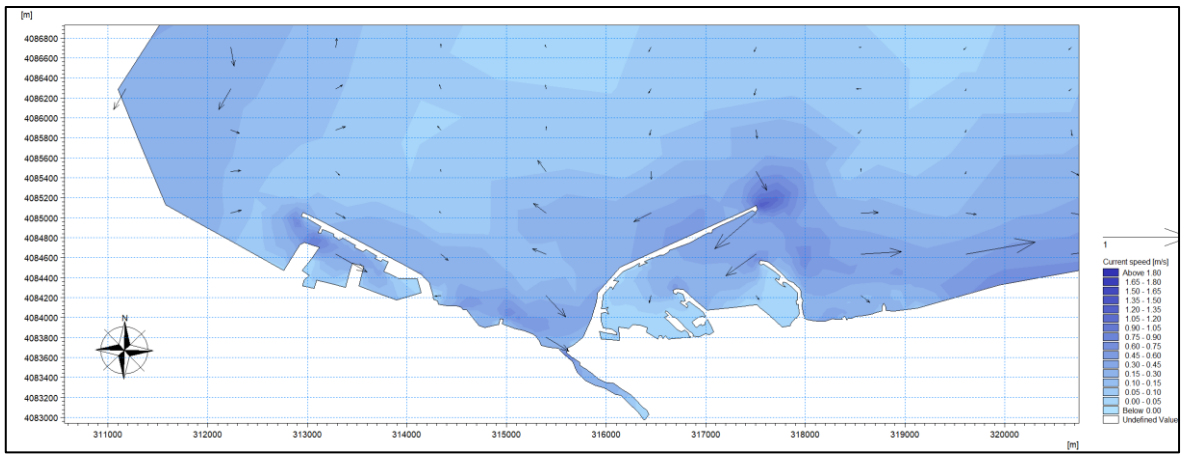


Figure 74: Current conditions in Oued Saf-Saf for the WNW direction (100).

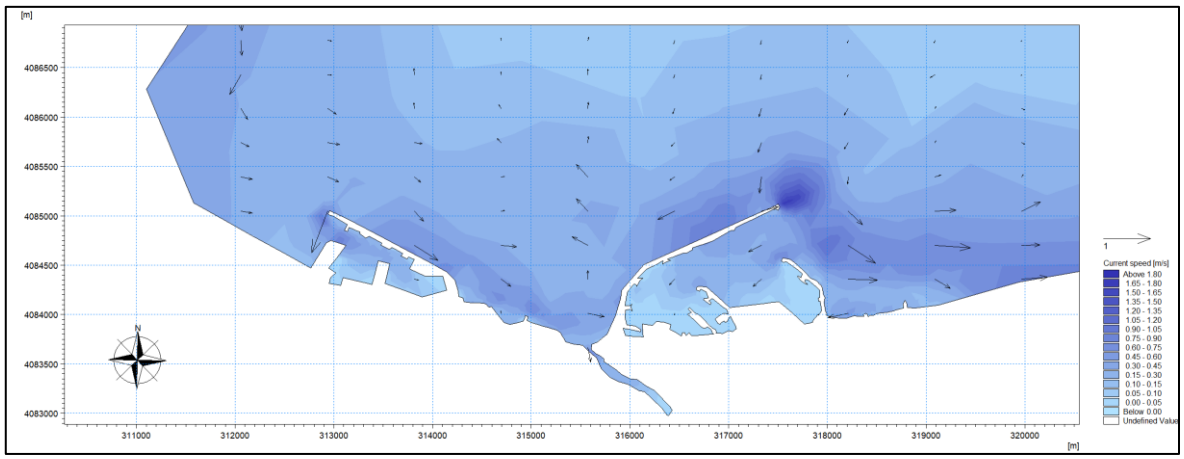


Figure 75: Current conditions in Oued Saf-Saf for the NW direction (100).

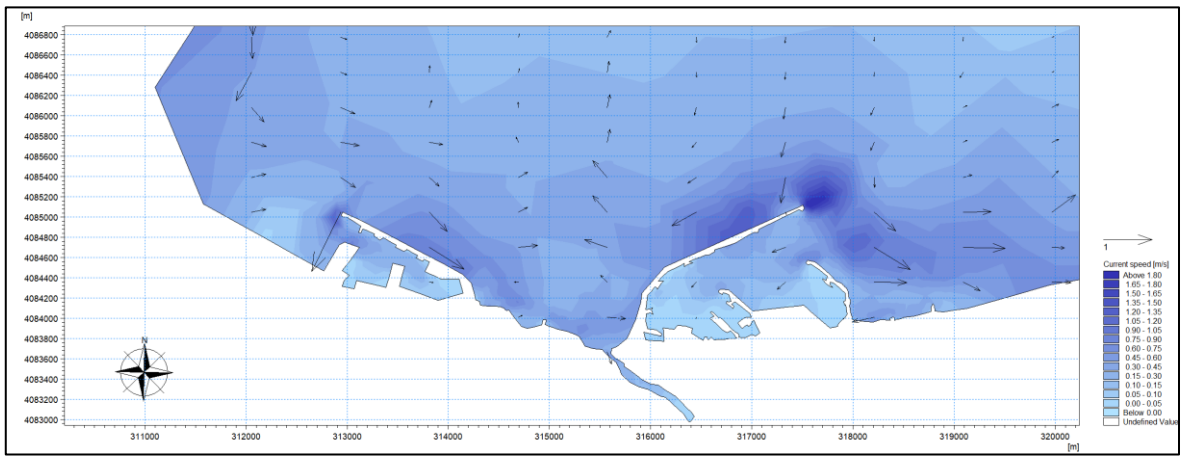


Figure 76: Current conditions in Oued Saf-Saf for the NNW direction (100).

**Conclusion**

The hydrodynamic analysis of Skikda Bay and its surrounding areas highlights the complex interactions between waves, currents, and coastal structures. Offshore, waves and currents retain significant energy, with wave heights exceeding 4.7m in exposed areas and currents exhibiting relatively uniform but strong velocities. As these hydrodynamic forces approach the coast, they undergo transformation due to seabed friction, diffraction, refraction, and bathymetric variations. In certain regions, such as headlands and narrow passages, current velocity intensifies due to flow constriction, whereas in more sheltered areas, including port infrastructures and enclosed bays, both wave energy and current speeds decrease due to dissipation and recirculation effects.

In the specific case of Oued Saf-Saf, current circulation remains highly heterogeneous across different return periods, with some areas experiencing significant acceleration while others exhibit stagnation zones. These findings emphasize the crucial role of coastal morphology, human-built structures, and local hydrodynamic conditions in shaping wave and current behaviors, ultimately influencing coastal erosion, sediment transport, and navigability.

# Chapter VI: Coastal Flooding

# VI.1 Introduction

Coastal flooding is a significant environmental hazard that threatens coastal communities worldwide, especially in the context of climate change and rising sea levels. The city of Skikda, located along the northeastern Mediterranean coast of Algeria, is particularly vulnerable due to its low-lying topography, growing urban infrastructure, and proximity to the sea. Understanding the dynamics of coastal flooding in this region is critical for effective risk management and sustainable coastal planning.

This study help us to analyze the risk and extent of coastal flooding in Skikda by analyzing historical and recent datasets, including satellite imagery, topographic and bathymetric data, and wave and tide patterns. The research will also consider the influence of extreme weather events, sea-level rise, and human interventions such as coastal infrastructure and land reclamation.

By integrating Geographic Information System (GIS), this study will identify zones at risk of flooding, quantify the potential effects.

# VI.2 Coastal Flooding simulation methodology

As part of this study, the delineation and mapping of coastal areas potentially exposed to marine flooding were carried out based on sea level rise scenarios. These scenarios were modeled using ArcGIS 10.4 software, with the goal of estimating potential effects at various future time horizons, namely the years 2030, 2050, and 2120.

The method adopted for estimating the coastal flooding hazard is based on:

- The calculation of extreme coastal water levels corresponding to return periods of 10 years, 30 years, and 100 years was carried out by taking into account several contributing factors: wave set-up, wind set-up and sea level rise associated with a drop in atmospheric pressure.
- In the second step, the simulated water levels were overlaid onto a Digital Elevation Model (DEM) of the study area with a spatial resolution of 30m, in order to identify and map potentially flood-prone areas. It is important to note, however, that for greater accuracy, a high-resolution DEM (between 0.5m and 1m) would be preferable. Nevertheless, the methodology applied remains the same.

### VI.2.1 Extreme water level scenarios

In the absence of data regarding storm surges, water level drops, tide gauge records, and offshore storm activity along the study area's coastline, flood levels were calculated using the equation developed by Hoozmans et al. (1993), this equation is widely used to estimate coastal areas that are potentially prone to flooding due to sea level rise. This equation allows for the simulation of inland water propagation by assuming a uniform rise in sea level, and is primarily based on overlaying the projected water level onto a Digital Elevation Model (DEM). It assumes that, under certain conditions (absence of coastal defenses, freely floodable terrain, etc.), any area with an elevation lower than or equal to the simulated water level is likely to be inundated.

Equation 12

$$Dft = MHW + St + Wf + Pf$$

$MHW$: Mean High Water level.
$St$: Relative Sea level rise.
$Wf$: Storm wave height responsible for flooding.
$Pf$: Sea level elevation due to atmospheric pressure.

In our study case:

The mean high water level ($MHW$)was obtained from the Tides4Fishing website.

Relative sea level rise ($St$) data were extracted from NASA's Sea Level Change website.

Based on the simulation results obtained from the numerical modeling and the bathymetric data, NNW is the direction from which the highest waves come during all the three return periods so the storm wave height for flooding ($Wf$) were calculated and are summarized in the table below:

Table 8: Mean heights of extreme waves at breaking point.

| **Return period (years)** | **10** | **30** | **100** |
|---|---|---|---|
| **Average wave heights (m)** | 2,4 | 3,2 | 3,5 |

Sea level is influenced by fluctuations in atmospheric pressure, a phenomenon known as the inverse barometric effect. When atmospheric pressure decreases, sea level rises (storm surge). Conversely, a rise in pressure causes the sea level to drop (negative surge). So, the sea level elevation due to atmospheric pressure ($Pf$) can be approximated using the following mathematical formula:

Equation 13

$$Z = 0.01 \times (1013 - p)$$

P: atmospheric pressure in hectopascals (hPa).
1013 hPa: standard sea level pressure at rest.

The atmospheric pressure data were extracted from the Wofrance website.

Ultimately, this leads us to the following table:

Table 9: Extreme flood levels.

| **Return period (years)** | **MHW (m)** | **St (m)** | **Wf (m)** | **Pf (m)** | **Dft (m)** |
|---|---|---|---|---|---|
| **10** | 0.50 | 0.10 | 2.4 | 0.12 | 3.12 |
| **30** | 0.50 | 0.20 | 3.2 | 0.12 | 4.02 |
| **100** | 0.50 | 0.87 | 3.5 | 0.12 | 4.99 |

### VI.2.2 Cartographic Study and Flood Scenarios

**Digital Elevation Model (DEM)**

Mapping is an essential tool for enhancing the visualization of scenario outcomes. For this purpose, a simulation was carried out in ArcGIS using a Digital Elevation Model (DEM) with a spatial resolution of 30m, in order to generate inundation maps for three return periods: 10, 30, and 100 years.

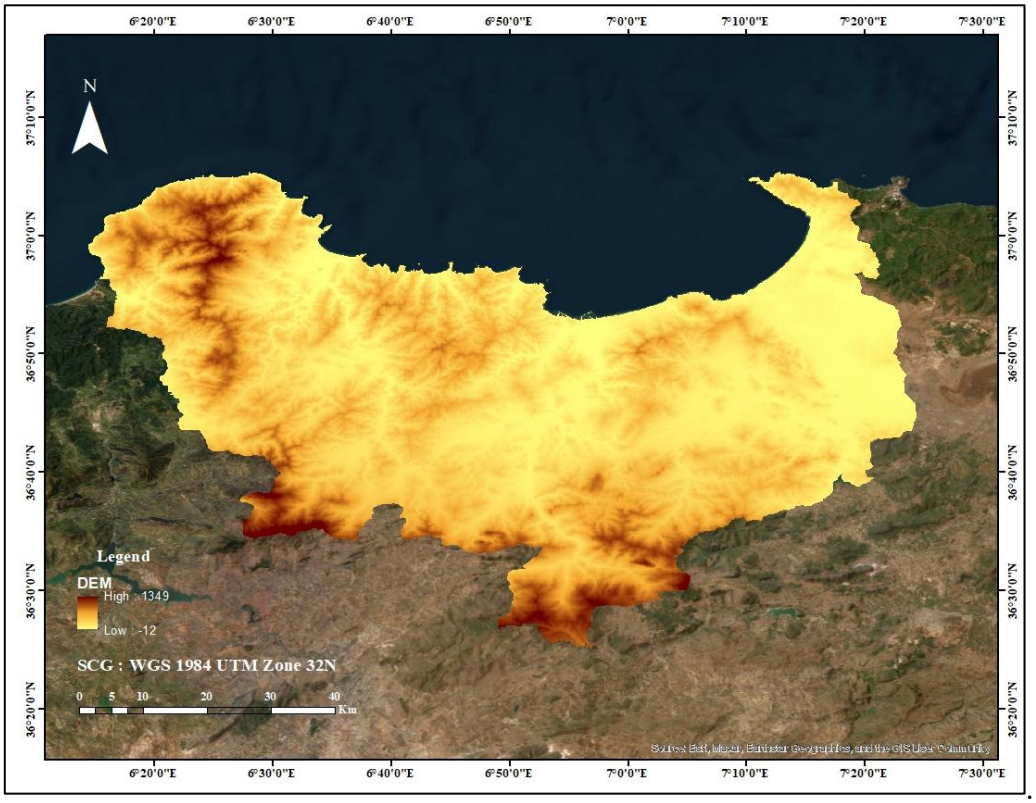


Figure 77: The Digital Elevation Model (DEM) of Skikda.

**Coastal Flooding**

**Interpretation**

**Submersion at 3m:**

According to the map, a sea level rise of 3m results in significant flooding of several coastal areas in Skikda Bay. The most affected zones are mainly located around oueds mouths and low-lying coastal regions. The marine intrusion in these areas is explained by the relatively flat topography and the proximity of hydrographic networks. The total area submerged is estimated at approximately 2583.4 ha, posing a serious threat to infrastructure, agricultural land, and nearby human settlements.

**Submersion at 4m:**

With a sea level rise of 4m, marine intrusion intensifies considerably. Flooded areas expand, especially around oueds mouths, where water reaches further inland. This progression is due to

the combined effects of low coastal elevation and oueds valleys that act as natural channels for water penetration. The affected surface area reaches around 3836.3 ha, increasing the risk to human activities and coastal ecosystems.

**Submersion at 5m:**

Under an extreme scenario of a 5m sea level rise, there is a dramatic inland advancement of seawater, potentially reaching several kilometers in vulnerable zones. Oueds mouths play a critical role in channeling water inland, leading to widespread flooding of both urban and agricultural areas. About 5022.3 ha of land would be submerged, highlighting a major risk for territorial development and the region's resilience to climate change consequences.

The following. Figures (78 to 81) illustrate the increasing impact.


Figure 78: Coastal Flooding map Skikda Bay.


Figure 79: Coastal Flooding map Oued El Kebir.

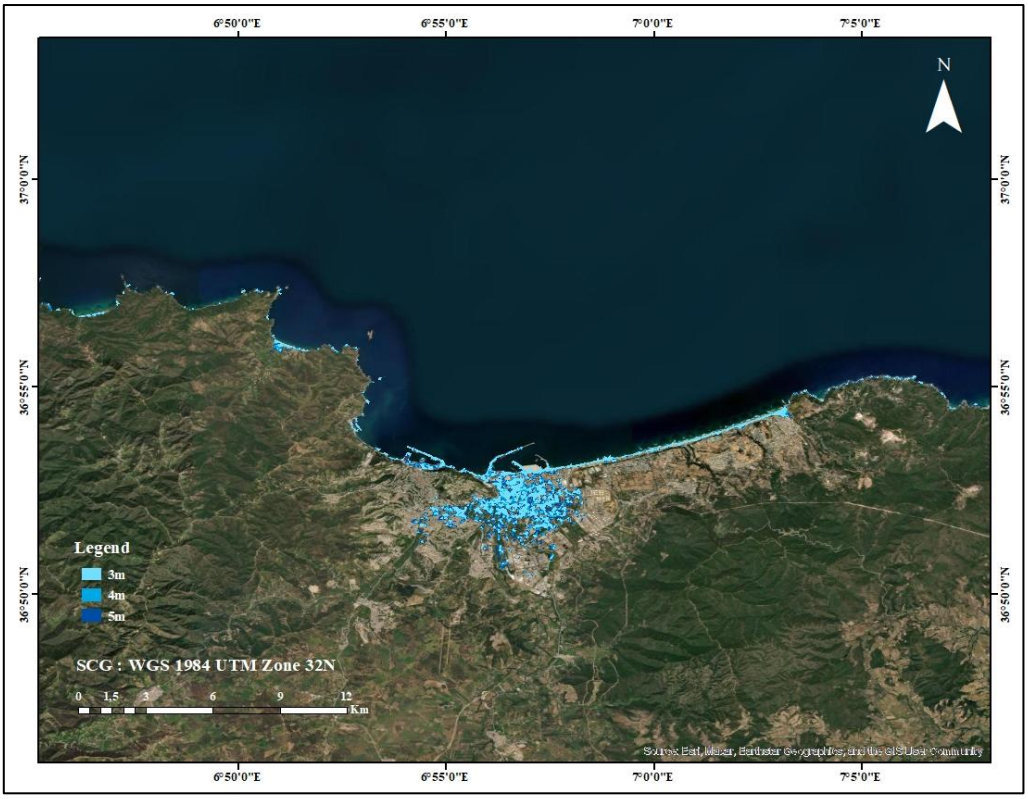


Figure 80: Coastal Flooding map of Oued Saf-Saf.


Figure 81: Coastal Flooding map of Oued El Guebli.

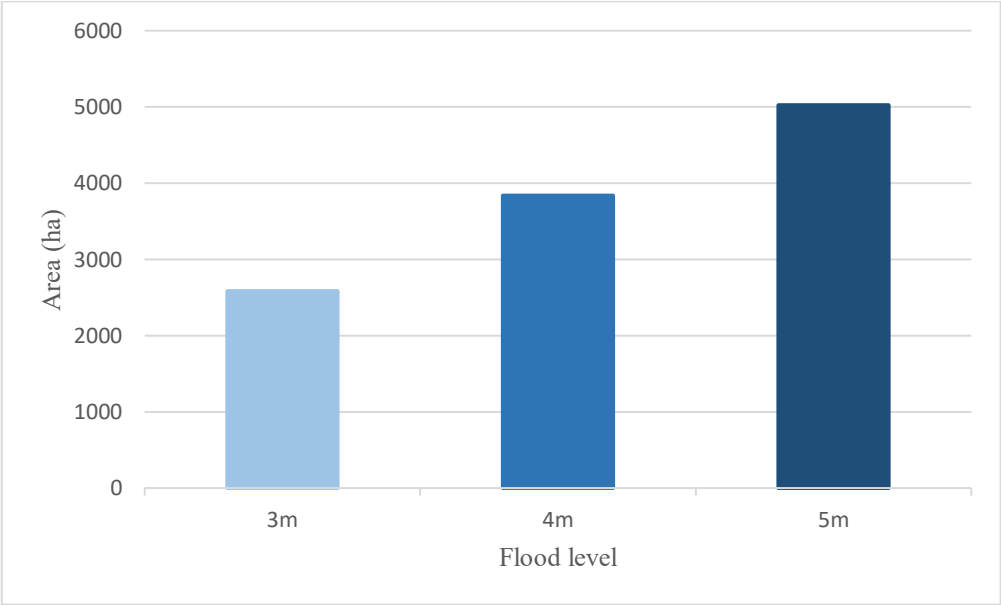


Figure 82: Bar Graph Showing Total Land Area Affected by Different Flood Levels.

## Land Cover

Land cover in the Skikda province is characterized by a diversity of environments, including forested, agricultural, and urban areas, as well as water bodies, wetlands, and bare soil. This distribution results from both the natural characteristics of the territory and human

development. It plays an important role in analyzing vulnerability to natural hazards, particularly the risk of marine submersion.

The data presented in the figure below was extracted from the ESRI Land Cover website, which provides reliable global land use information based on satellite imagery with a resolution of 10m.

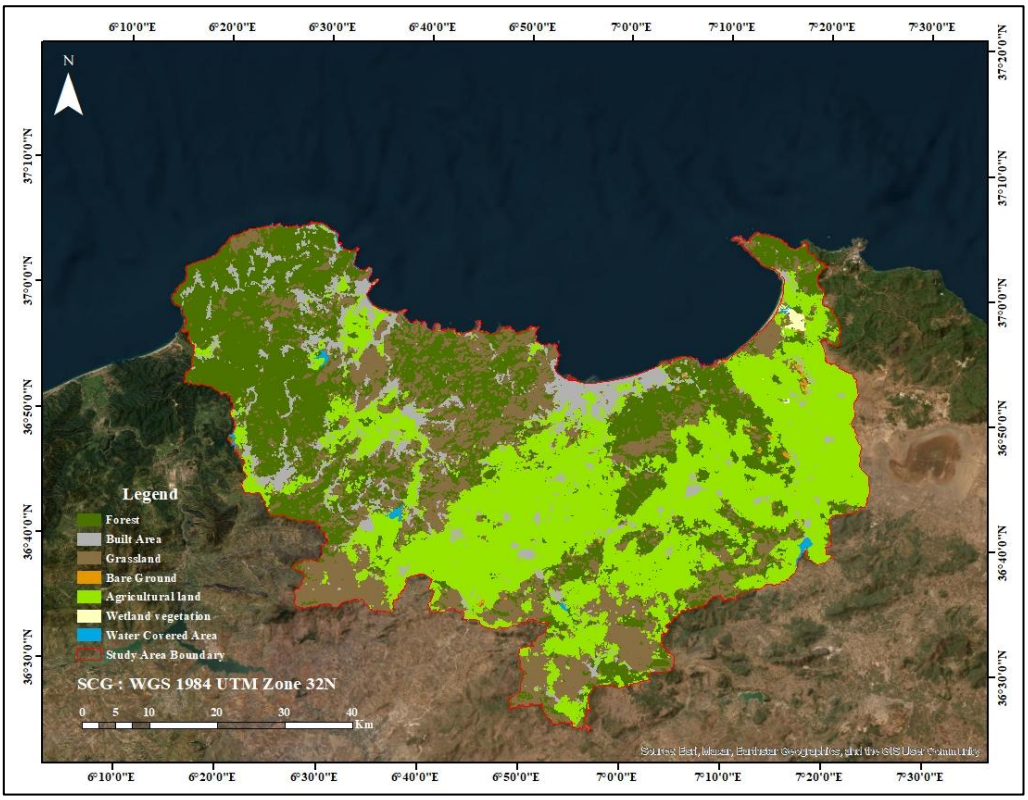


Figure 83: Land Cover map of Skikda.

By overlaying the coastal flooding results with the land cover map, it is possible to calculate the areas affected by flooding according to the type of land use. Table 9 summarizes these results.

The table shows that flood effect increases with rising flood levels across all land cover types. Wetland vegetation is the most vulnerable, with over 96% affected at a 5-m flood level, followed by bare ground (22%) and water-covered areas (9.21%). While forests are the least affected (0.10%), built-up and agricultural lands show significant absolute impacts, reaching 951.3 ha and 2422.7 ha respectively at the highest flood level. This highlights that even land types with lower percentage exposure can face substantial damage due to their large total area, indicating rising flood risks with longer return periods.

Table 10: Results of areas at risk of flooding.

| Land cover type | Total Area (ha) | Flood level 3m (Return period = 10 years) | | Flood level 4m (Return period = 30 years) | | Flood level 5m (Return period = 100 years) | |
|---|---|---|---|---|---|---|---|
| | | Area (ha) | Area (%) | Area (ha) | Area (%) | Area (ha) | Area (%) |
| **Water Covered Area** | 3132.5 | 233.3 | 7.45 | 267.7 | 8.55 | 288.6 | 9.21 |
| **Forest** | 180758.3 | 69.1 | 0.04 | 126.6 | 0.07 | 179.7 | 0.10 |
| **Grassland** | 73186.9 | 299.8 | 0.41 | 398.7 | 0.54 | 474.4 | 0.65 |
| **Bare Ground** | 658.9 | 122.3 | 18.56 | 135.0 | 20.49 | 144.9 | 22.00 |
| **Built Area** | 32515.8 | 482.9 | 1.49 | 725.1 | 2.23 | 951.3 | 2.93 |
| **Agricultural land** | 123608.8 | 930.5 | 0.75 | 1664.3 | 1.35 | 2422.7 | 1.96 |
| **Wetland vegetation** | 399.9 | 318.3 | 79.59 | 371.3 | 92.85 | 385.9 | 96.50 |

## Conclusion

The results indicate that sea level rise, combined with extreme weather conditions, could lead to significant coastal flooding in the Skikda region. The mapping of potentially flooded areas reveals that approximately 2583,4 ha could be submerged in the event of a 3m marine flood, while a 4m level would affect around 3836,3 ha, and an extreme scenario of 5m could inundate up to 5022,3 ha.

These values reflect an increasing vulnerability of the coastline as sea levels rise. The low elevation of coastal terrain, particularly near the mouths of oueds, facilitates the inland intrusion of seawater. Regardless of the flood level considered, the impacts on urban areas, harbor infrastructure, and coastal agricultural land would be significant highlighting the urgent need for integrated coastal planning and adaptation strategies in response to climate change.

# Chapter VII: Inundation

# VII.1 Introduction

Hydraulics plays a fundamental role in the study and management of flood events, which can severely affect infrastructure, natural environments, and human settlements. Flooding is often triggered by a combination of factors, including the intensity, duration, and spatial distribution of precipitation, as well as extreme events occurring in estuarine and downstream areas.

This chapter focuses on studying the flood vulnerability of the Oued Saf-Saf and the bridge that spans it. The study is limited exclusively to Oued Saf-Saf, as it is the only watershed for which high-resolution data is available. The objective is to identify areas at risk, analyze the hydrological behavior of the watercourse, and evaluate the potential impacts of flooding on the structural integrity of the bridge and the surrounding environment.

Figure 84: Image of the studied section of Oued Saf-Saf.

# VII.2 Methodology

## VII.2.1 Data collection

The data used in this study include

- A topographic survey.
- Intensity-Duration-Frequency (IDF) curves.

- Field data collected on site.

This data was provided by SAETI (Société Algérienne d'Études Techniques et d'Infrastructure).

### VII.2.2 Hydrological and Hydraulic Parameter Estimation

In our study, the watershed in question is considered ungauged, meaning that there are no measurement stations available to directly record the streamflow. In the absence of hydrometric data, it becomes necessary to estimate the peak discharge using indirect methods. For this purpose, we apply the Rational Method, which is commonly used for small urban or rural catchments. This method is based on the principle that the peak discharge is proportional to the rainfall intensity, the watershed area, and a runoff coefficient that reflects the land's ability to generate surface flow.

Equation 14

$$Q = \frac{C \cdot I \cdot S}{3.6}$$

Where:

- $C$: Runoff coefficient for a return period T.
- $I$: Average rainfall intensity (in mm/h) corresponding to a return period T and a Rainfall duration $T_c$.
- $S$: Watershed area (km²).
- $Q$: Projected peak discharge for a given return period (m³/s).

**Runoff coefficient**

The runoff coefficient is a parameter used in hydrology to estimate the proportion of rainfall that flows over the land surface rather than infiltrating into the soil. It reflects the amount of water that becomes surface runoff in relation to the total rainfall received. This coefficient is influenced by various factors, including soil type and permeability, land slope, vegetation cover, drainage area size, and prevailing weather conditions. It is commonly used in the design of drainage systems, the study of rainfall impact on the environment, and the management of water resources.

According to the Rational Method, the calculation of rainwater runoff involves three key coefficients: $C_1$, which represents the influence of slope; $C_2$, which accounts for the type of soil; and $C_3$, which reflects the vegetation cover of the area. These individual coefficients are summed to obtain the overall runoff coefficient (C), a key parameter used to estimate the discharge resulting from rainfall. By evaluating these three factors, the method provides a more accurate understanding of how different landscape characteristics impact rainwater runoff. The specific values of these coefficients are detailed in the following tables.

- Coefficient C1: Slope (%)

Table 11: The values of the runoff coefficient C1 based on the terrain slope **(SAETI, 2023)**.

| Slope (%) | C1 | | |
|---|---|---|---|
| **≤ 3.5 %** | 0.01 | 0.03 | 0.05 |
| **Between 3.5 and 11 %** | 0.06 | 0.08 | 0.10 |
| **Between 11 and 35 %** | 0.12 | 0.16 | 0.20 |
| **> 35 %** | 0.22 | 0.26 | 0.30 |

- Coefficient C2: Soil type

Table 12: The values of the runoff coefficient C2 according to the soil type **(SAETI, 2023)**.

| Soil type | C2 | | |
|---|---|---|---|
| **Impermeable** | 0.22 | 0.26 | 0.30 |
| **Slightly permeable** | 0.10 | 0.15 | 0.20 |
| **Permeable** | 0.06 | 0.08 | 0.10 |
| **Very permeable** | 0.03 | 0.04 | 0.05 |

- Coefficient C3: Vegetation cover

Table 13: The values of the runoff coefficient C3 based on land cover or vegetation **(SAETI, 2023)**.

| Vegetation cover | C3 | | |
|---|---|---|---|
| **Rocky** | 0.22 | 0.26 | 0.30 |
| **Grassland** | 0.17 | 0.21 | 0.25 |
| **Plowed fields** | 0.07 | 0.11 | 0.15 |
| **Forest and sandy areas** | 0.03 | 0.04 | 0.05 |

### Average rainfall intensity

The average rainfall intensity for a given duration and return period can be estimated using the Intensity–Duration–Frequency (IDF) empirical relationship. This formula is widely used in hydrology to evaluate rainfall intensities associated with specific return periods.

Equation 15

$$I = \frac{P(t)}{P\,jmax} = a \times {T_c}^{-b}$$

Where:

- $I$: Average rainfall intensity (mm/h) for a rainfall event of duration t.
- $P(t)$: Rainfall depth over a duration t (generally equal to the time of concentration), in mm.
- $P\ jmax$: Maximum daily rainfall (over 24 hours), in mm.
- $T_c$: Rainfall duration (hours).
- $a, b$: Empirical (or climatic) parameters, specific to each region and return period this is known as the MONTANA method

The application of this model to our station yielded the following form:

Equation 16

$$I(t,T) = \frac{a(T)}{t^{0,62}}$$

This means the exponent $b$ = 0.62, and is considered constant for this location and the coefficient a varies with the return period T.

Table 14: Values of the parameter a(T).

| T(years) | 2 | 5 | 10 | 20 | 50 | 100 |
|---|---|---|---|---|---|---|
| a(T) | 21,4 | 29,2 | 34,4 | 39,3 | 45,7 | 50,5 |

The Rainfall duration is the time it takes for a water particle falling at the highest and most distant point of a watershed to reach the outlet (the downstream exit point of the basin). In other words, it represents the time required for water to travel across the entire watershed through its natural drainage network.

The calculation of the Rainfall duration depends on the surface area of the watershed, as flow dynamics vary with basin size. Different empirical formulas are therefore used depending on the watershed's extent:

- For a watershed area less than 5 km²: Ventura's formula is used:

Equation 17

$$T_c = 0,127 \times \sqrt{\frac{S}{I_m}}$$

Where:

$T_c$: Rainfall duration (hours).

$S$: Watershed area (km²).

$I_m$: Average slope of the watershed (m/m).

- For a watershed area between 5 km² and 25 km²: Passini's formula is applied:

Equation 18

$$T_c = 0{,}11 \times \frac{\sqrt[3]{S \times L}}{\sqrt{I_m}}$$

Where:

$L$: Length of the main watercourse (km).

- For a watershed area between 25 km² and 200 km²: Giandotti's formula is used:

Equation 19

$$T_c = \frac{4\sqrt{S} + 1{,}5 + L}{0{,}8\sqrt{H_{moy} - H_{min}}}$$

Where:

$H_{moy}$ : Average altitude of the basin (m).

$H_{min}$: Minimum altitude of the basin (m).

In the case of the Skikda watershed, with a surface area of 1155 km², the size exceeds the typical upper limit of 200 km². Nevertheless, Giandotti's formula is still commonly used for large basins because it takes into account not only the surface area, but also the main stream length and key elevation differences within the basin. Therefore, Giandotti's formula is adopted for calculating the concentration time in our study.

Table 15: Results table of the Rational Method.

| T (years) | S (km2) | P (km) | L (km) | Slope (%) | C1 | C2 | C3 | C | Hmin (m) | Hmoy (m) | Tc (h) | I (mm/h) | Q (m3/s) |
|---|---|---|---|---|---|---|---|---|---|---|---|---|---|
| **2** | 1155 | 182 | 73 | 2% | 0.03 | 0.15 | 0.15 | 0.33 | 30 | 317 | 18.11 | 3.55 | 376 |
| **10** | 1155 | 182 | 73 | 2% | 0.03 | 0.15 | 0.15 | 0.33 | 30 | 317 | 18.11 | 5.71 | 605 |
| **100** | 1155 | 182 | 73 | 2% | 0.03 | 0.15 | 0.15 | 0.33 | 30 | 317 | 18.11 | 8.39 | 888 |

### VII.2.3 Data Processing of the Topographic Survey Conducted in Oued Saf-Saf

In this critical stage of the hydraulic modeling process, two complementary software programs are utilized: AutoCAD Civil 3D, for processing topographic data, and HEC-RAS, for simulating hydraulic flow. The work begins with the manipulation of the topographic survey conducted along the Oued Saf-Saf using Civil 3D. This operation involves utilizing the terrain's altimetric data to digitally reconstruct the configuration of the oued bed and its banks.

Initially, the main flow line is defined. It represents the longitudinal axis followed by the water along the watercourse. This line is important for identifying the natural direction of

flow, calculating the flow lengths between cross-sections, and modeling the evolution of water heights along the Oued.

Next, 14 cross-section lines were generated. These are profiles created perpendicular to the oued bed, allowing the precise capture of the hydraulic section geometry at different points along the route. These lines are essential for representing the variations in shape and slope of the oued bed, and they form one of the key elements of hydraulic analysis.

Once these geometric elements are properly established, they are exported in a specific format compatible with the HEC-RAS software. This export marks the transition to the next phase of the project, namely the actual hydraulic simulation. HEC-RAS will then simulate the behavior of flow under normal or extreme conditions and analyze the areas potentially exposed to flooding risks.

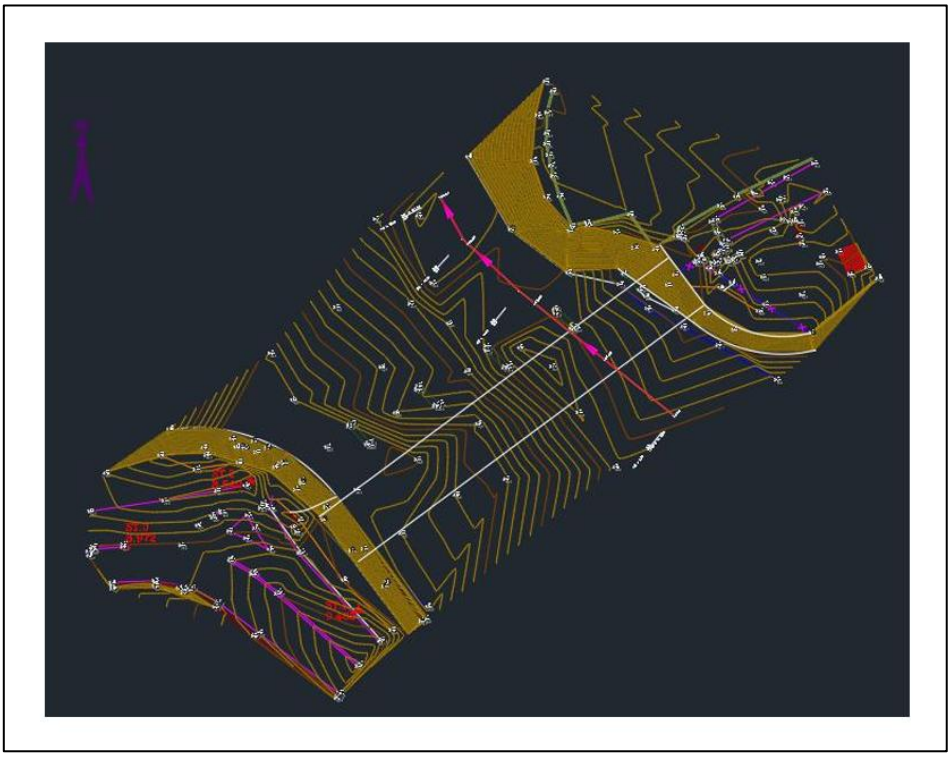

Figure 85: 3D Topographic Model of the Oued Saf-Saf Oued bed with the Flow Line.

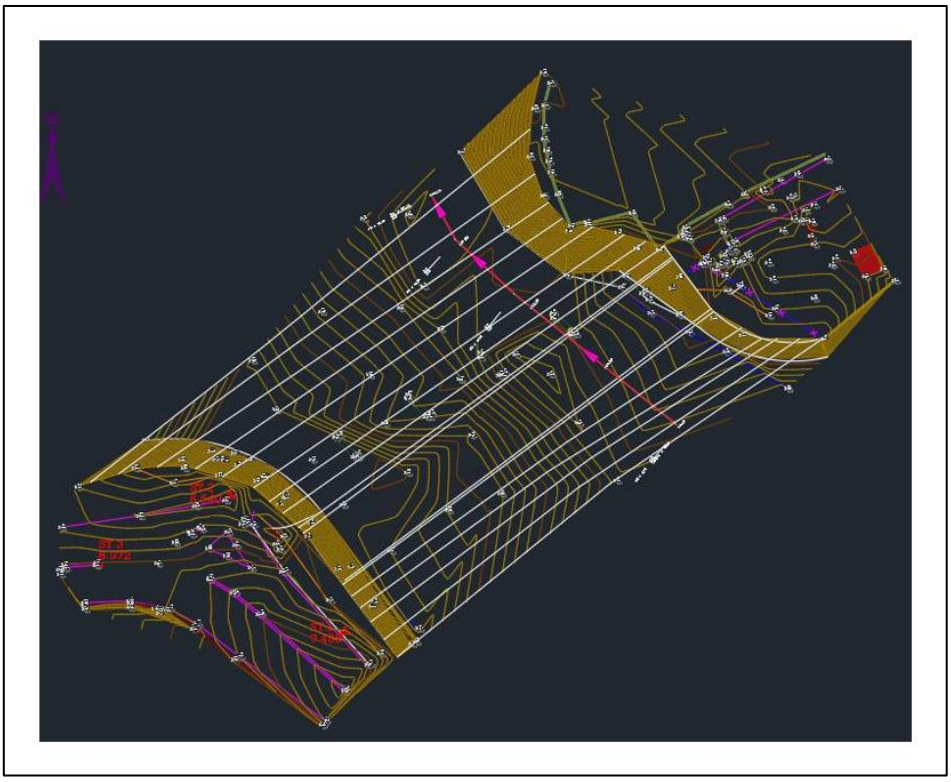

Figure 86: 3D Topographic Model of the Oued Saf-Saf Oued bed with the Flow Line and Cross-Section Lines.

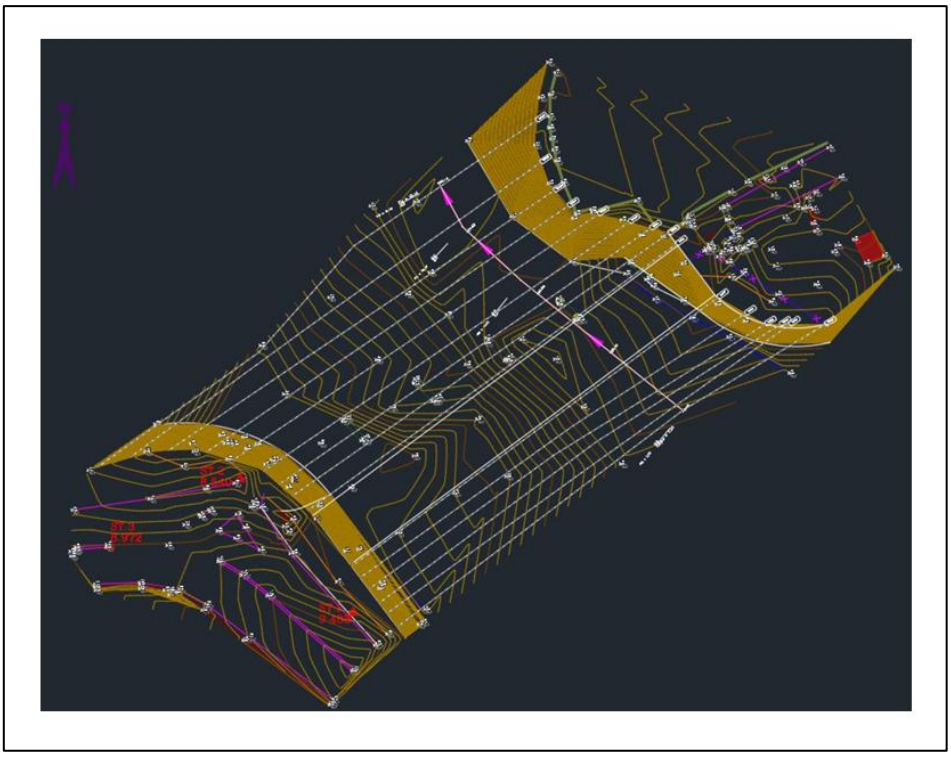

Figure 87: 3D Topographic Model of the Oued Saf-Saf Oued bed with the Flow Line and Cross-Section Lines after treating.

### VII.2.4 Hydraulic Modeling of Oued Saf-Saf Using HEC-RAS

This stage of the study involves simulating the hydraulic behavior of Oued Saf-Saf using the HEC-RAS software. The goal is to evaluate the variations in water surface elevation for return periods of 2, 10, and 100 years, while accounting for both the current oued bed morphology and planned hydraulic structures.

To carry out these simulations, two core datasets are required. The first consists of geometric data generated in AutoCAD Civil 3D, which includes the topographic model, cross-section profiles, and the main flow path. This geometric foundation accurately represents the physical characteristics of the oued and underpins the hydraulic modeling process.

The second essential input is the discharge (Q), previously estimated based on hydrological analysis. This value reflects the peak flow expected for each return period and is a critical driver of the model's output.

Beyond these primary inputs, two boundary conditions must be defined: the channel slope and the roughness coefficient. The slope corresponds to the longitudinal gradient of the oued bed, while the roughness coefficient commonly known as Manning’s coefficient reflects the resistance exerted by the channel surface on the water flow.

Manning’s coefficient plays a central role in determining flow behavior. It expresses the friction between the moving water and the channel boundaries, directly influencing both flow velocity and water depth along the oued course. Its value varies depending on the composition and condition of the oued bed whether natural, vegetated, or engineered. For this reason, precise estimation of this parameter is vital to ensure realistic and reliable simulation outcomes.

Once all necessary parameters are defined and input into the HEC-RAS environment, the model is run to simulate water flow dynamics. The output will allow for an in-depth interpretation of how the oued responds to extreme flow conditions, particularly in terms of potential overtopping, submersion, and stress on the designed infrastructure.

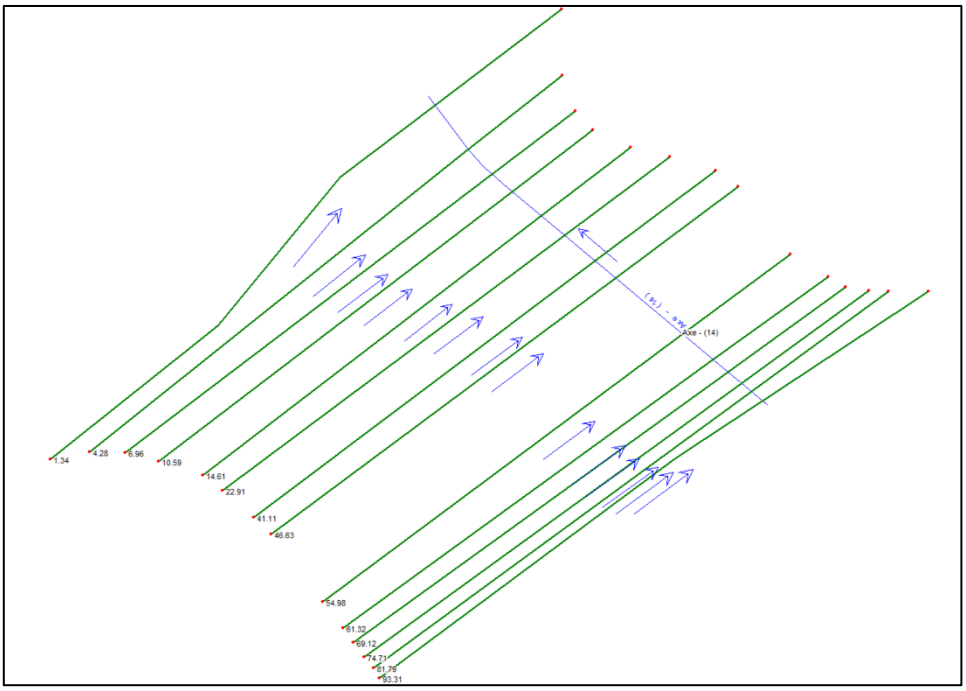


Figure 88: Representation of Cross-Sections and Flow Path in the HEC-RAS Geometric Interface.

## VII.3 Hydraulic Simulations

In hydraulic modeling with HEC-RAS, it is essential to define both the upstream and downstream boundaries of the oued reach. These boundaries represent the entry and exit points of the flow within the system and play a key role in guiding the simulation. In this study, a slope value of 0.007 was assigned to both the upstream and downstream boundaries. This uniform value was selected to reflect a relatively consistent longitudinal gradient observed along the modeled reach of Oued Saf-Saf. Using the same slope at both ends helps ensure a stable flow profile, particularly in simplified modeling scenarios where the terrain does not show abrupt changes in elevation. To study the hydraulic behavior of Oued Saf-Saf under different hydrological conditions, a series of simulations were carried out using the HEC-RAS software. These simulations seek to model the water surface profiles corresponding to flood events with return periods of 2, 10, and 100 years. Each scenario provides valuable insight into how the oued system responds to varying flow magnitudes, particularly in terms of water level distribution and potential flood risks. The analysis was conducted along 14 cross-sections, which were previously defined and imported into the model from topographic data processed in AutoCAD Civil 3D. Each cross-section is uniquely identified by a River Station number; a system used in HEC-RAS to organize the geometry along the oued reach. These numbers generally surge in the upstream direction and are based on the distance from the end of the oued, providing a clear reference for analyzing flow characteristics from downstream to upstream. As a result, each simulation (corresponding to a different return period) produces a set of 14 water surface elevation outputs, one for each cross-section. Each result includes the Energy Grade Line (EG) and the Water Surface (WS), which together describe the hydraulic profile and flow energy at every location. This structured approach allows for a detailed comparison of hydraulic behavior along the entire modeled reach, highlighting the sections most vulnerable to high water levels or overflow under extreme conditions.

### VII.3.1 Results of the Hydraulic Simulations

**Return period of 2 years**

**Interpretation**

The cross-section profiles for the 2-year return period (Figures 89 and 90) indicate a stable and well-contained flow throughout the modeled section of the oued. At stations such as 10.59 and 4.28, the water surface (WS) remains well below the elevation of the banks, and the energy grade line (EG) stays close to the WS, reflecting a uniform and subcritical flow regime. Even at station 1.34, where a small surge in WS is observed, the water remains comfortably within the channel. There are no signs of overtopping, irregularities, or critical conditions, and the flow remains mild and predictable. Overall, the oued handles this level of discharge with ease, showing that under the 2-year return period, it operates efficiently and safely within its natural capacity.

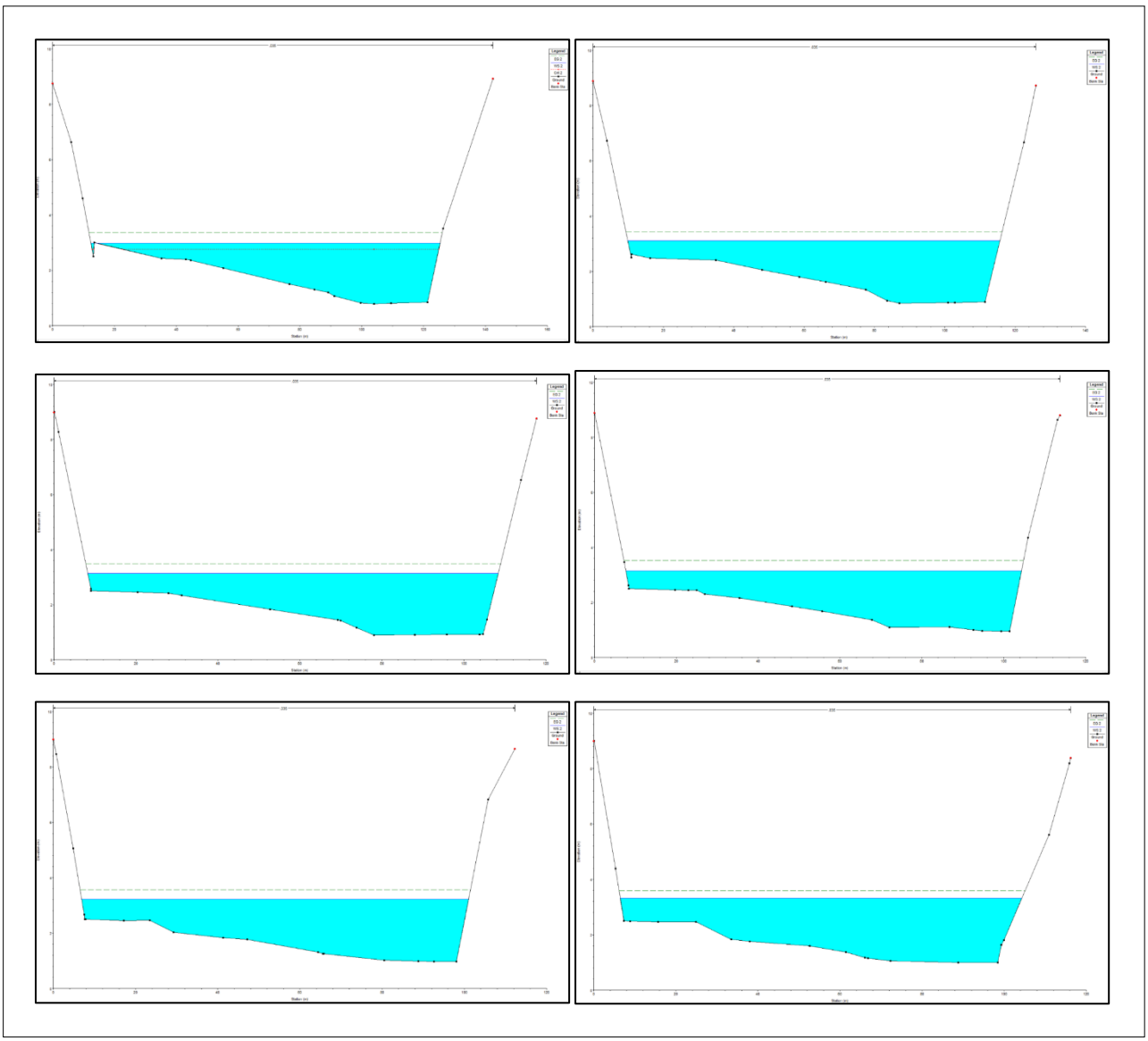

Figure 89: Simulation results of Oued Saf-Saf at River Stations 1.34m to 22.91m (2 years).

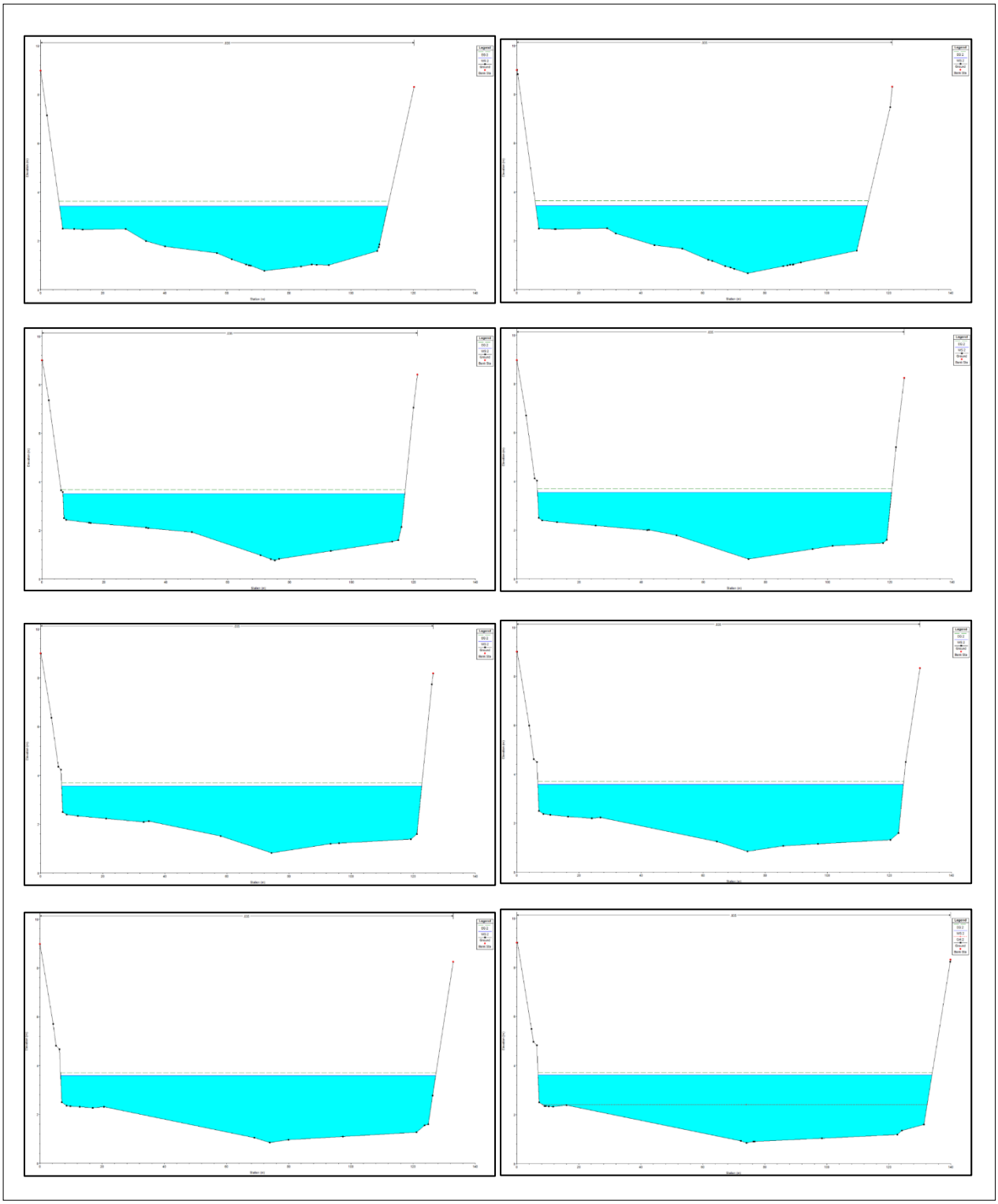

Figure 90: Simulation results of Oued Saf-Saf at River Stations 41.11m to 93.31m (2 years).

### Return period of 10 years

### Interpretation

Under the 10-year return period (Figures 91 and 92), the oued begins to respond more noticeably to the increased discharge. At station 10.59, the water surface rises compared to the

2-year scenario, moving closer to the top of the banks, and the energy grade line becomes more inclined, indicating a rise in flow velocity and energy. As we move downstream to stations like 4.28 and especially 1.34, the WS remains within the banks but with significantly less freeboard. The critical depth line becomes visible at 1.34, signaling a local shift in flow regime and approaching critical conditions. However, even with these changes, the oued still manages to contain the flow without flooding. The increased water levels and energy indicate that the system is under greater hydraulic stress, but no overtopping is observed, and the oued continues to function within its capacity.

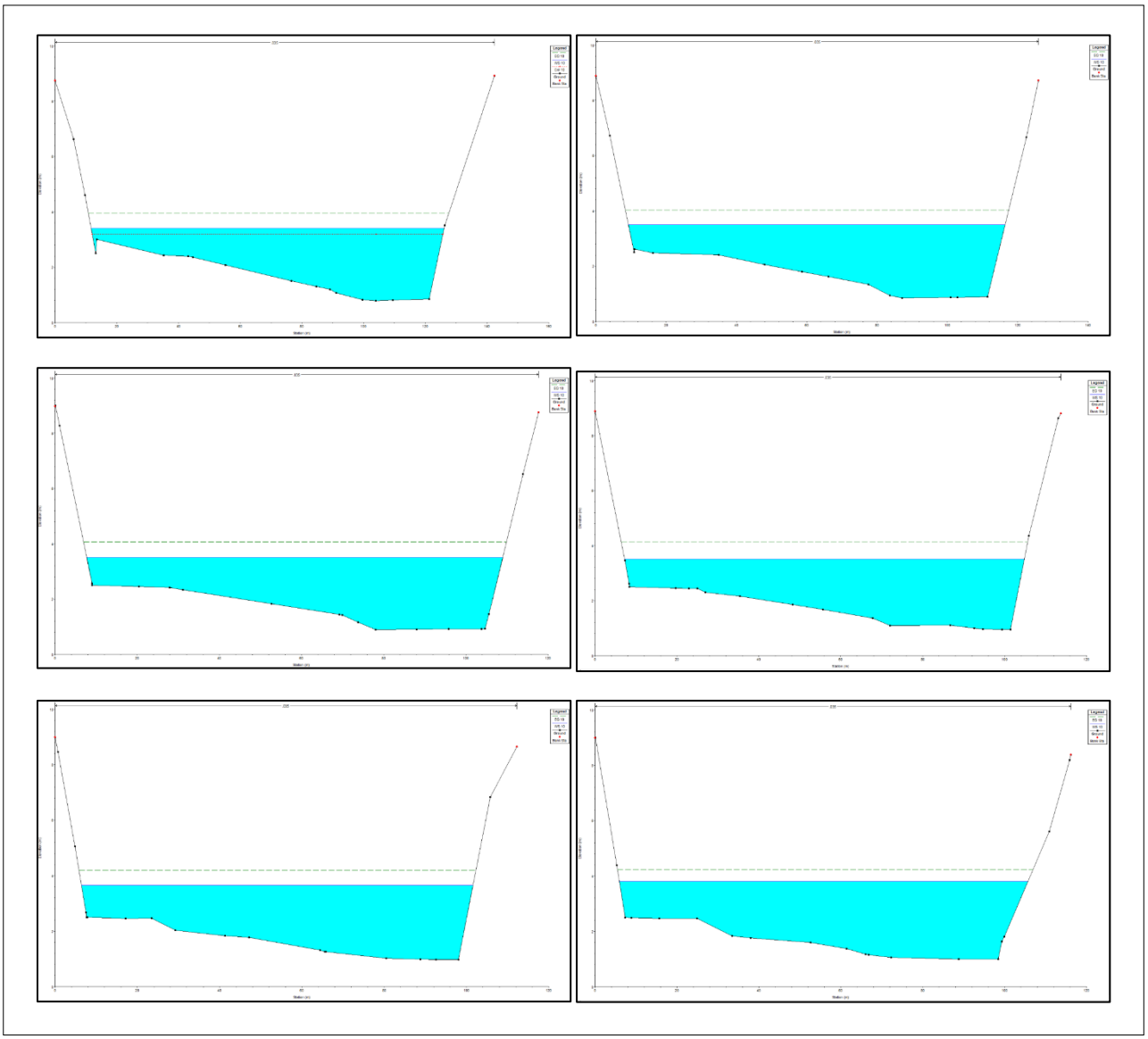

Figure 91: Simulation results of Oued Saf-Saf at River Stations 1.34m to 22.91m (10 years).

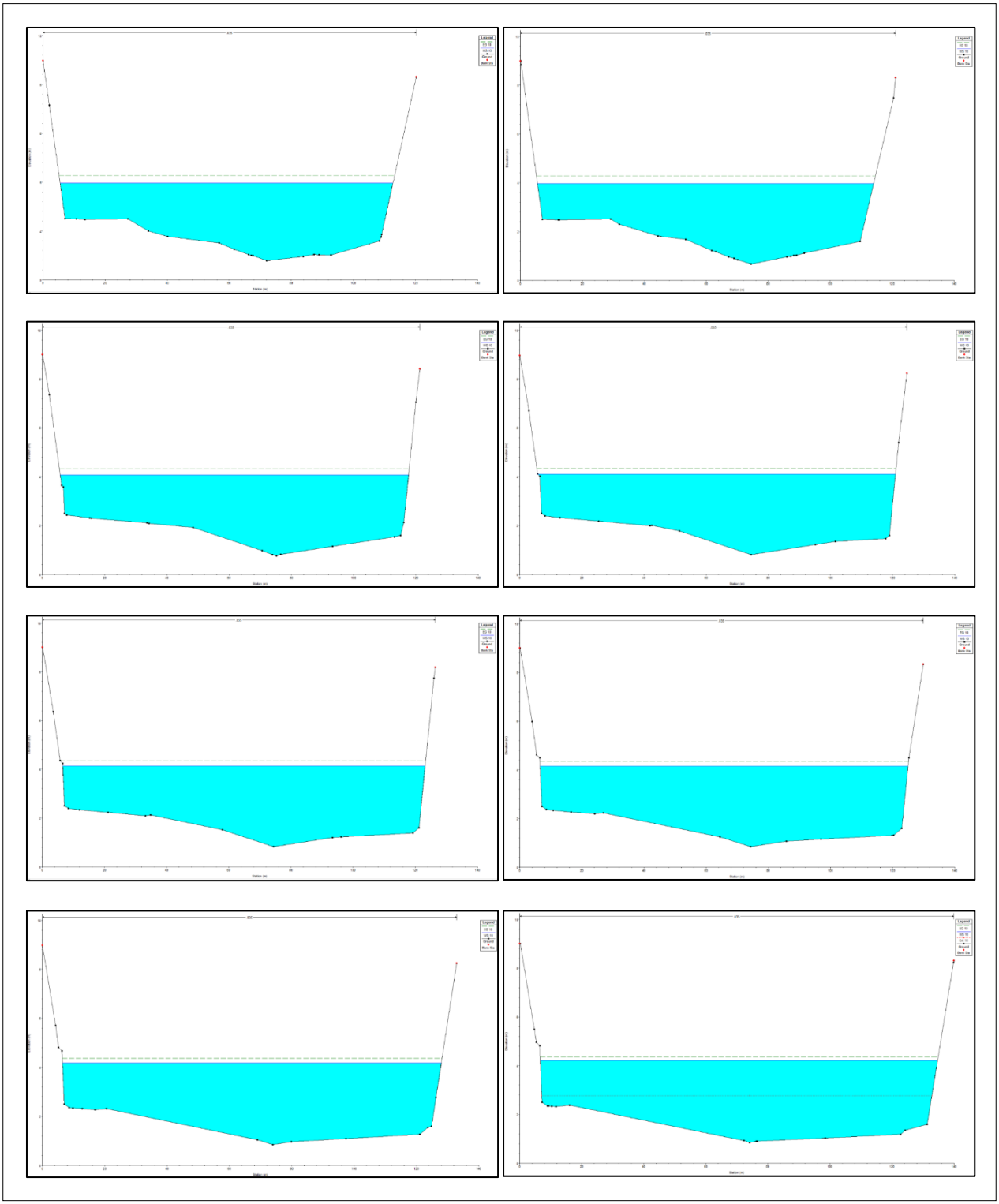

Figure 92: Simulation results of Oued Saf-Saf at River Stations 41.11m to 93.31m (10 years).

**Return period of 100 years**

**Interpretation**

Despite being the most extreme scenario, the cross-section profiles for the 100-year return period (Figures 93 and 94) show that the oued Saf-Saf continues to contain the flow without any overtopping or inundation. At upstream station 10.59, the water surface is very close to the top of the banks, and as we move downstream to stations like 4.28 and 1.34, the

WS continues to rise but never exceeds the bank elevation. The energy grade line is steep, and the critical depth line is clearly marked at 1.34, indicating higher velocities and a more energetic flow. However, the fact that no part of the WS crosses the banks demonstrates that the oued has a surprisingly strong capacity, even under extreme return periods. This highlights the resilience and effectiveness of the natural channel geometry in Saf-Saf, which is able to manage large discharges without causing flooding, making it a stable system under both normal and extreme hydrological conditions.

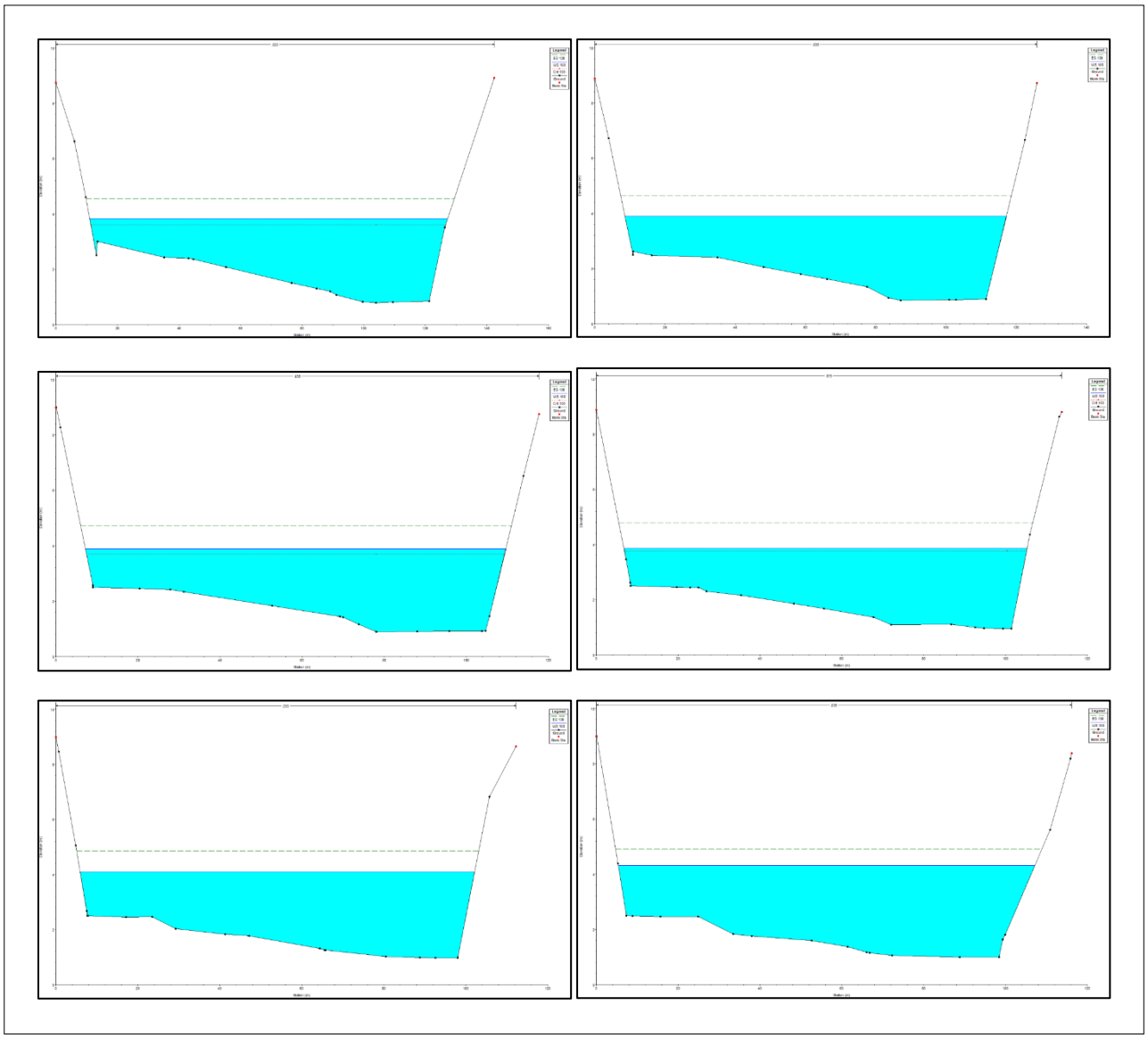

Figure 93: Simulation results of Oued Saf-Saf at River Stations 1.34m to 22.91m (100 years).

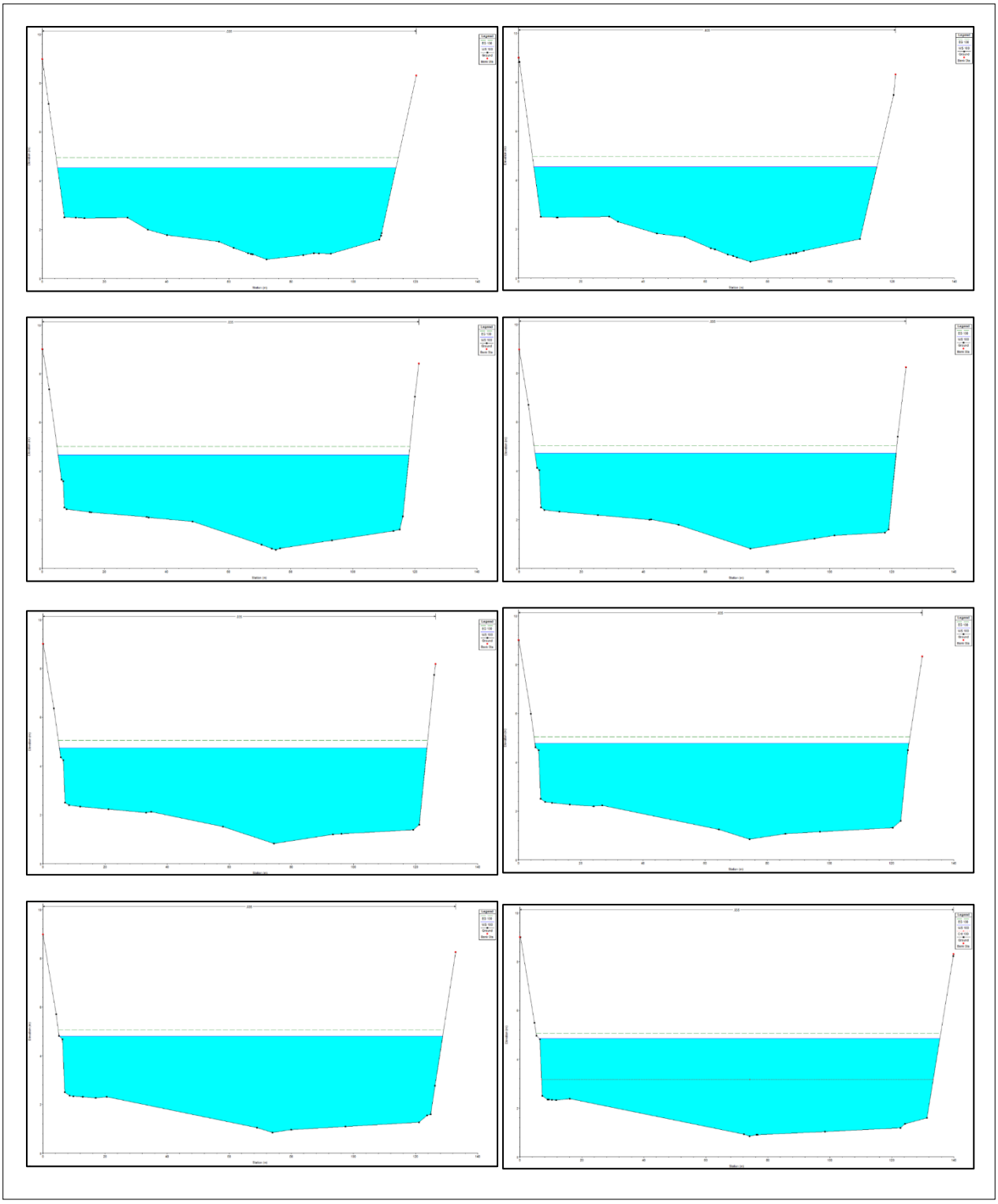

Figure 94: Simulation results of Oued Saf-Saf at River Stations 41.11m to 93.31m (100 years).

## VII.4 Inserting the Structure into HEC-RAS

In this phase of our study, a crucial step involves the integration of the hydraulic structure (specifically, a basin accompanied by a bridge) into the HEC-RAS modeling environment. This operation is fundamental for a comprehensive understanding of how the structure interacts with the natural flow regime of Oued Saf-Saf, a key component of our area of interest. Through this integration, we want to evaluate the influence of the bridge and its associated features on water movement, sediment transport, and erosion patterns within the oued. Moreover, this process

enables us to interpret the outcomes of the hydraulic simulation more accurately and to determine the vulnerability of the structure to phenomena such as local scour (which tends to develop in the vicinity of bridge piers).

The bridge under consideration is strategically positioned between cross sections 54.98m and 46.63m, with its central alignment located precisely at station 50.895m upstream from the downstream outlet of Oued Saf-Saf. Structurally, the bridge is supported by three piers, which are placed along the centerline of the flow at stations 19.5m, 53.5m, and 87m respectively. These locations were chosen based on both hydraulic alignment and structural considerations.

To enable HEC-RAS to simulate the physical processes with a high degree of reliability, it is essential to input specific geotechnical and hydraulic parameters. Among the most critical is the $D_{50}$ value (a measure of the median grain diameter of the riverbed material). This value was determined through in-situ sediment core sampling carried out near the piers. In our case, the median sediment size was found to be 3mm (indicating a coarse-grained bed composition which directly affects the resistance to erosion).

Another important modeling consideration is the orientation of the piers relative to the direction of the water flow. The angle between the pier axis and the direction of the hydraulic current can significantly influence the formation of vortices and localized scour holes. To simplify and stabilize the simulation while maintaining accuracy, we assigned an angle of 0° (meaning the piers are perfectly aligned with the direction of flow, minimizing asymmetric flow separation and simplifying the scouring dynamics).

By incorporating these carefully selected input parameters (including sediment characteristics and geometric alignment), HEC-RAS is able to simulate, with a high degree of fidelity, the interaction between the flow in Oued Saf-Saf and the bridge structure. This approach not only enhances the accuracy of our hydraulic analysis but also provides a solid foundation for identifying effective mitigation strategies (to reduce scouring risks and ensure the long-term stability and safety of the bridge infrastructure).

Figure 95: Image of the bridge studied over Oued Saf-Saf.

### VII.4.1 Results of the insertion

**Return period of 2 years**

**Interpretation**

The six cross-sectional profiles in Figures 96 to 101 represent the hydrodynamic simulation results of the Oued Saf-Saf at the bridge location (station 50.895 m), for three different return periods: 2 years, 10 years, and 100 years. For each return period, two scenarios are modeled (instantaneous and average discharge), providing a better visualization of flow conditions.

Upon analyzing the results, it is evident that the water surface elevation remains consistently below the bridge deck, regardless of the return period. In the most extreme scenario (100 years), the maximum water level reaches approximately 5m, while the bridge deck is positioned at an elevation of 7.5m. This implies a safety margin of 2.5m, even during extreme conditions.

This situation shows that the bridge is designed to withstand extreme hydrological events without being directly flooded or overtopped.

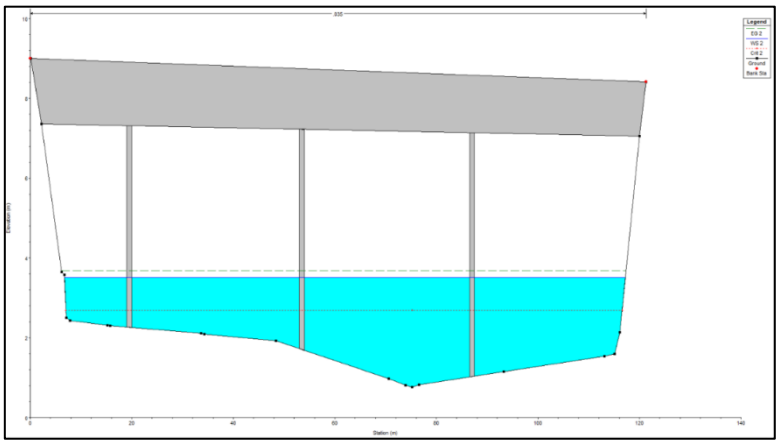

Figure 96: Upstream cross-sectional profile simulation with bridge insertion on Oued Saf-Saf (2 years).

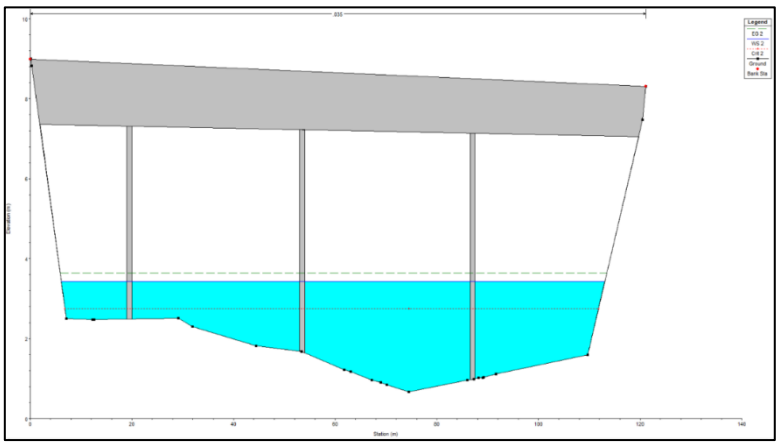

Figure 97: Downstream cross-sectional profile simulation with bridge insertion on Oued Saf-Saf (2 years).

### Return period of 10 years

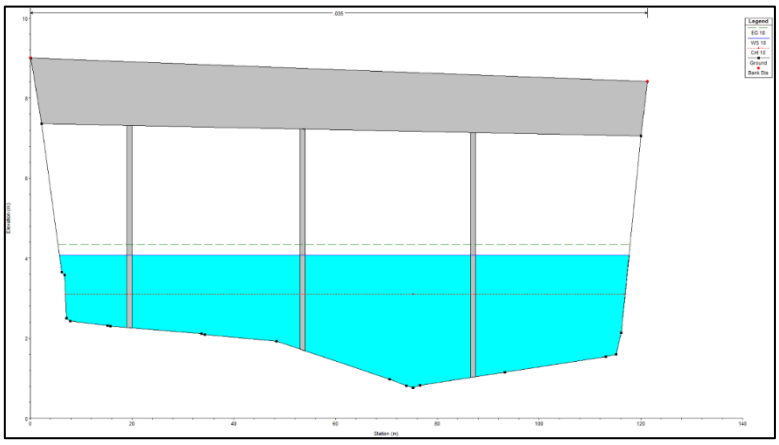

Figure 98: Upstream cross-sectional profile simulation with bridge insertion on Oued Saf-Saf (10 years).

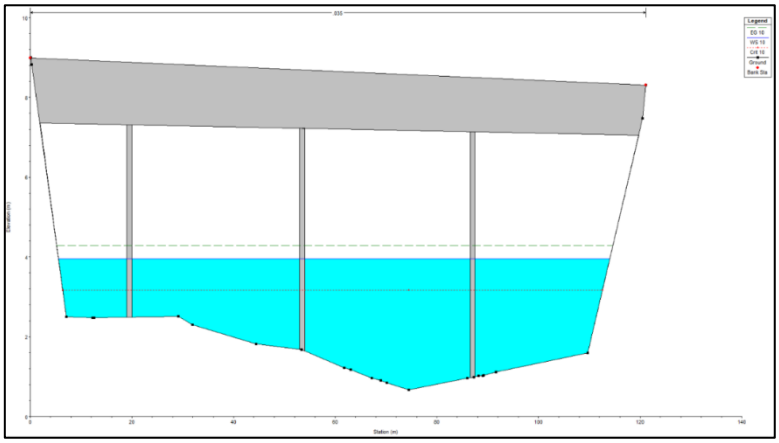

Figure 99: Downstream cross-sectional profile simulation with bridge insertion on Oued Saf-Saf (10 years).

### Return period of 100 years

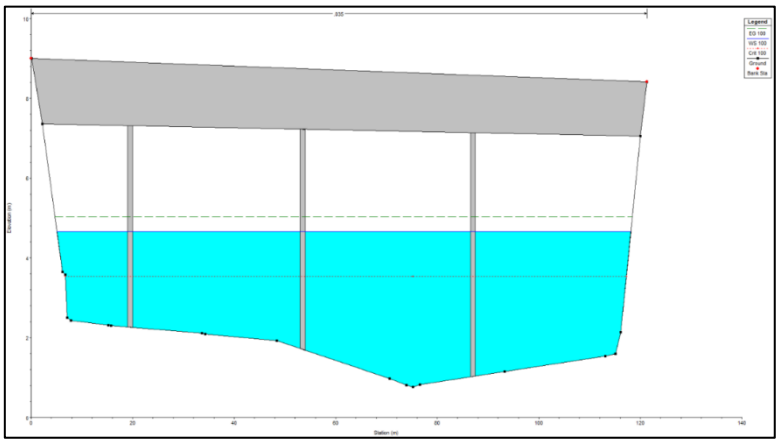

Figure 100: Upstream cross-sectional profile simulation with bridge insertion on Oued Saf-Saf (100 years).

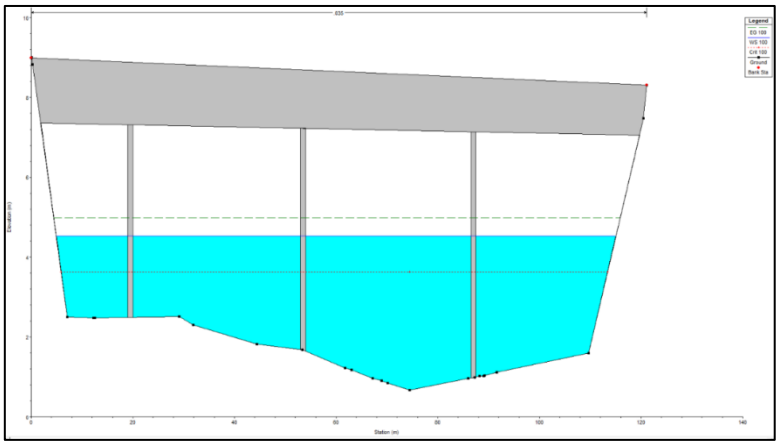

Figure 101: Downstream cross-sectional profile simulation with bridge insertion on Oued Saf-Saf (100 years).

### VII.4.1 Cases of scour at the pier level

Bridge structures over watercourses are inherently exposed to the risk of scour, a hydraulic phenomenon characterized by the erosion of sediment around piers and abutments due to flowing water. To determine the vulnerability of a specific bridge located at river station 50.805, a detailed scour analysis was conducted using hydraulic modeling software under three distinct flood scenarios corresponding to return periods of 2, 10, and 100 years. These scenarios simulate progressively increasing flow conditions, offering insights into potential changes in scour depth and bridge foundation stability over time. The analysis was carried out under controlled parameters: a pier angle of 0°, a sediment median size ($D_{50}$) of 3 mm, and a fixed riverbed geometry. While no major hydraulic overloads were detected at the piers, suggesting a limited immediate scour risk, the simulations underline the importance of considering long-term erosion and external influencing factors such as climate variability and sediment transport.

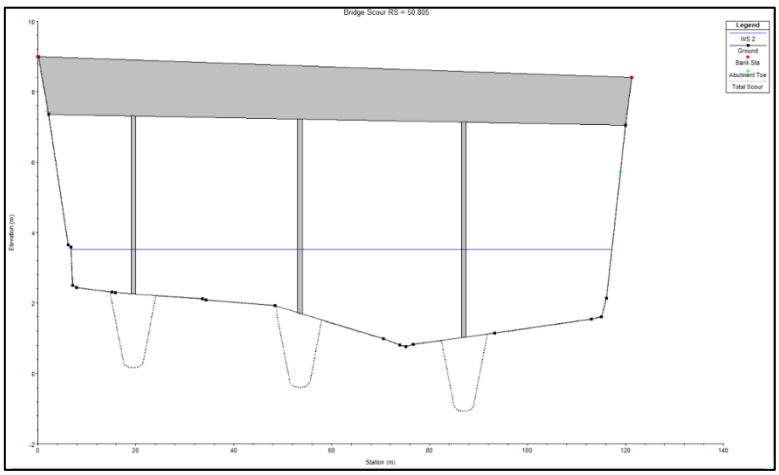

Figure 102: Scour Profile for Flood Event with a Return Period of 2 Years.

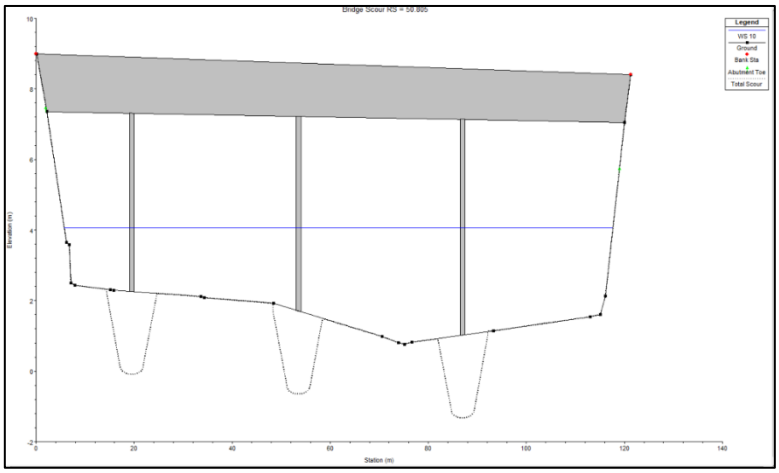

Figure 103: Scour Profile for Flood Event with a Return Period of 10 Years.

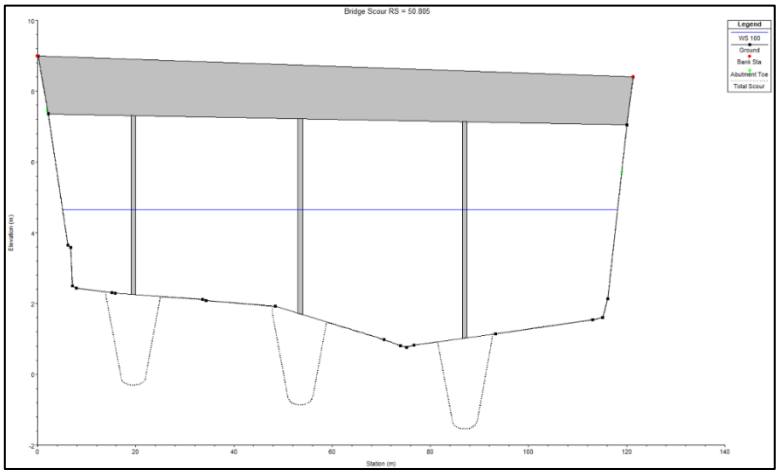

Figure 104: Scour Profile for Flood Event with a Return Period of 100 Years.

**Interpretation**

The three profiles presented in the previous Figures illustrate water surface elevations and scour depths for flood events with return periods of 2, 10, and 100 years. As the return period increases, so does the depth of local scour observed around the bridge piers:

- Return period of 2 years: Ys = 2.10 m
- Return period of 10 years: Ys = 2.35 m
- Return period of 100 years: Ys = 2.57 m

This trend clearly demonstrates that higher-intensity floods generate stronger erosive forces, leading to deeper scour at the base of the piers.

The CSU equation, which was used in the calculations, effectively reflects how scour behavior evolves with increasing hydraulic intensity. Developed by Colorado State University, this empirical formula estimates local scour depth around bridge piers based on factors such as pier width, flow depth, flow velocity (via the Froude number), and correction coefficients for pier shape, flow angle, and bed conditions. The general form of the equation is as follows:

Equation 20

$$y_s = 2.0 \cdot K_1 \cdot K_2 \cdot K_3 \cdot K_4 \cdot \left(\frac{a}{y_1}\right)^{0.65} \cdot Fr^{0.43}$$

where:

- $y_s$: local scour depth
- $a$: pier width
- $y_1$: approach flow depth
- $Fr$: Froude number of the flow
- $K_1, K_2, K_3 \, and \, K_4$: correction factors for pier shape, flow angle, bed condition, and debris, respectively.

Although the current modeling doesn't point to an immediate structural concern, it's important to consider how long-term factors (such as recurring floods, shifting flow patterns, or gradual changes in the riverbed) could amplify scour risks in the future.

To mitigate these risks and ensure the bridge remains stable over time, two technical solutions have been evaluated:

**Expanded Excavation with Structural Reinforcement**

Widening the excavation around the piers to enhance their stability, which may be paired with techniques like soil consolidation or the installation of reinforced concrete piles, depending on local geotechnical conditions.

**Rock Riprap Protection**

Placing a strategically designed layer of artificial riprap around the foundations to protect against erosion, with the size and arrangement of the rocks tailored to withstand local flow dynamics.

Both approaches require detailed geotechnical and hydraulic studies to ensure effective implementation. Considering the increasing scour potential under higher return period flood events, ongoing monitoring and adaptive maintenance are essential to safeguard the long-term integrity of the structure.

## VII.5 Mapping of the studied cases

### Interpretation

The three maps in Figures 105, 106 and 107 represent the hydraulic simulation results of the Saf-Saf oued for three different return periods: 2 years, 10 years, and 100 years, respectively. These maps, generated using the RAS Mapper module in the HEC-RAS software, illustrate the spatial distribution of water depths and flow vectors at the studied bridge location. The maximum depth is mainly concentrated within the main channel, indicating that the flow remains well-contained even during the most significant simulated flood events. The bridge, shown in gray, causes a slight backwater effect upstream without generating any significant overflow. The flow vectors confirm a downstream flow direction, with increasing intensity according to the return period. After analyzing the three scenarios, it was found that none of the cases present a risk of flooding in the studied area, even under the extreme 100-year return period. These results confirm the sufficient hydraulic capacity of the section and the effective integration of the bridge within the dynamics of the Saf-Saf oued.

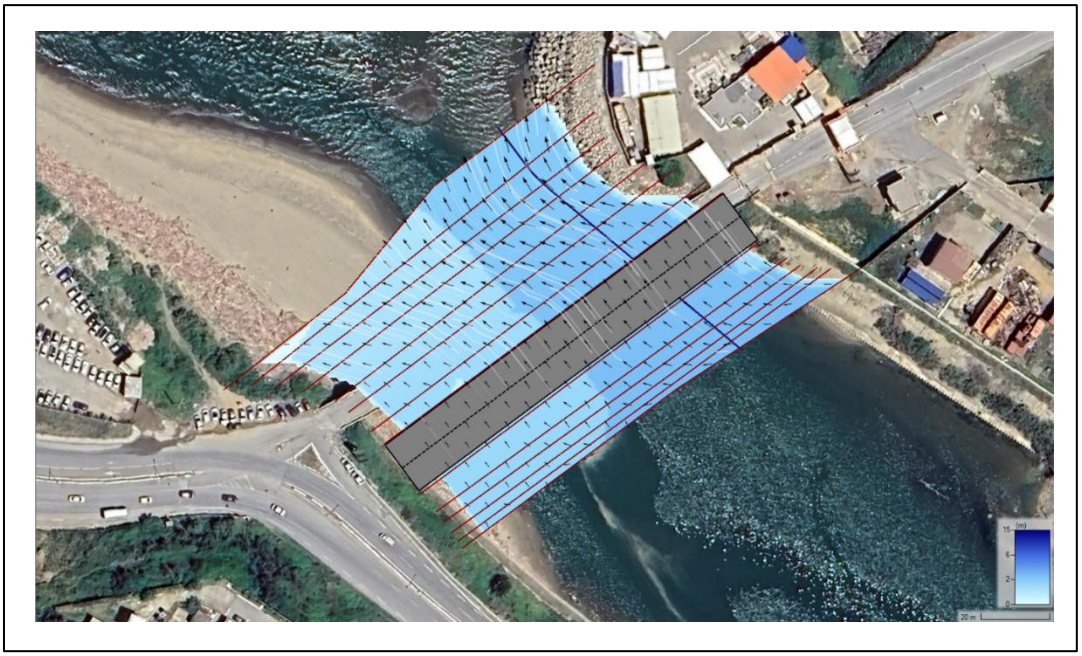

Figure 105: Map of Hydraulic Simulation of Oued Saf-Saf (2 years).

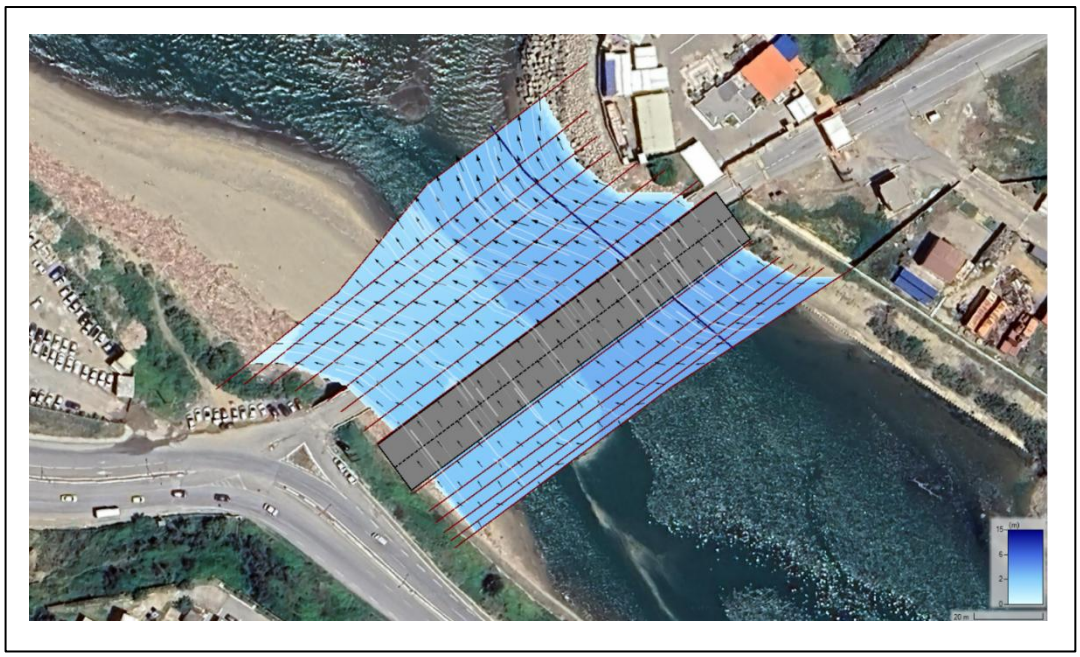

Figure 106: Map of Hydraulic Simulation of Oued Saf-Saf (10 years).

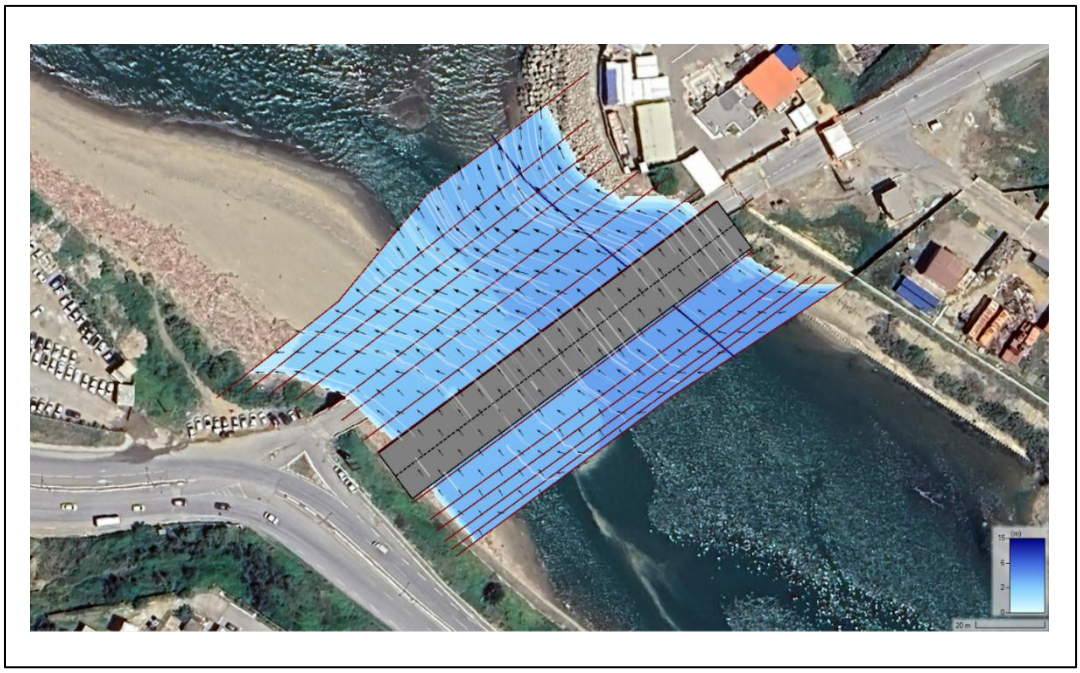

Figure 107: Map of Hydraulic Simulation of Oued Saf-Saf (100 years).

**Conclusion**

The overall results from the cross-sectional profiles and hydrodynamic maps of the Saf-Saf oued demonstrate the remarkable stability of the river system under the different simulated flood scenarios, ranging from the 2-year to the 100-year return period. Throughout the longitudinal and cross-sectional analysis, the water surface consistently remains below the bank elevation, with no signs of overtopping or hydraulic overload, even under extreme conditions. The studied bridge also maintains a sufficient safety margin, with a freeboard of approximately 2.5m in the 100-year scenario. Furthermore, the hydraulic maps confirm the oued's strong

conveyance capacity and the effective integration of the bridge within its natural hydrological dynamics. These observations highlight the robustness of the current design and the efficiency of the natural geometry of the Saf-Saf oued in managing flows without immediate risk of flooding or critical scour. However, regular monitoring remains essential to anticipate long-term changes caused by morphological evolution, erosion, or the potential effects of climate change.

# General Conclusion

# General Conclusion

This study set out to better understand which parts of the Skikda coastline are most at risk from erosion, coastal flooding, and inundation, especially as these threats become more serious with ongoing climate change. By combining shoreline change analysis, hydrodynamic modeling, and flood risk mapping, we were able to build a clearer picture of how different areas of the coast are reacting to natural forces.

One of the most important findings is the contrast between the western and eastern parts of the coastline. The rocky western coast has stayed largely stable over the past 30 years (1993–2023), showing little to no movement. Forecasts for 2033 and 2043 suggest that this stability will likely continue over the next 10 to 20 years. Its natural resistance to wave action helps protect it. In the other hand, the eastern coast, made up mostly of sandy beaches, is much more active and vulnerable, with clear signs of ongoing erosion. The results show that the shoreline is moving back and might keep getting worse, especially in places that don't have protection.

The behavior of waves and currents also plays a major role. Our hydrodynamic analysis showed that in offshore exposed areas, wave heights can go over 4.7m, and current velocities remain strong and relatively uniform. As these forces approach the shore, they are modified by seabed friction, refraction, and coastal structures.

Sea level rise adds another layer of risk. Our simulations indicate that a 3m coastal fooding could submerge about 2583.4 hectares, a 4m flood would effect around 3836.3 hectares, and an extreme 5m flood could inundate up to 5022.3 hectares. These zones include urban areas, harbors, and agricultural land especially in low-lying regions near oued mouths, which allow seawater to travel inland more easily. This highlights the growing vulnerability of the region to coastal flooding under future climate scenarios.

Despite these vulnerabilities, some systems show notable resilience. In the case of Oued Saf-Saf, hydrodynamic simulations across multiple return periods (from 2-year to 100-year floods) demonstrated the oued's strong capacity. Even under the extreme 100-year scenario, the water surface remained below bank elevation, with no overtopping or structural failure. The bridge over the oued retained a freeboard of approximately 2.5m, confirming the system's strength under stress.

**Looking Ahead**

This research offers valuable insight into the risks facing the Skikda coastline, but it also highlights the need for continued work. More precise data will be essential. This includes updated topographic and bathymetric surveys, recent wave and climate records, and reliable field observations. Supporting open data sharing between researchers and institutions can also help strengthen future studies.

With these improvements, future research will be better equipped to support effective planning and adaptation strategies. This will be key to protecting both the natural environment and the communities that rely on the Skikda coast.

# References

**ABRAR, Y., & MANMOHANJIT, S. (2020).** *Watershed Hydrology, Management and Modeling.* USA: Taylor & Francis Group, LLC.

**ALGERIE 360. (2025, 03 04).** *Skikda / Tourisme Les atouts de Ben M'hidi*. Retrieved from algerie 360: https://www.algerie360.com/skikda-tourisme-les-atouts-de-ben-mhidi/?utm_source=chatgpt.com

**Alim, D. A. (2023).** *Evolution morpho-dynamique de la baie d'Alger : Observation et Modélisation hydrodynamique et sédimentaire* . Dely Brahim: ENSSMAL.

**AUGUSTINUS, P. (2003).** COASTAL SYSTEMS. *Encyclopedia of Life Support Systems(EOLSS)*, 6.

**BENALLOU, I. (2020).** *Evaluation des impacts des changements climatiques et des activités anthropiques sur le littoral de la baie de Zemmouri : Vulnérabilité et Adaptation.* Dely Brahim: ENSSMAL.

**BERKANI, M., & Wajih, M. S. (2021).** *Etude et valorisation des terres perdues par la submersion marine dans la région Ouest d'Alger.* Dely Brahim: ENSSMAL.

**BHATTACHARYYA, M., & RITOLIA, G. (2006).** Conditional VaR using EVT – Towards a planned. *International Review of Financial Analysis*, 5.

**BOUHIDEL, K. E. (2022).** Vegetation and landscape dynamics of the Guerbès-Benazouz. *Ukrainian Journal of Ecology*, 10.

**BOUKHENNAF, A., & MEZOUAR, K. (2023).** Long and short-term evolution of the Algerian coastline using remote sensing and GIS technology. *Marine Science*, 11.

**BREBBIA. (1982).** *Computational Methods and Experimental Measurements.* Southampton: Keramidas.

**CEMALI, N., BENAZZOUZ, M. T., & RAMOUL, S. (2019).** La contribution des GIS dans la quantification de l'évolution du littoral de Skikda entre 1960 et 2002 et impact des aménagements. *JOURNAL OF MATERIALS AND ENGINEERING STRUCTURES*, 14.

**DHI. (2017).** *MIKE 21 Flow Model, Hydrodynamic Module, Scientific Documentation.* Denmark: DHI.

**DHI. (2017).** *MIKE 21, Spectral Wave module, Scientific Documentation.* Denmark: DHI.

**DHI. (2025, 3 19).** *MIKE 21 and MIKE 3*. Retrieved from DHIGROUP: https://www.dhigroup.com/technologies/mikepoweredbydhi/mike-21-3

**ESRI. (2025, 04 10).** *ESRI Land Cover*. Retrieved from Land Cover: https://livingatlas.arcgis.com/landcoverexplorer/#mapCenter=-117.20000%2C34.06000%2C11&mode=step&timeExtent=2017%2C2024&year=2024

**GOUGUET, L. (2018).** *Guide de gestion des dunes et des plages associées.* Versailles Cedex: Editions Quae.

**GRICHE, H., & GREBICI, M. L. (2024).** *Modélisation et cartographie de la vulnérabilité du littoral centre algérien face aux risques d'inondation et de submersion marine.* Dely Brahim: ENSSMAL.

**GUEDDAH, D. (2003).** *Evaluation de la pollution industrielle et urbaine dans la région de Skikda : impact sur l'écosystème marin côtier.* Annaba: Université Badji Mokhtar.

**Historique-Météo. (2025, 03 05).** *Historique météo : archives météo pour le monde entier*. Retrieved from Historique-Météo: https://www.historique-meteo.net/

**IPCC (Intergovernmental Panel on Climate Change). (2019).** *Sea Level Rise and Implications for Low-Lying Islands, Coasts and Communities.* Cambridge: IPCC.

**IPCC (Intergovernmental Panel on Climate Change). (2021).** *Climate Change 2021: The Physical Science Basis.* Cambridge: IPCC.

**IPCC. (2013).** *CLIMATE CHANGE 2013.* Cambridge: Working Group I Technical Support Unit.

**JOHNSEN, J. P., HESOUG, B., & SOLAS, A. M. (2014).** The creation of coastal space – how local ecological knowledge becomes relevant. *Maritime Studies*, 20.

**LOBETO, H., SEMEDO, A., LEMOS, G., DASTGHEIB, A., MENENDEZ, M., RANASINGHE, R., & BIDLOT, J. R. (2024).** Global coastal wave storminess. *Scientific Reports*, 18.

**MARINE SCIENCE CONSERVATION. (2012).** *Sandy Beaches.* Miami: Deering Estate.

**MAUNDER, J. (1992).** *Dictionary of global climate change.* New york: UCL Press.

**MEGHZILI, H. (2015).** *Modèles d'aménagement et d'urbanisation des Zones d'Expansion Touristique de la wilaya de Skikda (Algérie).* Bretagne: UNIVERSITÉ DE BRETAGNE OCCIDENTALE.

**MOUSSAOUI, M. (2024).** *Gestion et Valorisation des zones littorales à intérêt stratégique cas de la wilaya de Tipaza.* Dely Brahim: ENSSMAL.

**NASA Sea Level Change . (2025, 09 04).** *Sea Level Change* . Retrieved from Sea Level Projection Tool: https://sealevel.nasa.gov/ipcc-ar6-sea-level-projection-tool

**NATIONS UNIES ALGERIE. (2025, 03 03).** *Des dunes pour préserver les zones humides de Guerbes- Sanhadja*. Retrieved from NATIONS UNIES ALGERIE: https://algeria.un.org/fr/37272-des-dunes-pour-pr%C3%A9server-les-zones-humides-de-guerbes-sanhadja?utm_source=chatgpt.com

**NOAA . (2016).** *Glossary of Terminology.* Maryland: NOAA.

**NOVICO, F., & PRIOHANDONO, Y. A. (2012).** Analysis of Erosion and Sedimentation Patterns Using Software of Mike 21 HDFM-MT in The Kapuas Murung River Mouth Central Kalimantan Province. *Bulletin of the Marine Geology*, 4.

**PASKOFF. (2010).** *La gestion du trait de cote.* Versailles Cedex: Editions Quae.

**PERERA, U., & RATNAYAKE, A. S. (2023).** Grain size distribution of modern beach sediments in Sri Lanka. *Anthropocene Coasts*, 1-2.

**RUGGIERO, P., KRATZMANN, M., HIMMELSTOSS, E., REID, D., ALLAN, J., & KAMINSKY, G. (2025, 4 29).** *National Assessment of Shoreline Change: Historical Shoreline Change Along the Pacific Northwest Coast.* Retrieved from USGS: https://pubs.usgs.gov/of/2012/1007/

**SIVAPALAN, M., TAKEUCHI, K., FRANKS, S. W., GUPTA, V. K., KARAMBIRI, H., LAKSHMI, V., . . . ZEHE, E. (2003).** IAHS Decade on Predictions in Ungauged Basins(PUB), 2003–2012: Shaping an exciting future forthe hydrological sciences. *Hydrological Sciences–Journal–des Sciences Hydrologiques*, 4.

**STANDER, C. (2015).** *Analysis of Extreme Events in the Coastal.* Stellenbosch: Stellenbosch University.

**STEPANIAN, A. (2002).** *Evolution morphodynamique d'une plage macrotidale à barres: Omaha beach (Normandie).* Caen: HAL open science.

**STULL, R., & JAMES, S. (2019).** *Wave Characteristics.* Columbia: Weather for Sailing, Flying & Snow Sports.

**SURESH, R. (2020).** *Watershed Hydrology.* Samastipur: College of Agricultural Engineering.

**TAMAZIRT, M. (2023).** *MODÉLISATION DES EFFETS DE LA HOULE SUR LA STABILITÉ ET FRANCHISSEMENT DES OUVRAGES MARITIMES.* Dely Brahim: ENSSMAL.

**TIDE FORECAST. (2025, 3 18).** *Tide Times and Tide Charts Worldwide*. Retrieved from TIDE FORECAST: https://www.tide-forecast.com/

**TIDES FOR FISHING. (2025, 3 18).** *TIDES AND SOLUNAR CHARTS*. Retrieved from TIDES4FISHING: https://tides4fishing.com/dz/algeria/skikda

**UNDP Algérie. (2025, 03 03).** *Protection des Zones Humides du Complexe Guerbes-Sanhadja de Skikda - Signature d'un nouveau projet*. Retrieved from UNDP: https://www.undp.org/fr/algeria/actualites/protection-des-zones-humides-du-complexe-guerbes-sanhadja-de-skikda-signature-dun-nouveau-projet?utm_source=chatgpt.com

**VALIQUETTE, S. (2020).** *Théorie des valeurs extrêmes dans le cadre des mélanges de.* Sherbrooke: UNIVERSITÉ DE SHERBROOKE.

**VITAMINEDZ. (2025, 03 05).** *Les Plages Skikda*. Retrieved from Vitaminedz: https://www.vitaminedz.com/fr/Skikda/Les-plages-17087-1.html

**WOFRANCE. (2025, 09 04).** *WOFRANCE*. Retrieved from Weather Online: https://www.wofrance.fr/weather/maps/city?LANG=fr&WMO=60355&ART=LDR&CONT=afri&R=0&LEVEL=150&REGION=0011&LAND=AL&NOREGION=1&MOD=&TMX=&TMN=&SON=&PRE=&MONAT=&OFFS=&SORT=

**ZORN, M., & KOMAC, B. (2013).** *Encyclopedia of Natural Hazards.* London: Springer Nature.

# Appendices

# I. Current conditions in El Marsa fishing harbor

## Return period of 10 years

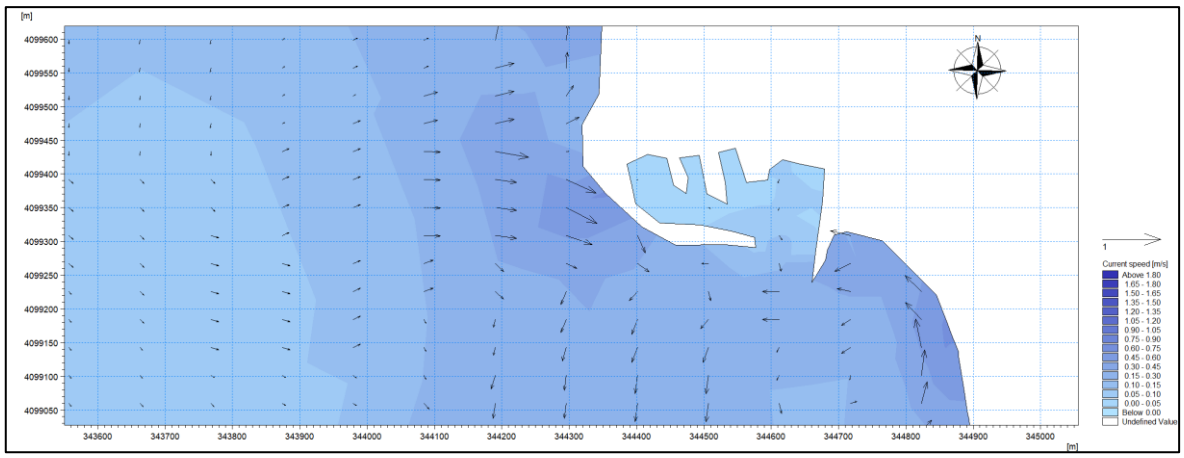


Figure A. 1: Current conditions in El Marsa fishing harbor for the WNW direction (10).

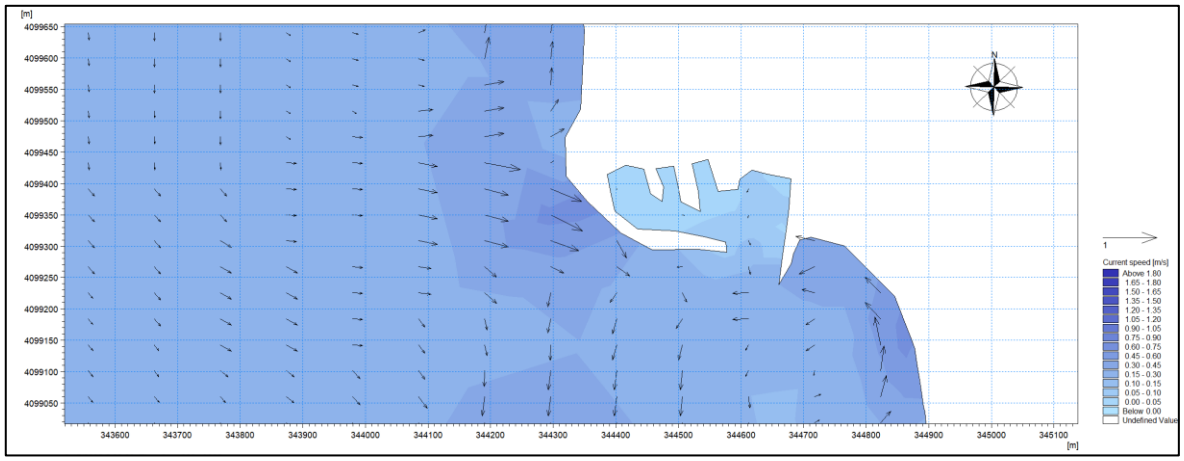


Figure A. 2: Current conditions in El Marsa fishing harbor for the NW direction (10).

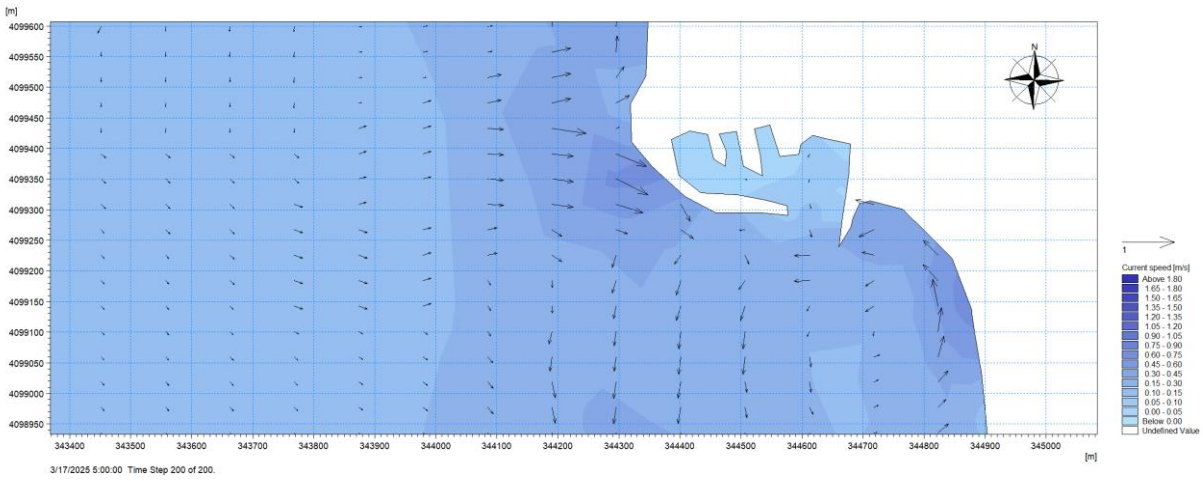


Figure A. 3: Current conditions in El Marsa fishing harbor for the NNW direction (10).

## Return period of 30 years

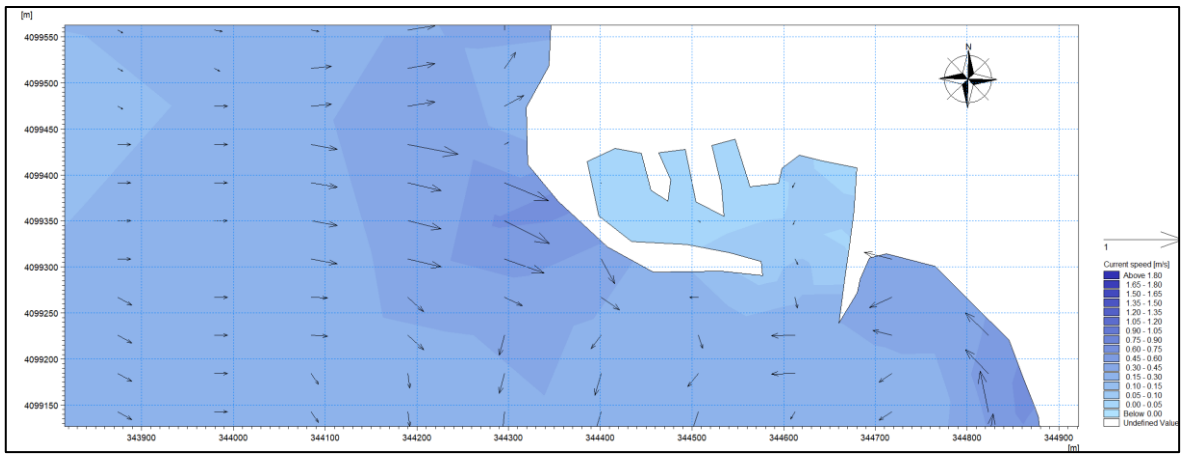


Figure A. 4: Current conditions in El Marsa fishing harbor for the WNW direction (30).

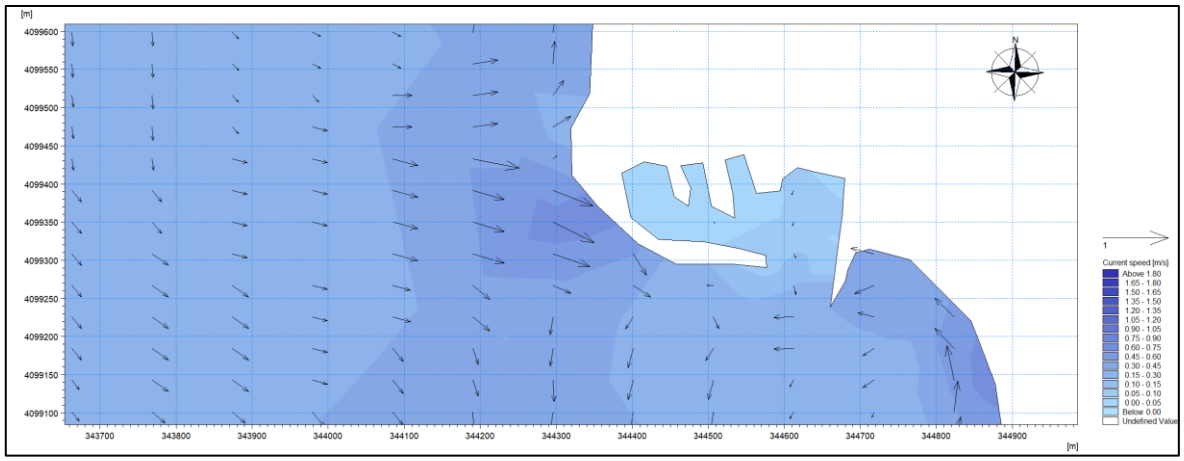


Figure A. 5: Current conditions in El Marsa fishing harbor for the NW direction (30).

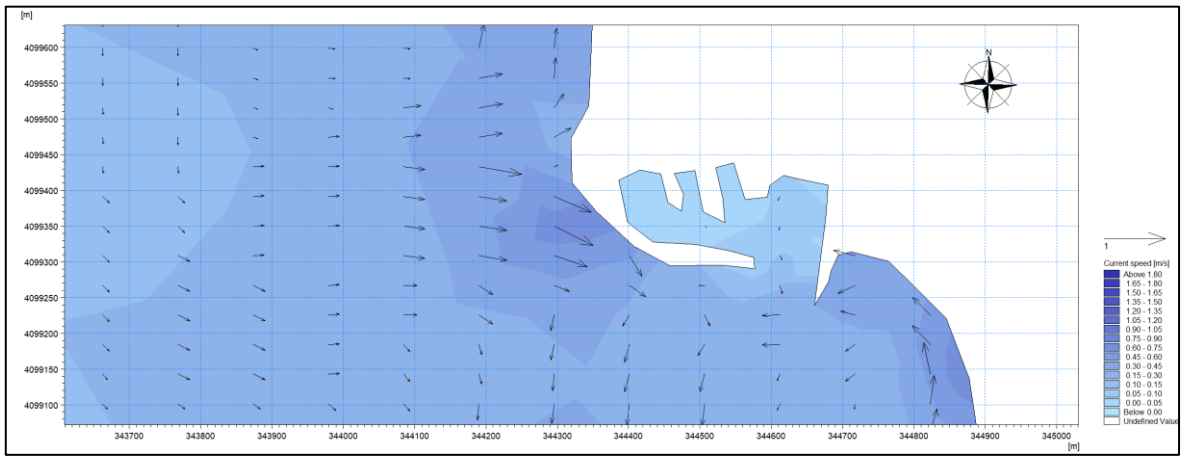


Figure A. 6: Current conditions in El Marsa fishing harbor for the NNW direction (30).

## Return period of 100 years

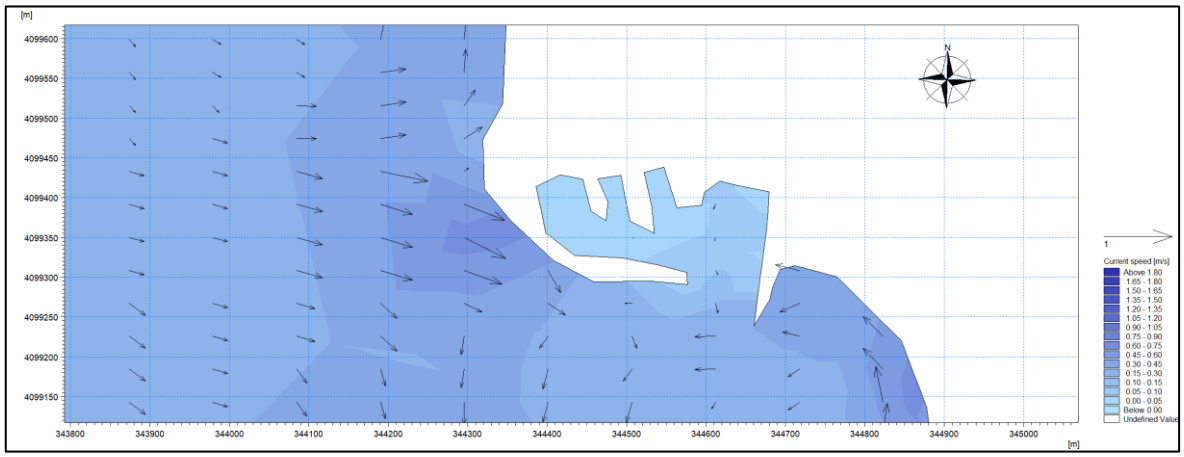


Figure A. 7: Current conditions in El Marsa fishing harbor for the WNW direction (100).

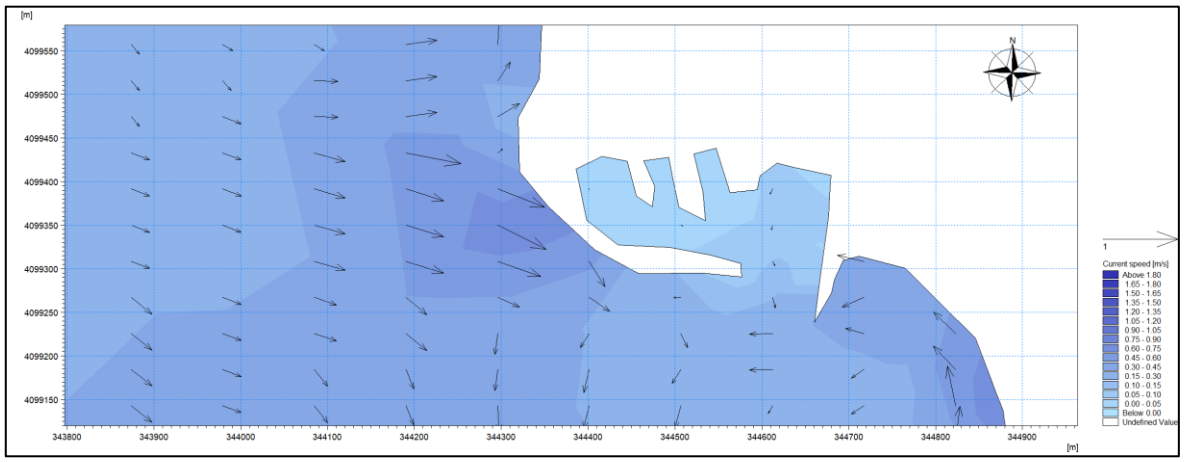


Figure A. 8: Current conditions in El Marsa fishing harbor for the NW direction (100).

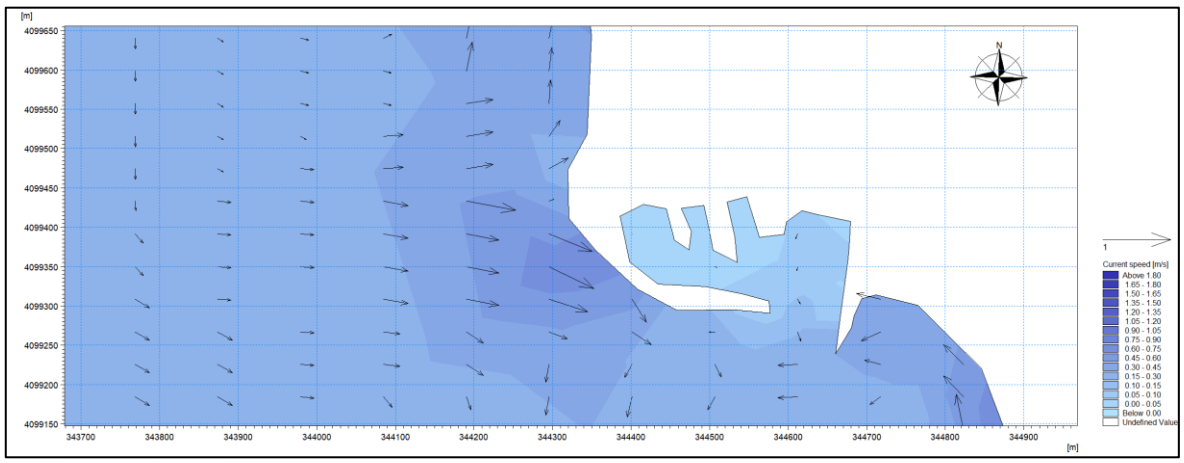


Figure A. 9: Current conditions in El Marsa fishing harbor for the NNW direction (100).

## II. processing using Civil 3D and HEC-RAS

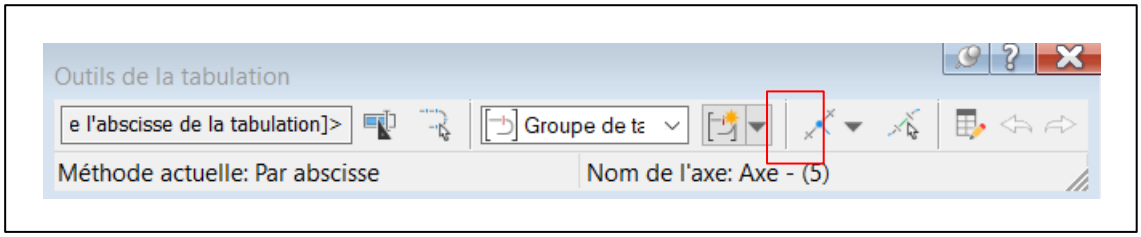


Figure A. 10: Generation of sample lines based on tabulated stations in Civil3D.

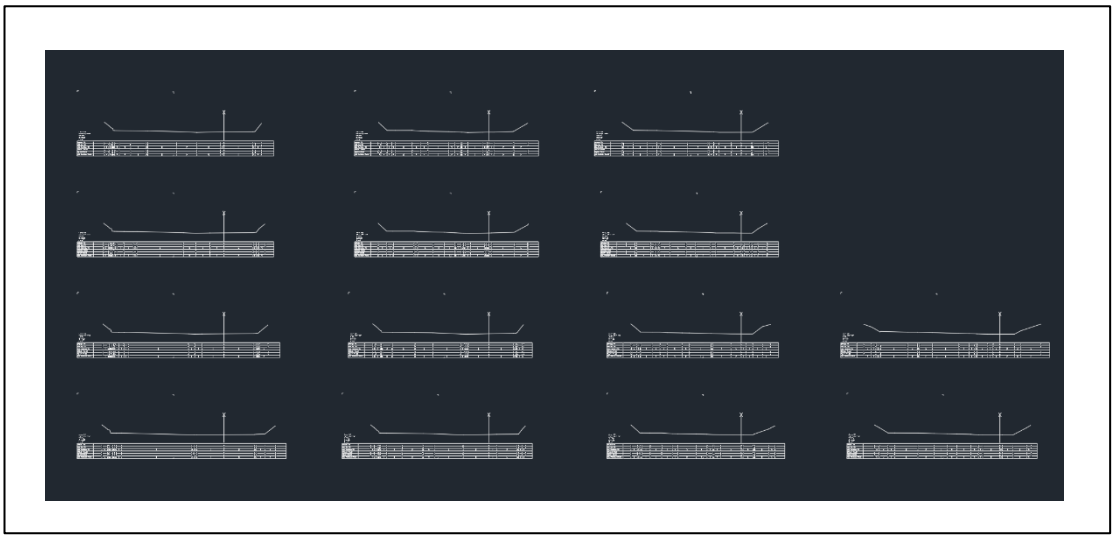

Figure A. 11: Cross section drawings along the tabulated lines in Civil3D.

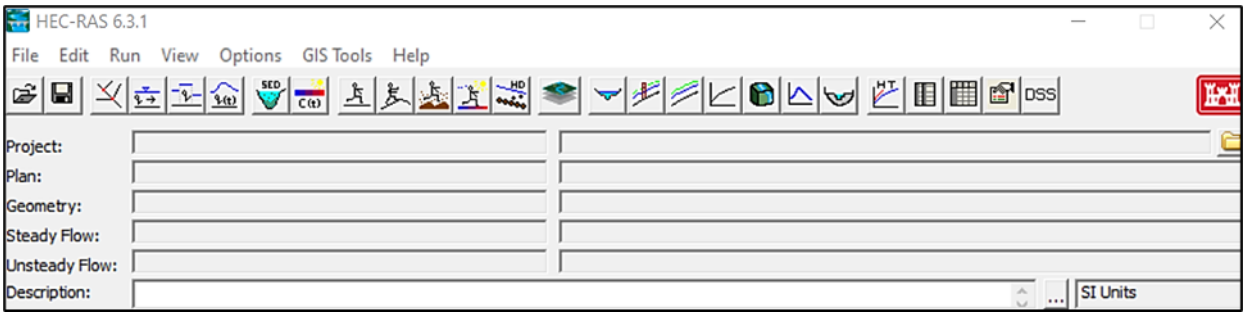


Figure A. 12: HEC-RAS Interface

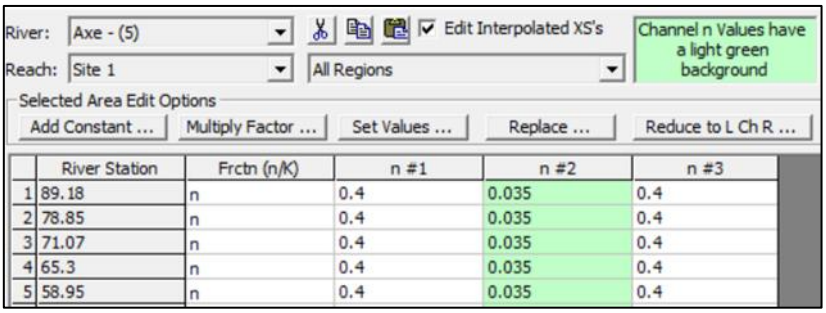


Figure A. 13: Roughness coefficient input.

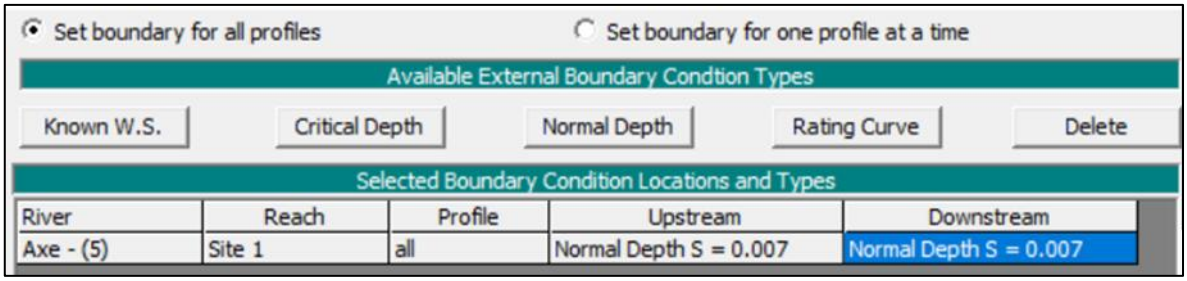


Figure A. 14: Slope value input.

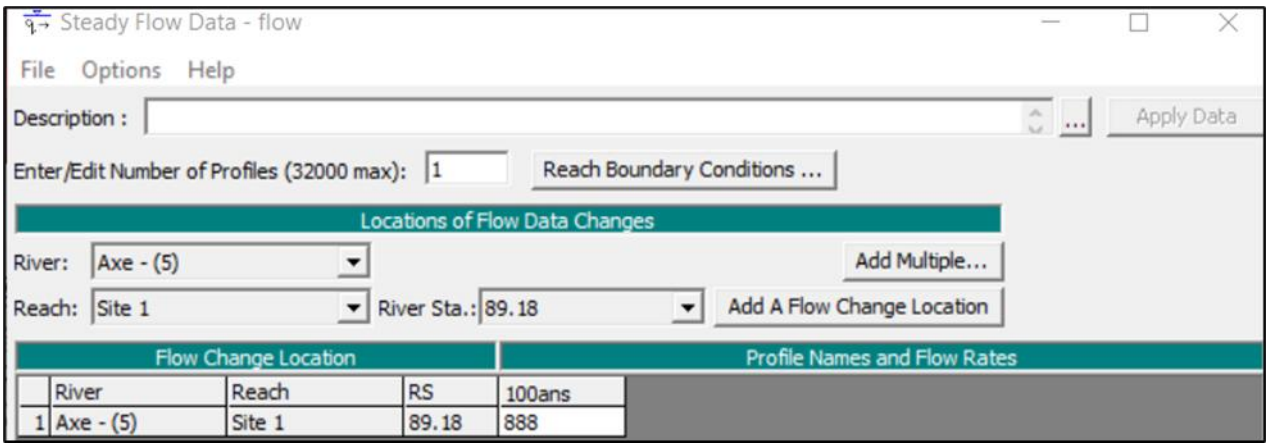


Figure A. 15: Flow rate input.

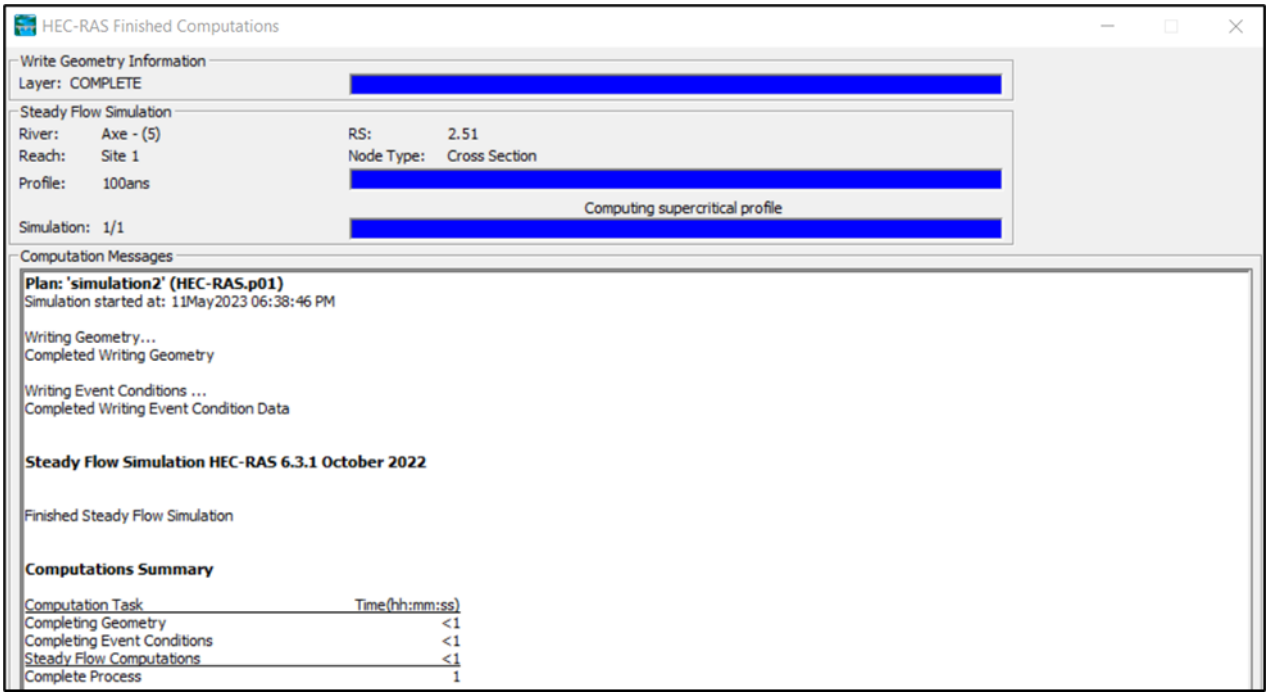


Figure A. 16: Computation Summary of Steady Flow Simulation in HEC-RAS.

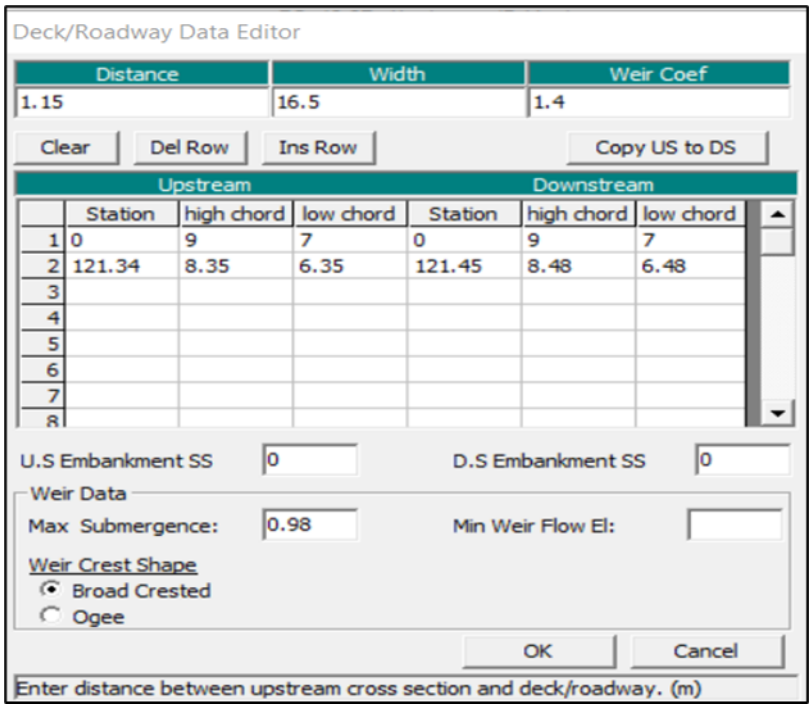


Figure A. 17: Bridge deck information input.

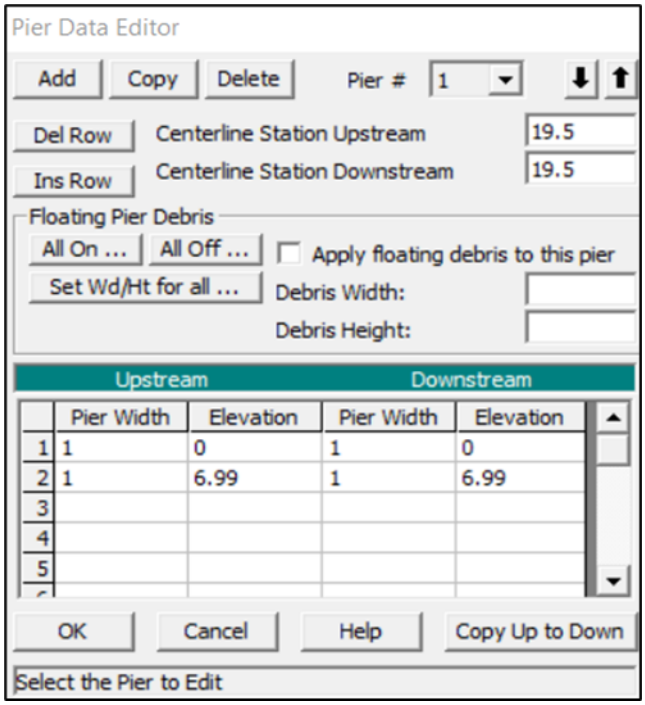


Figure A. 18: Pier information input.

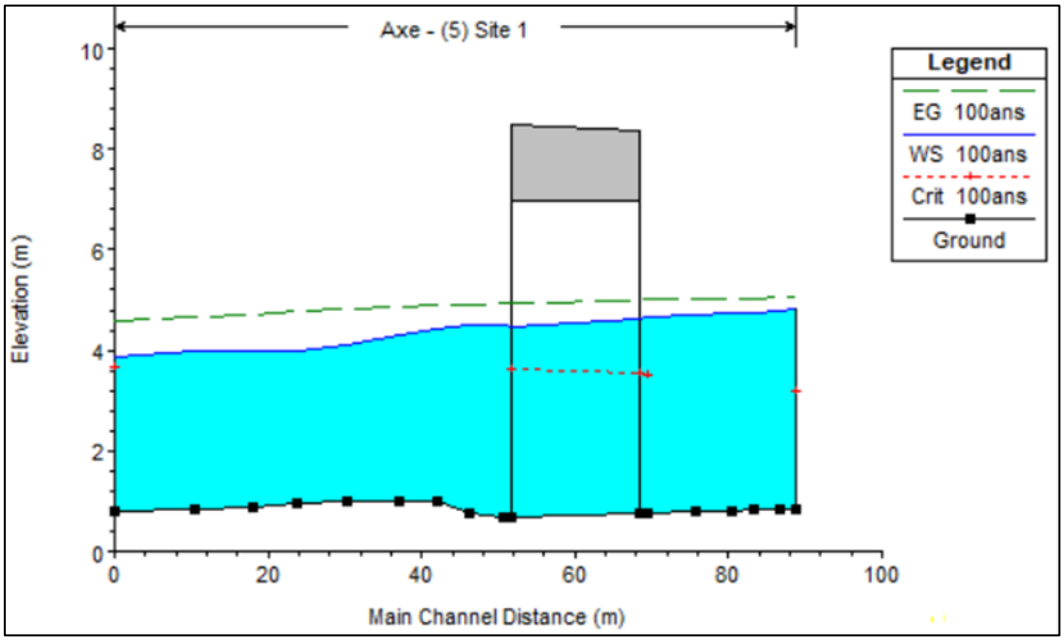


Figure A. 19: Vertical view of the bridge.

# Abstract

## Abstract

Coastal regions are among the most vulnerable to the impacts of climate change, with increasing threats from shoreline erosion, coastal flooding, and inundation. The Skikda coastline, located in northeastern Algeria, is particularly susceptible to these hazards due to its geographical features, low-lying areas, and proximity to river mouths. In this study we want to analyze the vulnerability of the Skikda coastline by focusing on the dynamics of shoreline erosion, coastal flooding, and inundation, using a combination of field data, hydrodynamic modeling, and risk evaluation techniques. The research analyzes the behavior of waves and currents in the area, incorporating both natural and human-induced factors that influence coastal processes. Hydrodynamic models, including the MIKE21 simulation tool, were used to evaluate the effect of various storm scenarios, while hydraulic modeling with the HEC-RAS system provided insights into the extent of potential flooding in critical zones. The findings reveal significant regional differences, with the eastern part of the coastline showing a higher level of vulnerability to erosion and flooding compared to the more stable western regions. The study emphasizes the growing threat posed by rising sea levels and extreme weather events, highlighting the urgent need for sustainable coastal management and adaptive strategies. By mapping high-risk zones and understanding the driving forces behind coastal dynamics, this research offers valuable information for decision-makers to develop effective mitigation and adaptation measures to protect both the environment and local communities.


**Keywords**: Skikda coastline, coastal hazards, shoreline erosion, coastal flooding, inundation, hydrodynamics, MIKE21 model, HEC-RAS model, climate change.


## Résumé

Les régions côtières sont parmi les plus vulnérables aux impacts du changement climatique, avec des menaces croissantes liées à l'érosion du littoral, aux inondations côtières et aux submersions. Le littoral de Skikda, situé dans le nord-est de l'Algérie, est particulièrement exposé à ces risques en raison de ses caractéristiques géographiques, de ses basses terres et de sa proximité avec les embouchures des rivières. Cette étude vise à évaluer la vulnérabilité du littoral de Skikda en se concentrant sur la dynamique de l'érosion du littoral, des submersions côtières et des inondations, en utilisant une combinaison de données de terrain, de modélisation hydrodynamique et de techniques d'évaluation des risques. La recherche analyse le comportement des vagues et des courants dans la région, en tenant compte des facteurs naturels et anthropiques qui influencent les processus côtiers. Des modèles hydrodynamiques, dont l'outil de simulation MIKE21, ont été utilisés pour évaluer l'impact de divers scénarios de tempête, tandis que la modélisation hydraulique avec le système HEC-RAS a permis de mieux comprendre l'étendue des inondations potentielles dans les zones critiques. Les résultats révèlent des différences régionales significatives, la partie orientale du littoral étant plus vulnérable à l'érosion et aux submersions que les régions occidentales plus stables. L'étude met l'accent sur la menace croissante que représentent l'élévation du niveau de la mer et les phénomènes météorologiques extrêmes, soulignant le besoin urgent d'une gestion durable des côtes et de stratégies d'adaptation. En cartographiant les zones à haut risque et en comprenant les forces motrices de la dynamique côtière, cette recherche fournit des informations précieuses

aux décideurs pour développer des mesures d'atténuation et d'adaptation efficaces afin de protéger à la fois l'environnement et les communautés locales.

**Mots-clés** : Littoral de Skikda, risques côtiers, érosion du littoral, inondation côtière, inondation, hydrodynamique, modèle MIKE21, modèle HEC-RAS, changement climatique.

**الملخص**

تُعد المناطق الساحلية من أكثر المناطق عرضة لتأثيرات التغير المناخي، حيث تواجه تهديدات متزايدة من تآكل السواحل، الغمر والفيضانات الساحلية. ويُعتبر الساحل السكيكدي، الواقع في شمال شرق الجزائر، من المناطق الأكثر هشاشة بسبب خصائصه الجغرافية، وانخفاض مستواه، وقربه من مصبات الأودية. تهدف هذه الدراسة إلى تقييم هشاشة الساحل السكيكدي من خلال التركيز على ديناميات التآكل الساحلي، الغمر والفيضانات الساحلية، وذلك باستخدام بيانات ميدانية، ونماذج هيدروديناميكية، وتقنيات تقييم المخاطر. وقد تم تحليل سلوك الأمواج والتيارات في المنطقة، مع مراعاة العوامل الطبيعية والبشرية التي تؤثر على العمليات الساحلية. تم استخدام نماذج هيدروديناميكية، من بينها برنامج MIKE21، لتقييم تأثير سيناريوهات العواصف المختلفة، بينما وفّرت النمذجة الهيدروليكية باستخدام نظام HEC-RAS رؤى حول مدى الفيضانات المحتملة في المناطق الحرجة. كشفت النتائج عن فروقات إقليمية واضحة، حيث تبين أن الجزء الشرقي من الساحل أكثر عرضة للتآكل والغمر مقارنة بالجزء الغربي الأكثر استقرارًا. وتبرز الدراسة التهديد المتزايد الناتج عن ارتفاع مستوى سطح البحر والظواهر الجوية القصوى، مشددة على الحاجة الملحة لإدارة ساحلية مستدامة واستراتيجيات تكيف فعالة. من خلال رسم خرائط للمناطق الأكثر عرضة للخطر وفهم القوى المحركة للديناميات الساحلية، توفّر هذه الدراسة معلومات قيّمة لصناع القرار من أجل تطوير إجراءات فعالة للتخفيف من المخاطر والتكيف لحماية البيئة والمجتمعات المحلية.

**الكلمات المفتاحية:** ساحل سكيكدة، المخاطر الساحلية، تآكل السواحل، الفيضانات الساحلية، الغمر، الهيدروديناميك، نموذج MIKE21، نموذج HEC-RAS، التغير المناخي.